Habilitation à Diriger des Recherches

Turbulent transport of particles and fields

Mickaël Bourgoin

2012

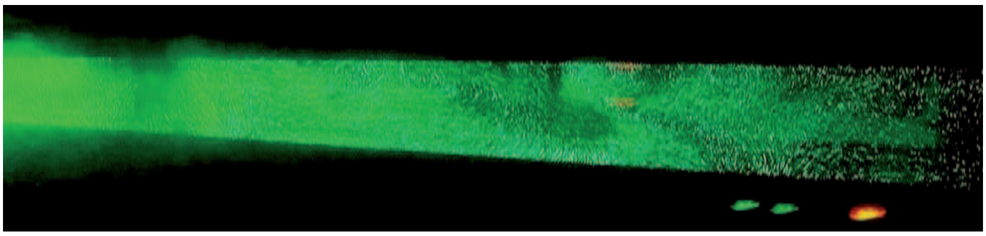

Table of contents

Chapter 1

Introduction

In spite of almost two centuries of active research, a complete frame for describing and accurately predict turbulent flows has not emerged yet. The difficulty in describing turbulence appears at the very early stage. As noted by Tennekes and Lumley [101], giving a definition of the phenomenon is already a challenge. This might be related to the very fundamental character of turbulence and to its ubiquitousness, which makes it at the same time familiar and mysterious. As most of such fundamental things, a definition can only be approached by an enumeration of empirical properties. A series of key words serving this purpose can be clearly identified from classical turbulence textbooks : for instance, without being exhautsive, *statistics, complexity, irregularity, randomness, multi-scaling, whirls, intermittency, mixing, dispersion* form part of the semantic field which globally defines what we mean by *turbulence*.

In parallel with the semantic issue, comes the technical difficulty of turbulence theoretical description. Though an exact theory for turbulence does *a priori* exist, the strong non-linearities of Navies-Stokes equations seem to vanish any hope of ever finding an analytical solution of the problem. As for the definition matter, unless a relevant radical change of paradigm is ever found, we are therefore committed to simply find the best possible description of the phenomenon in terms of an enumeration (which ought to be as complete as possible) of the mathematical and physical properties –mainly in a statistical sense– of these unknown solutions, seeking in particular for universal behaviors.

The first stone in building such a statistical description in modern history of turbulence starts with Richardson, who proposed in the 1920s a multi-scale description of the phenomenon in terms of an energy cascade, where turbulence appears as a hierarchy of random eddies with sizes ranging from the scale where energy is injected down to the scale where it is dissipated by viscosity. This range of scales defines the inertial range of turbulence. Though we know today that this cascade results from the non-linear interaction of Fourier modes of the velocity field, we are still unable to quantitatively model and predict turbulence statistics over the entire range of inertial scales. Since 1941, Kolmogorov's ideas dominate the common way to describe turbulence, essentially by means of the moments of velocity increments (the so-called *structure functions*). In spite of some successes (as the 5/3 turbulent spectrum, the 4/5 law or recent progresses in multi-fractal description) it is a constative fact that our *toolbox* for turbulence investigation remains incomplete and not suited yet to produce an accurate and predictable description (finite Reynolds number effects, anisotropy effects, intermittency phenomenon, turbulent transport, etc. are, for instance, just a few of the remaining mysteries).

As a consequence of this situation, from a fundamental point of view, it is an usual feeling that the mysteries and the blockage we face in turbulence may be due to a wrong angle of attack of the problem, related to the lack of an appropriate tool to look at it properly. To put it in other words, it may simply be to early to find precise answers as very likely we didn't find yet the good questions. This manuscript follows, somehow, this idea : the general tone is intentionally more interrogative than affirmative. It is often driven by the motivation of proposing new investigation tools which may offer different –or at least complementary– points of view and which may help questionning common *credos*, in an unblocking scope.

These pages give a synthetic view of my personal research contribution to this effort, in the field of turbulent transport phenomena. Three major topics will be discussed :

- the Lagrangian structure of turbulence ;
- the turbulent transport of material particles ;
- the magnetohydrodynamic transport of magnetic field in turbulent flows of liquid metals.

This work is primarily experimental (including conception and developments of innovating instrumentation and facilities), though the modeling effort of the studied phenomena is constant and has often motivated fruitful collaborations.

These topics have in common the fact that they concern transport properties of turbulence, in a broad sense, which can be taken as a unifying guideline. Though the research presented here is mainly academic, it is also motivated by the increasing requirements for modeling practical applications where turbulent transport is crucial (pollution dispersion, mixing, combustion, etc.). The capacity of turbulence to transport, mix and disperse substances, particles and fields is indeed one of its main characteristics. Establishing models to predict accurately mixing properties of turbulence remains an important challenge. In industrial systems for instance, this is directly related to processes efficiency, with important economical and environmental issues. Such models have been developed since the pioneering work by Taylor and Richardson in the 1920's [100, 88], but their experimental validation is still ambiguous. Some of these descriptions are naturally developed in a Lagrangian framework, where the flow is described from the trajectories of its fluid elements. For instance, a key ingredient in the statistical modeling of mixing relies on the dipersion of pairs of fluid particles, the separation of two nearby fluid elements being naturally related to concentration fluctuations of a dispersed passive substance [68, 94]. Similarly, the coupling between a conducting fluid and a passive magnetic filed (this is the domain of magnetohydrodynamics) is directly related to the advection of material lines in the flow.

An important effort of my work aims at improving our capacity to analyze and investigate such turbulent transport phenomena. For an experimentalist, this pairs with the development of new experimental tools. In the present case, I have implemented highly resolved Lagrangian techniques (both acoustical and optical), made accessible in the last decade thanks to impressive technological advances.

I have then applied such Lagrangian measurements to investigate fundamental properties of turbulence itself but also the transport properties of material particles whos dynamics deviates from that of tracers. My contributions to the Lagrangian turbulence investigation are presented in the first chapter, with a particular focus on relative dispersion, small scale intermittency and anisotropy. The second chapter is dedicated to the turbulent transport of material particles. Predicting the dynamics of such particles dispersed and transported in a turbulent flow remains a challenge with important applications in industrial and natural systems (dust and pollutants dispersion, industrial mixers, sediments in rivers, dispersion of gametes of marine animals, water droplets in clouds, atmospheric balloons, etc.). However our modelling capacity of these phenomena is still very limited as writing the equation of motion of a single particle in a turbulent field is already problematic, not to mention the subtle couplings which appear as the seeding density is increased.

In parallel to the transport of particles, I have investigated the advection of a magnetic field by a turbulent flow of liquid metal. A remarkable property of this advection is that, under specific conditions, the stretching and folding of magnetic field lines can sustain the spontaneous amplification of magnetic energy. This instability, known as dynamo effect, has been proposed by Larmor in 1919 as being responsible of the magnetic filed of planets and stars. It is only at the beginning of the 21st centuries that three laboratory experiments became capable of reproducing this mechanism. The last chapter of this manuscript is dedicated to the VKS experiment –which is the first, and so far only, successful experimental dynamo in a fully turbulent flow of liquid Sodium– and to related investigations of magnetohydrodynamic (MHD) induction mechanisms in a smaller liquid Gallium experiment.

The final chapter of this manuscript is dedicated to a short description of my perspective research, including some ongoing projects.

To finish this introduction, I would like to emphasize that the personal contributions which are presented here, have benefited from unvaluable collaborations without whom they won't have been possible. These include in particular the EDT team at LEGI, Jean-François Pinton's group at Laboratoire de Physique de l'École Normale Supérieure de Lyon, Eberhard Bodenschatz's group at Cornell University and the VKS team.

Chapter 2

Lagrangian structure of turbulence

2.1 General context

Turbulence governs the vast majority of fluid flows in nature and industrial applications from atmospheric dynamics to mixing and combustion. Despite its ubiquitousness, turbulence remains one of the deepest unsolved mysteries of classical physics. Even if the equations of motion of turbulent flows are perfectly known since Navier and Stokes, more than a century ago, its complexity (primarily driven by its non-linearity) annihilates any hope of finding analytical solutions. We are then forced to turn to phenomenological modeling to gain insight into the behavior of turbulent flows. In 1922 L. F. Richardson introduced the first description of turbulence as a multiple scale phenomenon (Richardson cascade) where mechanical energy is injected at large eddies, and as they become unstable, they split into smaller eddies to which energy is transferred, and so on until eventually viscous dissipation stops the cascade at some small scale where viscosity becomes dominant. In 1941 A. Kolmogorov proposed a quantitative statistical description of turbulence [54] as a self-similar cascade with universal properties.

Taken together, Kolmogorov's hypotheses state that in intense turbulence and well away from any boundaries or singularities the statistics of turbulent flow should be universal at length and timescales that are small compared with the injection of energy into the flow. This implies in particular that at sufficiently small scales, turbulence becomes homogeneous and isotropic, an hypothesis known as *local isotropy*. In Kolmogorov's approach the mean energy dissipation rate $\langle\epsilon\rangle$ then becomes the only relevant parameter governing the dynamics of structures in the inertial range. Since then, statistical turbulence modeling has been dominated by Kolmogorov's ideas, whose 1941 hypotheses have so influenced the field that they are simply known as the 'K41' phenomenology. The great utility of the K41 model lies in its prediction of universal scaling laws for velocity increments statistics. However, K41 is known to fail describing important features of real turbulent flows, as for instance the *intermittency* phenomenon. This has stimulated many theoretical studies trying to refine K41 phenomenology, including Kolmogorov's refined hypotheses of self-similarity in 1962 (known as K62) and more recently multifractal models [77].

In the same spirit of finding alternative, or at least complementary, descriptions of turbulence, new modeling paths have emerged during the last decades, based on a stochastic Lagrangian description of turbulence [93]. In a Lagrangian point of view, fluid statistics (velocity, acceleration, pressure, etc.) are considered along fluid particles trajectories, contrary to the traditional Eulerian approach where the same statistics are considered at fixed points in space where fluid particles do stream continuously. Whereas most of our experimental knowledge of turbulence (including Kolmogorov's ideas) comes from an Eulerian approach, the Lagrangian approach offers complementary observations. Moreover in several cases the Lagrangian point of view offers a more natural framework [112]. This is the case for instance for dispersion issues (and related mixing problems) for which a particulate description (rather than a field approach) is often more relevant. However, direct Lagrangian measurements in fully developed turbulence have only become possible in the last decade thanks to the advent of optical and acoustical technologies which allows to accurately track tracer particles with a sufficiently high spatial and temporal resolution, in order to characterize their dynamics over the entire range of inertial scales. For this reason, until very recently, models and theoretical advances in the Lagrangian framework could not be confronted to or guided by reliable experimental data.

With this perspective I have explored three important questions related to the Lagrangian properties of turbulence :

- The relative dispersion of pairs ;
- The Lagrangian intermittency ;
- The validity of Kolmogorov's local isotropy hypothesis ;

This required the development of a high resolution particle tracking setup [21] (figure 2.1) which I have entirely implemented as a postdoctoral associate in E. Bodenschatz group at Cornell University between 2003 and 2005, together with Haitao Xu (also postdoctoral associate) and Nick Ouellette (PhD student).

Beyond the experimental challenge of achieving such Lagrangian measurements, my motivation to investigate these specific questions relies on their fundamental and practical importance : (i) pair dispersion is directly related to mixing properties of turbulence and also to fundamental scaling laws which remained to be investigated experimentally ; (ii) intermittency is one of the biggest fundamental mysteries of small scale turbulence, whose accurate description is in turn important for the development of accurate sub-scale models (for instance for *larg eddies simulations*) and (iii) the local isotropy hypothesis is the basis of most theoretical descriptions of turbulence and directly impacts the relevance of most turbulence models. As we will see, the results I present farther appear to question some usual positions and have stimulated interesting debates and exchanges in the turbulence community. This is particularly the case for the relative dispersion and local isotropy studies ; intermittency investigation is more *factual* and its importance relies on the unprecedented resolution of the measurements of Lagrangian anomalous exponents.

After a brief description of the experimental setup and its technological challenges, I present in the following sections the main results on these topics.

2.2 3D - high resolution optical Lagrangian tracking

In the experiments presented in this chapter, turbulence is genrated by counter-rotating two baffled discs in a closed plexiglass cylindrical chamber containing 120 liters of water, described in detail in [108]. This is the well-known von Kármán flow configuration. While this flow is both anisotropic and inhomogeneous, it can be used to achieve very high Reynolds numbers (approaching $R_\lambda \sim 10^3$) in a relatively small amount of laboratory space. In addition, the size and the confinement of the flow makes it well-suited to Lagrangian measurements compared to wind tunnels or other configurations with strong mean flows, where it is significantly more difficult to follow tracer particles for long periods of time [5, 85, 84]. Several techniques can then be used for direct Lagrangian tracking, which are essentially separated in two families : optical tracking and scattering tecnhics (mostly based on Laser and acoustic doppler velocimetry). For the present study, I have implemented a multiple high-speed camera system capable of tracking optically, in 3D, hundreds of trajectories of particles with sufficient spatial and temporal resolution to resolve the smallest and fastest turbulent scales in fully developed turbulence.

The flow is seeded with very small neutrally-buoyant tracer particles which behave as fluid elements. These tracers are tracked using three high speed cameras. Optical three-dimensional Lagrangian particle tracking can broadly be broken into three steps. First, the particle images are identified from the recorded camera frames and their centers are located, ideally with sub-pixel resolution. Next, the two-dimensional coordinates of the particle centers found from each camera are correlated to produce three-dimensional particle positions. This stereomatching step has the added benefit of filtering out spurious particles, since they will not match images from the other cameras. Finally, the three-dimensional coordinates of the particles are followed in time, generating particle tracks. An analysis of Lagrangian particle tracking algorithms was given by Ouellette *et al.* [75]. Using three or more cameras (instead of two theoretically sufficient for a stereo-tracking) has two main benefits : (i) when a particle is visible from the three cameras simultaneously, we get redundant 3D information on particles position which is then located with a higher resolution (typically equivalent to $1/10^{\text{th}}$ of a pixel) and (ii) when many particles are present in the measurement volume, situations occur where a particle may be hidden by another along the line of view of one of the cameras ; increasing the number of cameras increases the probability that all the particles are seen by at least two cameras, making the 3D positioning always possible for most of them ; we have empirically shown that 3 cameras (at 256×256 pixels each) allow to simultaneously track around 300 particles with sub-pixel resolution. These particle tracks are then used to study multi-particle statistics such as the relative dispersion discussed in 2.3.

It is important to note that resolving particle motions in intense turbulence requires an imaging system with a very high temporal and spatial resolution. In terms of time resolution, for efficient and accurate particle tracking, such a system must over-resolve the Kolmogorov timescale $\tau_\eta = \sqrt{\nu/\epsilon}$, the smallest turbulent timescale, especially when time derivatives of the particle motion are desired (to investigate velocity or acceleration for instance). τ_η is typically very short ; for example, in our water flow at $R_\lambda = 815$ (the highest Reynolds number reported here, $\tau_\eta = 0.544$ ms). Making at least ten measurements per τ_η thus corresponds to a minimum imaging rate of 18 000 frames per second ; even faster recordings are required to make very accurate measurements. Previously, due to the lack of commercial cameras capable of recording images at these speeds, this technique was limited to the measurement in flows with low level of turbulence [74, 105]. For high turbulence level, a similar technique using optical silicon strip detectors in the vertex detectors of high-energy particle accelerators has been implemented by Voth *et al.*. [108, 57]. These strip detectors, however, have proved to be unsuitable for measuring multiple particles simultaneously. The same difficulty remains for Doppler techniques (either acoustic or optic). For the work presented here, we have used the best available commercial high-speed cameras (at the time this research was done). We have used Phantom v7.3 CMOS cameras from Vision Research Inc., which are capable of recording images at a rate of 27 000 frames per second at a resolution of 256×256 pixels. In terms of spatial resolution, considering the subpixel accuracy (of the order of 1/10th when three cameras are used simultaneously), the effective resolution is therefore of the order of "2560x2560" pixels what ensures that more than three decades of spatial scales are resolved and covers, in most cases,

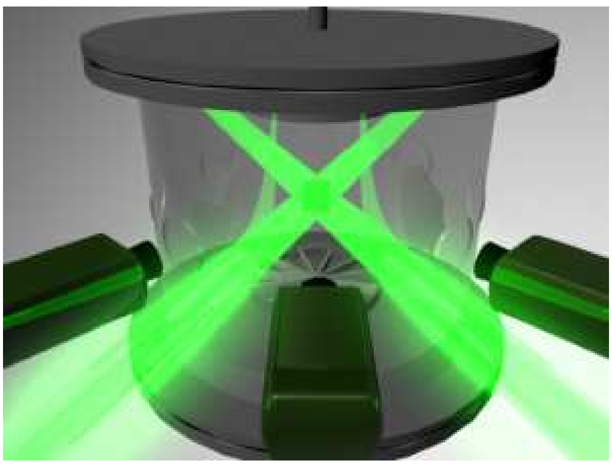

FIG. 2.1 – Sketch of the experimental apparatus.The trajectories of tracer particles were recorded by three high-speed cameras in a $5 \times 5 \times 5$ cm^3 subvolume in the centre of the tank. The tracers were illuminated by two pulsed Nd :YAG lasers with a combined power of roughly 150 W. The cameras were arranged in a single plane in the forward scattering direction from the lasers with an angular separation of roughly 45°. The discs rotated about the z-axis.

the entire range of inertial scales.

Another requirement concerns the size of the tracked particles which must be smaller than the dissipation scale of the flow ($\eta = (\nu^3/\epsilon)^{1/4}$) in order to ensure that the particle does behave just like a real fluid element. I used transparent polystyrene microspheres with a diameter of 25 μm and a density 1.06 times that of water. These particles are smaller than or comparable to η for all the Reynolds numbers reported in this work, and have previously been shown to act as passive tracers in this flow [109]. On this point, I also refer the reader to chapter 3 which discusses inertial particles issue and the departure from tracer behavior.

I would also like to stress the huge amount of data to be recorded and processed in such measurements. At the considered repetition rates to the cameras (of several 10^4 frames per second) and sensor resolution, the overall data rate exceeds several gigabytes per second of acquisition. This is an important constraint, also found for instance in recent time resolved PIV systems, which defines a new era in experimental fluid dynamics, where instrumentation must be coupled to efficient network capacities and high performance computation systems. The tracking system I developed is indeed connected to a dedicated cluster where each node directly communicates with the cameras in order to improve the data transfer and processing.

In the following sections I describe the results I obtained with this apparatus on the questions of pair dispersion, Lagrangian intermittency and local isotropy hypothesis. I would like to emphasize however that these were only the first studies of many that followed after I left the group. This high resolution tracking system has now become the state of the art in terms of Lagrangian techniques and is nowadays among the most accurate measurements available in turbulence research. However, it should be noted this technique is still at its childhood, and the room for improvement is very important. For instance, several groups in the world are working now on the development of onboard pre-processing, using Field Programmable Gate Arrays (FGPAs) directly mounted in the cameras, prior to the data transfer. This will reduce the amount of data to be effectively transferred from the cameras, allowing for even higher repetition rates, hence improving the overall resolution of next generation tracking systems.

The system I built with H. Xu and N. Ouellette, has now moved to the Max Planck Institute in Göttingen (together with E. Bodenschatz group), and has been upgraded with newest cameras (faster and with higher resolution). It is now being used primarily to investigate the turbulent dynamics of material particles (which do not behave as tracers).

2.3 The relative dispersion of pairs

2.3.1 Superdiffusive regimes

In a quiescent fluid, the relative dispersion of two fluid elements (or tracer particles) is dominated by diffusion. The particles undergo Brownian motion, and the mean square separation $\langle \Delta^2 \rangle$ between them grows linearly in time. In a turbulent flow, however, if the two particles are separated by distances smaller than the characteristic size of the largest eddies in the flow, they will separate faster (superdiffusively). At large separation times and distances, the local correlations responsible for the superdiffusive separation will no longer be present, and, on average, the relative dispersion will again be linear in time, so that an effective large scale Brownian behavior is recovered. Despite almost 80 years of scientific inquiry into relative dispersion (2, 9–17), no clear experimental verification of the theoretical predictions has emerged. In particular a clear experimental characterization of the superdiffusive regime remained to be done. Two critical unresolved questions being the diffusive exponent and the extent to which the initial separation of the fluid particles influences their subsequent motion.

Predictions for the superdiffusivity of pair dispersion in turbulence date back to 1926, when Richardson [88] suggested that the mean square separation between two particles in the range of inertial scales

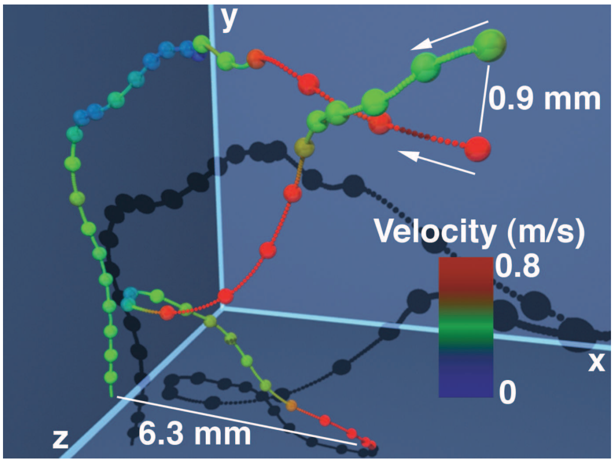

FIG. 2.2 – A pair of measured particle trajectories at $R_\lambda \sim 690$. The small spheres mark every other measured position of the particles and are separated by 0.074 ms (τ_η /13) in time ; the large spheres mark every 30th position. The color of the spheres indicates the magnitude of each particle's absolute velocity in units of m/s. The particles enter the measurement volume as indicated by the arrows and separate under the influence of the turbulence.

should grow superdiffusively in time as t^3. By applying Kolmogorov's scaling phenomenology [54], Obukhov [70] specified that in the inertial range of turbulence, where the only relevant flow parameter is the energy dissipation rate per unit mass ϵ, the mean square pair separation should grow as $\left\langle \Delta^2(t) \right\rangle = g\epsilon t^3$, whith g a universal constant. An important feature of the Richardson-Obukhov superdiffusive prediction is that the separation rate is cubic in time and independent of initial separation. The absence of initial separation is however more an assumption than a consequence of Richardson-Obukhov's prediction, since the t^3 law can indeed be derived by simple dimensional analysis only if initial separation is considered as an irrelevant parameters. In this case the only relevant parameters being $\left\langle \Delta^2(t) \right\rangle$, ϵ and t, Richardson-Obukhov is a direct result of Pi-Buckingam theorem as the only possible relation dimensionally consistent. In turbulence lectures, Richardson-Obukhov t^3 regime is generally considered as *the* law for turbulent disperions, although despite significant efforts, there has been no unambiguous experimental observation of the Richardson–Obukhov law, and best estimates of the Richardson constant span a full order of magnitude [94]. In 1950 Batchelor [8] refined Richardson and Obukbhov's work by considering initial separation as a possible relevant parameter of the problem. In this case, he predicted that two different dispersion regimes should exist for the dispersion of particles with initial separation at inertial range scales : for times shorter than a characteristic timescale t_0, which depends on the initial separation of the pair, the mean square separation should grow ballistically as t^2 ; the t^3 law being expected only for times longer than t_0. More precisely, if $\Delta(t)$ is the separation of two fluid elements at time t and defining Δ_0 as the initial separation between the fluid elements, Batchelor predicted that for Δ_0 in the inertial range

$$\left\langle \left[\vec{\Delta}(t) - \vec{\Delta}_0 \right]^2 \right\rangle = \begin{cases} \frac{11}{3} C_2 \left(\epsilon \Delta_0\right)^{2/3} t^2 & \text{if} \quad t \ll t_0 = \left(\frac{\Delta_0^2}{\epsilon}\right)^{1/3} \\ g\epsilon t^3 & \text{if} \quad t_0 \ll t \ll T_L \\ Dt & \text{if} \quad T_L \ll t \end{cases} \tag{2.1}$$

where C_2 is the universal constant in the inertial range scaling law for the Eulerian second-order velocity structure function, which has a well-known value of approximately 2.13 [97] (interestingly, this relation directly bridges Eulerian and Lagrangian approaches). In the classical cascade model of turbulence, t_0 corresponds to the eddy turnover time at the scale Δ_0 and may be interpreted as the time for which the two fluid elements "remember" their initial relative velocity as they move in the same eddy of size Δ_0.

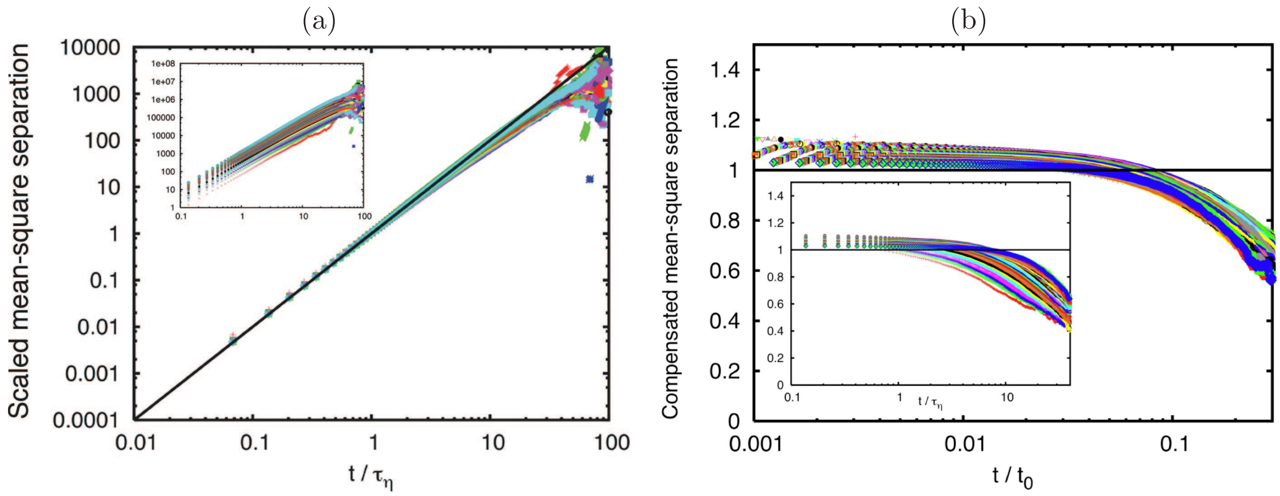

FIG. 2.3 – (a) Evolution of the mean square particle separation. The mean square separation between particle pairs is plotted against time for 50 different initial separations at a turbulence level of $R_\lambda \sim 815$, with the time axis normalized by the Kolmogorov scales. Each curve represents a bin of initial separations 1 mm wide (43η), ranging from 0 to 1 mm to 49 to 50 mm. The curves are scaled by the constant $11/3C_2(\epsilon\Delta_0)^{2/3}$ (Eq. 2.1).The data collapse onto a single universal power law. The bold black line is the power law predicted by Batchelor. Because the smallest Δ_0 measured is not in the inertial range, we do not expect it to scale perfectly as t^2, and indeed it does not scale as well as the larger Δ_0. The inset shows the same curves scaled simply by the Kolmogorov length, for which we see no scale collapse. For both plots, we see no Richardson-Obukhov t^3 scaling. (b) Mean square separation with time scaled by t_0. The mean square separation at $R_\lambda \sim 815$ compensated by Batchelor's scaling law (Eq. 2.1) is plotted against time in units of t_0. Plotted in this way, a plateau corresponds to Batchelor scaling. The inset shows the same compensated data plotted against time and scaled by the Kolmogorov time τ_η . The data clearly collapse significantly better with time scaled by t_0. The data begin to deviate from a t^2 power law at a universal time of about 0.1 t_0.

For times on the order of t_0, this eddy breaks up, and the growth of the pair separation is then expected to undergo a transition to Richardson-Obukhov scaling. According to this prediction, at short times (namely $t \ll t_0$), relative dispersion is ballistic and initial separation dependent, while it accelerates for $t_0 \ll t \ll T_L$ at the same time as it looses the memory of its initial separation. For times much larger (namely $t \gg T_L$) a Brownian-like dispersion is recovered as the two particles evolve then without any correlation. The aim of this study was to investigate this scenario by a systematic analysis of dispersion of pairs of particles in a highly turbulent flow, emphasizing the role of initial separation of the particles.

2.3.2 Richardson vs Batchelor regime

Figure 2.2 shows an example of two simultaneously particle tracks measured in our experiment. Figure 2.3a shows measurements of relative dispersion for turbulence levels up to $R_\lambda \sim 815$. We found that for experimentally accessible initial separations, our data scales as t^2 for more than two decades in time, with no hint of classical Richardson-Obukhov t^3 scaling. This behavior holds for initial separations throughout the entire inertial range, even for large initial separations (up to 70% of the largest length scale of the turbulence). When we scaled our relative dispersion data by the constant predicted by Batchelor, given in Eq. (2.1), the curves collapsed onto a single t^2 power law. The line drawn in figure 2.3a is $\frac{11}{3}C_2(\epsilon\Delta_0)^{2/3}t^2$ (with no adjustable parameter). It is important to stress the remarkable quality of the collapse in the main figure where 50 curves are represented, one for each initial separation. In figure 2.3b, where time is plotted in units of τ_η , the data for different initial separations start deviating from the t^2 law after a time t^* which depends on Δ_0 (see inset of figure 2.3b). If, however, time is rescaled by Batchelor's $t_0 = (\Delta_0^2/\epsilon)^{1/3}$ (main figure 2.3b), the data for each initial separation deviate from Batchelor's prediction at the same universal value of roughly $t^*/t_0 \sim 0.1$. This behavior prevails for all the Reynolds number explored (between R_λ 200 and 815). Above t^*, the measurements show that the separation rate is slower, suggesting the transition toward the fully uncorrelated brownian dispersion, with no hint of an intermediate accelerated Richardson-Obukhov t^3 law.

I would also like to stress that the Batchelor t^2 law appears to be very robust, what may seem in some sense surprising, given the large-scale inhomogeneity and anisotropy present in our flow. It is therefore very likely that the same law should be present in other real-world flows that are not perfectly homogeneous and isotropic.

Our measurements also confirm the importance of initial separation as predicted by Batchelor in Eq. (2.1) at two levels : (i) the extent of the ballistic regime (given by $t_0 = (\Delta_0^2/\epsilon)^{1/3}$) increases as $\Delta_0^{2/3}$; (ii) the ballistic separation rate is also proportional to $\Delta_0^{2/3}$. This initial separation dependence has important practical consequence since in any real situation of relative dispersion (let say for instance the dipersion of a cloud of polutant), the initial source will have a finite size and therefore most pairs will have a nonzero Δ_0.

2.3.3 Distance-neighbor function - another Richardson / Batchelor controversy

In Richardson's seminal paper [88], he suggested that turbulent relative dispersion can be described by a diffusion equation, although one where the diffusion constant $K(r,t)$ is a function of space and time (non-fickian diffusion). With the additional assumption that the flow is isotropic, the equation can be reduced to a single spatial dimension, namely

$$\frac{\partial}{\partial t}q(r,t) = \frac{1}{r^2}\frac{\partial}{\partial r}\left[r^2 K(r,t)\frac{\partial q(r,t)}{\partial r}\right]. \tag{2.2}$$

$q(r,t)$, which Richardson called the distance-neighbour function, represents the spherically averaged probability density function (PDF) of the relative dispersion. Assuming the boundary conditions $q(\infty,t) = 0$ and $q(r,\infty) = 0$, equation (2.2) admits a self-similar solution if we additionally assume the initial condition $q(r,0) = \delta(r)$, (*i.e.* diffusion from a point source).

The exact form of the distribution $q(r,t)$ then depends on the expression of the diffusivity coefficient $K(r,t)$ as a function of space and time. If for simplicity we assume time and space power laws for the diffusivity coefficient $K(r,t) = r^\alpha t^\beta$, dimensional consistency with K41 imposes that $3\alpha + 2\beta = 4$ [17]. In his original work, Richardson assumed $K \propto r^{4/3}$ (the celebrated 4/3 Richardson law), corresponding to $\alpha = 4/3$ and $\beta = 0$. Under these conditions, Richardson showed that

$$q_R(r,t) = A_R t^{-9/2} \exp\left[-B_R \frac{r^{2/3}}{t}\right], \tag{2.3}$$

where A_R and B_R are integration constant. Subsequently, Batchelor proposed instead that K could be timescale dependent rather than spatial scale dependent and proposed that $K(r,t) \propto t^2$ [9] ($\alpha = 0$, $\beta = 2$), leading to

$$q_B(r,t) = A_B t^{-9/2} \exp\left[-B_B \frac{r^2}{t^3}\right]. \tag{2.4}$$

Note that both the Batchelor and the Richardson analytical expressions for the distance neighbour function give a t^3 Richardson-Obukhov like dispersion regime for $\langle r^2 \rangle (t) = \int r^2 q(r,t) \mathrm{d}r$. This is a direct consequence of the fact that both laws are derived for the dispersion from a point source (particles with zero initial separation), and by dimensional constraint (as described before) the absence of initial scale imply in both cases a Richardson-Obukhov t^3 law for the mean separation evolution $\langle r^2 \rangle$. No analytical solution of (2.2) is known for a finite size dispersive source. Therefore this new Richardson-Batchelor controversy should not be confused with the t^2 vs t^3 controversy discussed previously.

We cannot easily replicate such a point source condition in the laboratory experiment. We therefore propose to empirically approximate this condition, by subtracting the initial separation of each particle

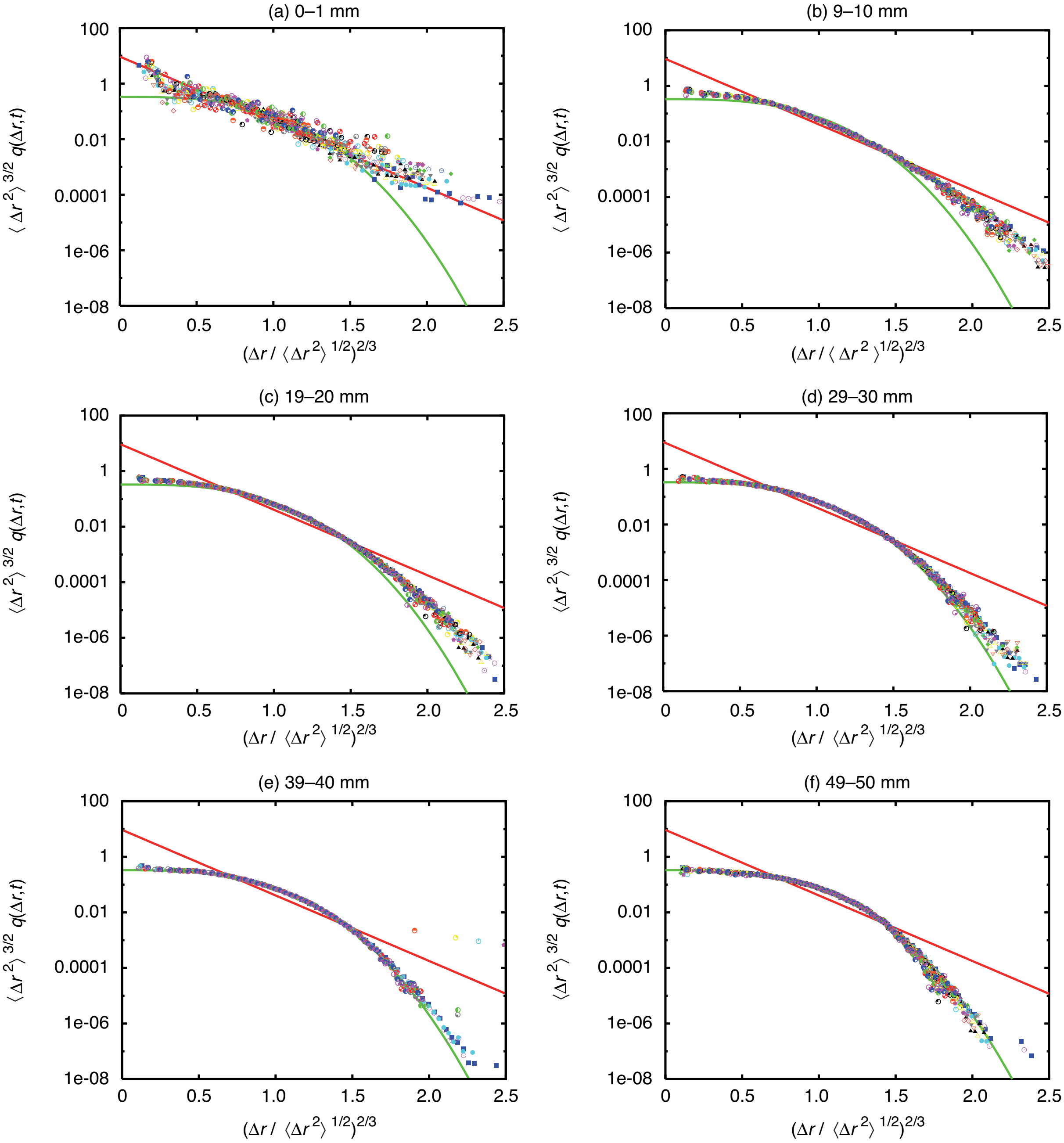

FIG. 2.4 – The distance neighbour function for different initial separations at $R_\lambda = 815$. The red straight line is Richardson's predicted PDF, while the green curved line is Batchelor's. The symbols show the experimental measurements. Each plot shows a different initial separation ; for each initial separation, PDFs from 20 times ranging from τ_η to $20\tau_\eta$ are shown.

pair componentwise and considering $q(\delta r, t)$, where we define $\delta r = |\Delta - \Delta_0|$. Moreover for consistency with the observed dispersion regime reported in previous section (which is clearly not Richardson-Obukhov), the expressions for the distance neighbour function can be rewritten as

$$q_R(\delta r, t) = A'_R \left\langle \delta r^2 \right\rangle^{-3/2} \exp\left[-B'_R \frac{\delta r^{2/3}}{\langle \delta r^2 \rangle^{1/3}} \right] \tag{2.5}$$

and

$$q_B(\delta r, t) = A'_B \left\langle \delta r^2 \right\rangle^{-3/2} \exp\left[-B'_B \frac{\delta r^2}{\langle \delta r^2 \rangle} \right]. \tag{2.6}$$

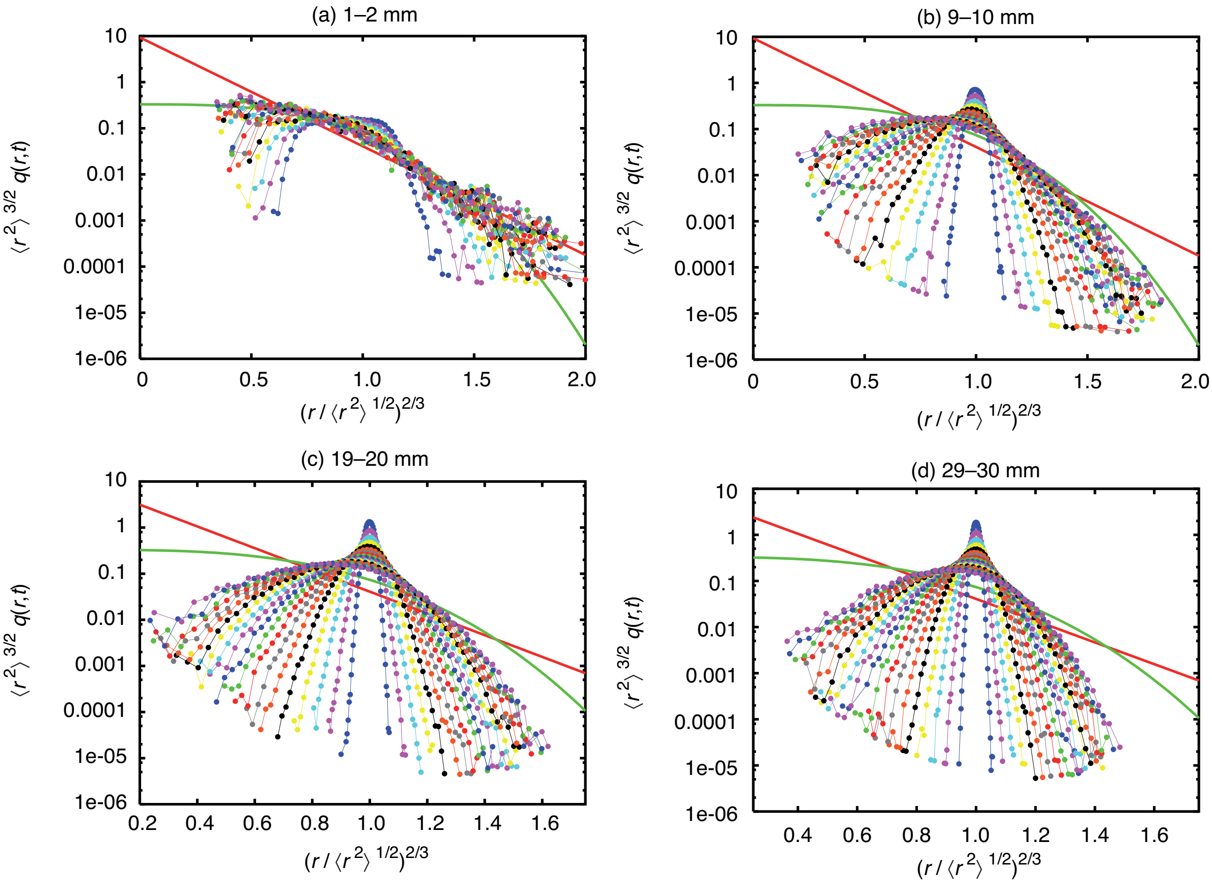

FIG. 2.5 – The distance neighbour function for different initial separations at $R_\lambda = 815$ without subtracting the initial separation. The red line is again Richardson's PDF, while the green line is Batchelor's. The short time data are peaked near the root-mean-square separation. The measured PDFs spread as time increases, approaching the Batchelor PDF.

where the time dependency is implicitly represented in $\langle \delta r^2 \rangle (t)$. In the case of an initial point source, this expressions are equivalent to (2.3) and (2.4). This approach is mostly empirical and has no real theoretical background ; it also has the unwelcome side effect of treating all pairs in the same fashion, whether they are separating or coming closer together. However, as presented below, it gives interesting results.

The measurements of $q(\delta r, t)$ are shown in figure 2.4 for six different initial separations at $R_\lambda = 815$. For each initial separation, the distance neighbour function is shown for 20 different times ranging from τ_η to $20\tau_\eta$. For small initial separations ($< 40\eta$), the measured distance neighbour function agrees well with Richardson's predicted form, while for large initial separations ($> 1100\eta$), data agree well with Batchelor's form. For intermediate initial separations, the data lie between the two predictions and undergo a transition between the two laws. The same qualitative trend is seen at all Reynolds numbers investigated.

Finally, it is interesting to note that $q(\delta r, t)$ is self-similar in t for all Reynolds numbers measured. This is not the case if we consider $q(r, t)$ without accounting for the nonzero initial separation of the pair (see figure 2.5), what gives an *a posteriori* empirical justification of the relevance of considering function $q(\delta r, t)$.

2.3.4 Discussion and conclusions

I have shown that the Batchelor's prediction for the pair separation growth rate is fulfilled for more than two decades in time at high turbulence levels (up to $R_\lambda \sim 10^3$). Although the data may be somewhat contaminated by the inhomogeneity and anisotropy present in our specific flow, the observed scale collapse onto the Batchelor law appears very robust. No hint of Richardson-Obukhov scaling, cubic in time and independent of initial separation, has been observed. I believe the reason is that this intermdiate regime not only requires a large separation between T_L and τ_η (hence a large Reynolds number) but also a large separation between T_L and t_0, so that initial separation could be actually "forgotten" by the two fluid elements before their dynamics becomes too uncorrelated. For the initial separations accessible in our experiments, the maximum value of the ratio of (T_L/t_0) was of order 10, with no fully developed t^3 scaling. In order to apply the Richardson-Obukhov scaling law to a practical situation, (T_L/t_0) must probably be much larger than 10, which implies that this law is limited either to very small initial separations (as observed for instance in numerical simulations [17, 13]) or to very high Reynolds numbers. Only then the memory of initial separation might be forgotten before large uncorrelated scales are reached. Interestingly, a recent numerical study by M. Rast and J.-F. Pinton [86] also points toward the possibility that such scaling laws may simply be sub-dominant compared to other effects, as the role of the "delay time" (which they define as the duration for which particle pairs remain together before their separation increases significantly).

This has two important consequences : (i) though the separation is still superdiffusive it is slower than the usually admitted cubic Richardson-Obukhov law and (ii) there is a memory effect as the initial separation remains an important parameter which influences the pair separation untill it reaches the decorrelation scale of the flow. Note that the role of initial separation also appears in the distance-neighbour function analysis, which has been shown to have self similar behaviour only when the initial separation is substracted to the instantaneous pair separation.

Let me emphasize the potential importance of these results : they show that the Richardson-Obukhov's law (which is generally taken for granted) may have to be replaced in most cases (in particular for modeling of turbulent mixing and transport phenomena), by the Batchelor's ballistic law in order to predict in a reliable manner turbulent dispersion effects. An important consequence is that in almost all flows with natural, industrial or biological significance, the initial separation will influence the subsequent spreading of the two fluid elements throughout the entire period of their turbulent superdiffusive separation. This can explain, for example, measurements of the decay of the fluctuations of a passive scalar injected into the flow [110], which was shown to become slower as the separation between two sources was increased. In more practical situations (as the dispersion of radioactive aerosols or volcanic ashes, for instance) the prediction of the decay rate and hence of the required time for the concentration of contaminants to drop below a given security threshold may also be affected by the choice of the appropriate dispersion law.

Finally these results raise the question of the status Richardson-Obukhov dispersion law, which is generally presented as *the* turbulent dispersion law in most textbooks and turbulence lectures. It is however important to emphasize the limitations of this law as well as the importance of the Batchelor's regime and the role of initial separation. Not doing so may lead to growing misconceptions. As a colateral aspect, this study also adresses the question of the relevance of a "large Reynolds number limit" which is often invoked in turbulence models. Is there such a limit for which a Richardson-Obukhov dispersion law would be present ?

2.4 Lagrangian intermittency

2.4.1 Velocity increments and intermittency phenomenon

The previous section dealed with the statistical analysis of fluid particles position, and more specifically position differences (or increments). I move now one step forward in the analysis of fluid tracer dynamics by considering their velocity increments. In the context of turbulence, statistics of velocity increments are of particular importance. In classical Eulerian approaches, spatial velocity differences are generally considered $\delta \boldsymbol{u}(r) = \boldsymbol{u}(\boldsymbol{r}+\boldsymbol{x}) - \boldsymbol{u}(\boldsymbol{x})$ and statistics are investigated in terms of their moments $< \delta \boldsymbol{u}(\boldsymbol{r})^p >$ also called structure functions. Such incremental quantities are important for several reasons. First because the classical inertial range similarity hypothesis since K41 is best suited to increments rather than to raw velocity field. Let me quote Batchelor who wrote, about the importance of velocity differences in this context, that "*it seems reasonable to suppose that when r is small enough the larger eddies make very little contribution to the velocity difference, so that this mean value is determined almost wholly by eddies whose diameters are of the same or smaller order than r, and we led to apply similarity hypotheses*" [8]. Increments are also important because they directly give common statistical quantities, particularly in the case of second order structure function $S_2(r) =< \delta u(r)^2 >$ which, for homogeneous turbulence, is directly related to the velocity correlation function $R_{uu}(r) = 2(\sigma_u^2 - S_2(r))$ (with σ_u^2 the velocity variance) which is itself related to the velocity spectrum by simple Fourier transform. A last important aspect of increments comes from the third order Eulerian structure function for which one of the only known exact analytical results (the celebrated Kolmogorov 4/5th law) is directly derivable from Navier-Stokes equations.

In the Eulerian framework, K41 phenomenology predicts that the moments $< \delta u(r)^p >$ should scale as $r^{\zeta_p^E}$ with $\zeta_p^E = p/3$ in the inertial range of turbulence where the only relevant flow parameter is the rate of energy dissipation per unit mass ϵ. Closer studies, however, have shown that the K41 scaling predictions are not obeyed, especially for high-order moments. Instead, the ζ_p^E increase nonlinearly and slower than p=3 [3, 4, 35, 26]. This anomalous scaling is usually attributed to the phenomenon of intermittency that destroys the perfect self-similarity underlying the K41 phenomenology, and reflects the fact that energy dissipation ϵ is highly unevenly distributed. As an attempt of definition of intermittency (a consensual definition has not emerged yet in the turbulence community) we may see it as the fact that statistical quantities of a turbulent field dependent on the scale at which they are explored. As a consequence, if we consider increments at a given scale r of a given velocity field intermittency causes their probability density function (PDF) to change depending on the observation scale r. Such a deformation of the increments PDF is now well-established and well characterized for Eulerian fields (though its physical origin remains mysterious) : increments PDF are gaussian at large scale ; they develop approximately exponential tails for separations in the inertial range ; tails become stretch exponential at even smaller scales. These evolution of the statistics across the scales reveals the non self-similar nature of turbulence, in contradiction with original Kolmogorov's hypotheses, which is responsible for the departure from K41 predictions for structure functions scalings. To account for these anomalous exponents, original Kolmogorov's self-similar hypotheses had to be refined. Kolmogorov himself proposed such a refinement in 1962 [56] incorporating Oukhov's suggestion of strongly non-Gaussian fluctuations of the energy dissipation rate [72] after Landau objected the averaged energy dissipation might not be a sufficient parameter to describe turbulent fields as assumed in original K41 hypotheses. Since then, several other descriptions of intermittency have emerged, among which the most popular has become the multi-fractal description introduced by Parisi and Frisch in 1985 [77].

Almost all of the observations of anomalous scaling have been made for Eulerian structure functions, measured with probes fixed relative to some laboratory reference frame. K41 phenomenology also applies, however, to Lagrangian quantities measured along the trajectories of individual fluid elements. In the Lagrangian framework, temporal increments along a particle trajectory are considered : $\delta u(\tau) = u(t + \tau) - u(t)$ (turbulence is assumed statistically stationary, so that Lagrangian velocity differences depend only on the time increment τ). Historically, as already mentioned, Lagrangian measurements have been very difficult to perform. For this reason, anomalous scaling and intermittency have not been fully investigated from the Lagrangian viewpoint. Given that the Lagrangian approach is more natural for many problems in turbulence, a more thorough understanding of Lagrangian intermittency is needed. In addition, experimental measurements of Lagrangian anomalous scaling provide data to test stochastic models of turbulence [27, 14, 15]. Before we carried the measurements reported in this section, only available experimental data on Lagrangian intermittency were those obtained by Mordant *et al.* [65, 67] from acoustical Lagrangian measurements where the deviation of Lagrangian anomalous exponents from the self-similar prediction was found to be significantly more pronounced than its Eulerian equivalent. The resolution of these measurements was however limited due to the size

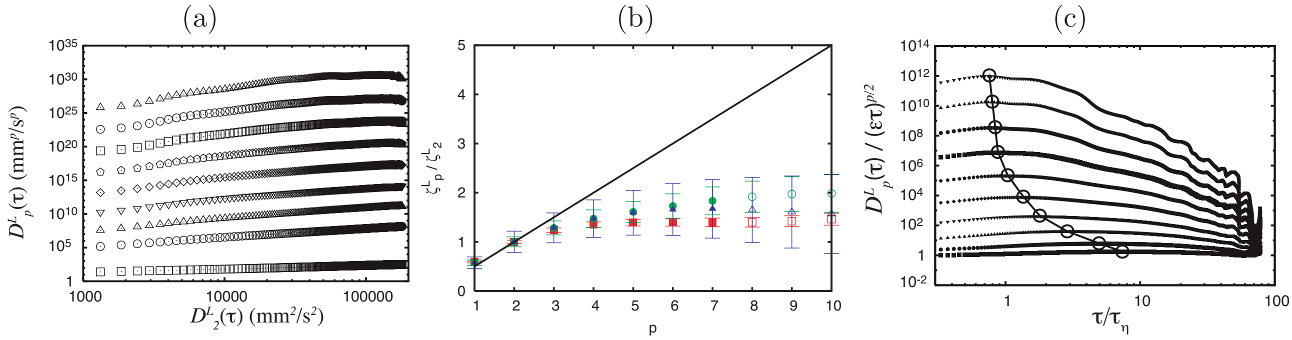

FIG. 2.6 – (a) ESS plot of the high-order Lagrangian structure func- tions at $R_\lambda = 815$. From top to bottom, the symbols correspond to our measurements of the tenth order through first order structure function, with second order omitted. The straight lines are fits to the data to extract the relative scaling exponents. The lines were fit only to values of $D_2^L(\tau)$ corresponding to times between $3\tau_\eta$ and $6\tau_\eta$, where $D_2^L(\tau)$ was found to display a K41 scaling range with $\zeta_2^L = 1$. (b) Anomalous exponents of the structure function relative scaling exponents ζ_p^L/ζ_2^L measured using ESS as a function of order. The solid line shows the K41 prediction for the scaling exponents, with $\zeta_2^L = 1$. Different symbols denote different Reynolds numbers : the red (■) are for $R_\lambda = 200$, the green (•) are for $R_\lambda = 690$, and the blue (▲) are for $R_\lambda = 815$. Strong departure from the K41 prediction is clear for all Reynolds numbers investigated. Equivalent results are found without using ESS (not shown). Moments of orders higher than 7 are not as well converged statistically as the lower-order moments, as suggested by their larger error bars. These high-order moments are plotted with open symbols. (c) High-order Lagrangian structure functions at $R_\lambda = 690$ compensated by the K41 predictions. The order of the structure function increases from 1 to 10 from the bottom curve to the top curve. A K41 scaling region is seen at all orders, but this plateau shifts to shorter times as the order of the structure function increases, as shown by the open circles.

of the tracked particles, significantly larger than the turbulent dissipation scale.

2.4.2 Experimental characterization of Lagrangian intermittency

Using the same Lagrangian tracking system previously described, I have measured the high-order moments of the Lagrangian velocity increments $\delta u(\tau) = u(t+\tau) - u(t)$. Following K41 phenomenology, these moments, also known as the Lagrangian structure functions, should scale as

$$D_p^L(\tau) =< |\delta u(\tau)|^p >\sim (\epsilon\tau)^{\zeta_p^L} \tag{2.7}$$

in the inertial range, with $\zeta_p^L = p/2$. As mentioned above, there have been few experimental studies of the deviation of the ζ_p^L from the K41 prediction, due both to the inherent difficulty in making Lagrangian measurements and to the high degree of temporal resolution required to measure high-order structure functions. Mordant *et al.* [65, 67] measured Lagrangian velocity statistics with an acoustical particle tracking system in a flow similar to ours, and found that the Lagrangian structure functions showed strong intermittency. Because of the requirements of their acoustical system, however, their tracked particles were much larger than the Kolmogorov length scale η and they recorded data at a rate slower than the Kolmogorov time scale τ_η . The measured particle tracks may therefore have smeared out the smallest length and time scales of the flow. This problem of resolution is easily solved in simulation. Biferale *et al.* [14, 15] investigated the Lagrangian structure functions in a direct numerical simulation (DNS) of the Navier-Stokes equations in the context of the multifractal formalism. As with many simulations, however, their results are limited by their low Reynolds number. This is also true of the simulation of Mazzitelli and Lohse [63], who studied Lagrangian statistics both for fluid elements and for bubbles.

In figure 2.6a, I have plotted the Lagrangian structure functions of orders 1 through 10 as measured in our experiment at a Reynolds number of $R_\lambda = 815$ using the Extended Self Similarity (ESS) representation. In recent years, the extended self-similarity ansatz introduced by Benzi *et al.* [12] has become a widely used tool for investigating the anomalous scaling of the Eulerian ζ_p^E. In Eulerian framework, this technique is based on the Kolmogorov 4/5 law stating, as an exact derivation from the Navier-Stokes equations, that $\zeta_3^E = 1$ [55]. Therefore, $< |\delta u(r)|^p > \sim < |\delta u(r)|^3 >^{\zeta_p^E}$ exactly. Based on this idea, it was empirically observed that plotting the structure functions of different orders against each other tends to produce cleaner scaling ranges since imperfections in the scaling behavior in the near dissipation range seem to be correlated among structure functions of different order [35]. Regardless, extended self-similarity (ESS) has been shown to produce very well-determined values of the ζ_p^E. Because of its great utility in determining the scaling exponents of the Eulerian structure functions, researchers have extended the ESS ansatz to the Lagrangian structure functions [14, 15, 67], using the fact that K41 scaling gives $\zeta_2^L = 1$.

Because of the lack of an exact equation for any of the ζ_p^L similar to the Kolmogorov 4/5 law, ESS can only be strictly used to measure relative scaling exponents in the Lagrangian case. Figure 2.6b shows our measurements of the relative exponents ζ_p^L/ζ_2^L computed using ESS. Since ζ_2^L should be close to unity, this ratio is expected to be close to the true value of ζ_p^L. In order to find the relative exponent as close as possible to ζ_p^L, we have fit straight lines to the ESS curves only between $D_2^L(3\tau_\eta)$ and $D_2^L(6\tau_\eta)$ for $R_\lambda = 690$ and 815 and $D_2^L(2\tau_\eta)$ and $D_2^L(4.5\tau_\eta)$ for $R_\lambda = 200$, where a very limited K41 scaling range for the second order structure function is evident. In analogy with the usual Eulerian definition, we take this range to be the Lagrangian inertial range. These fits are shown in figure 2.6a and are compared with the K41 predictions in figure 2.6b. It is clear that there is significant deviation from the K41 prediction, and that this deviation is stronger than in the Eulerian case. Additionally, since the ESS ansatz has not been fully justified theoretically, we have also measured the scaling exponents without using ESS ; these absolute scaling exponents are nearly identical to the ESS values.

2.4.3 Discussion and conclusions

The significance of these results may be seen as twofold : (i) they are the best resolved experimental measurements of high order Lagrangian anomalous exponents in fully developed turbulence and (ii) at the same time they contribute to the questioning process regarding our analysis capacity to quantify turbulence.

As a consequence of the first point, the anomalous exponents shown in figure 2.6b still remain the *standard* values for experimental chracterization of Lagrangian intermittency. This is for instance of primary interest for the investigation of multifractal models and in particular for testing bridging relations between Eulerian and Lagrangian intermittencies [18, 27, 11].

To illustrate the second point, we can notice that the scaling exponents shown in figure 2.6b are similar to those measured by Mordant *et al.* [67], who measured up to sixth order, but significantly lower than the findings from DNS by Biferale *et al.* [14, 15]. The difference with these numerical predictions seems largely dominated by the range of timelags for which the local ESS slopes are measured. While the exponents reported here were estimated from a narrow range where K41 scaling was clearly observed for D_2^L, values reported in [14, 15] considered a much larger range ($[10\tau_\eta, 50\tau_\eta]$) which fell outside these Lagrangian inertial range. The same numerical data fitted over a range comparable to ours gives a good agreement (in [15] Biferale *et al.* did find that fitting the ESS exponents for $\tau_\eta < \tau < 10\tau_\eta$ tend to give smaller values actually comparable to our measurements). More generally these ambiguities show the difficulty just to clearly quantify fine turbulence statistical properties. Somehow, they also point to the limitation of velocity increments (which remain the most widely used analytical tool to investigate turbulent signals) to characterize turbulence statistics. This limitation can be further illustrated by noting that the scaling properties of the high-order Lagrangian structure functions reported in figure 2.6a & b are found anomalous when measured for the narrow range of time lags where the second order structure function (D_2^L) does show a K41 scaling region. However if we scale the structure functions of order p by the non-intermittent K41 scalings ($\tau^{p/2}$), a different picture emerges. As shown in figure 2.6c, the higher order structure functions do show plateaus when compensated by the K41 predictions, albeit at shorter times than for the low order structure functions. The open circles in figure 2.6c show the centers of the K41 scaling ranges which are found to decrease and saturate at a value of the order of τ_η as the structure function order increases. In this picture one may for instance wonder if the anomaly should not be looked for in the fitting range rather than in the exponents. But beyond this rhetorical question, such ambiguities illustrate the incompleteness of the available *toolbox* to characterize turbulence. It is indeed a common feeling in every-days turbulence research, that we lack an appropriate tool to analyze the data (one often feels as driving in nails with a wrench or any other inappropriate tool). The ESS approach already appears as a phenomenological attempt to partially rectify the unsuitability of the direct structure function analysis, with the scope to emphasize the possible existence of universal, but hidden, scaling laws. In the semantic field of statistical turbulence this ressembles an *unbiasing* procedure trying to compensate some mismatch between the analysis tool and the object its applied to. Similarly, the attempt of recovering universal K41 scalings for velocity increments by appropriate conditionings [36, 50] (for instance on local energy dissipation), can also be considered as an *unbiasing* procedure which seems to make conditioned velocity increments more *suitable*. However, none of this manipulation of velocity increments has succeeded in giving a satisfactory characterization (not to mention comprehension) of turbulence. Our capacity to progress in understanding and characterizing fine properties of turbulence seems to be conditioned to the development of new statistical approaches to analyze data. In this context, Empirical Mode Decomposition (EMD), introduced by Huang *et al.* [51] in the late 1990's, may be particularly promising.

2.5 On the validity of Kolmogorov's local isotropy hypothesis

Kolmogorov's original self-similar hypotheses assumed that well away from any boundaries or singularities, the statistics of turbulent flows should be universal at length and timescales that are small compared with the injection of energy into the flow and that averaged energy dissipation $\langle\epsilon\rangle$ should be the only relevant parameter for inertial range dynamics.

Intermittency and anomalous scaling corrections (discussed in previous section) reveal the limitation of considering solely the averaged dissipation $\langle\epsilon\rangle$ in these hypotheses and remain an active topic in modern turbulence research, trying to understand the deep physical reasons of K41 self similar phenomenology failures and to outline more accurate descriptions of turbulence. Evidence of intermittency led Kolmogorov himself to reconsider, in 1962, the original formulation of self-similar hypotheses in order to account for local fluctuations of the dissipation rate ϵ.

However, little attention have been given to another even more fundamental aspect of Kolmogorov's hypotheses : if the small-scale statistics are to be universal, they must be independent of the large-scale flow structure. In particular, K41 assumes that at small scales the turbulence should "forget" any preferred direction of the large-scale flow and that the small-scale fluctuations should be statistically homogeneous and isotropic ; this is the *local isotropy* hypothesis. Models and simulations of turbulence therefore commonly assume such isotropic conditions. Real flows, however, are never homogeneous and isotropic at large scales. Careful study of the effects of large-scale anisotropy on the small-scale turbulent fluctuations is therefore very important for understanding the behavior of turbulent flows in real systems (either natural or manmade). In addition, such study is necessary in order to relate current turbulence theory, modeling, and simulation to practical applications.

Persistent anisotropy at small scales has been noted previously in Eulerian studies of homogeneous shear flows [83, 38] and in the context of the SO(3) symmetry group [16]. Available data is however usually limited to low or moderate Reynolds number and the trend of the persistence of small-scale anisotropy with Reynolds number remains unclear. Is small-scale isotropy somehow recovered for sufficiently large Reynolds number ? This remains an open question which I tackle here from the Lagrangian point of view.

We have investigated the K41 hypothesis of local isotropy in the von Kármán experiment presented above. Von Kármán geometry is particularly well suited for this study as it has a pronounced large-scale anisotropry (the geometry of the system imposes a large scale axisymetric forcing) at the same time as it produces easily very large Reynolds number turbulence. The effects of this large-scale anisotropy are investigated based on the comparison of different projections of the second order Lagrangian structure function $D^L_{2,ij}(\tau) =< \delta u_i(t+\tau)\delta u_j(t) >$. Axisymmetric turbulence has been the subject of prior theoretical work [7, 25, 76], but has not yielded any experimentally verifiable predictions similar to those made by the K41 model. Considering the second order structure function is of particular interest since it is known not to be significantly affected by intermittent corrections compared to higher order structure functions (as shown in previous section, see for instance figure 2.6b). This allows to unambiguously investigate effects of anisotropy limiting other spurious effects. K41 phenomenology predicts that the Lagrangian structure function tensor should scale as $D^L_{2,ij}(\tau) = C_0\epsilon\tau\delta_{ij}$ in the inertial range (with i and j representing the three spatial coordinates). According to K41 universality hypotheses, the structure function should be isotropic and C_0 should have a universal value for all turbulent flows (at least in the limit of high Reynolds number). It is an important parameter in stochastic models of turbulent transport and dispersion [90, 93, 111] and is, remarkably, also connected both to the Richardson constant governing the separation of fluid element pairs, assuming that the covariance of the relative acceleration of the pair is stationary, and to the structure functions of the fluctuations of a scalar field passively advected by the turbulence [94]. Previously measured values of C_0 range from 2.1 to 7.0, in part because Lagrangian experiments, where the trajectories of individual fluid particles are followed, have historically been very difficult. Hanna [48] measured the Lagrangian spectra in the atmospheric boundary layer using neutrally buoyant balloons, but acknowledged significant (as much as 50%) uncertainty in the measurements, reporting a value of 4 ± 2 for C_0. Lien *et al.* [58] measured 1D spectra using large floaters (roughly 1 m in scale) in the oceanic boundary layer. Due to the considerable noise in their measurements, they were only able to estimate that the value of C_0 lies somewhere between 3.1 and 6.2. Mordant *et al.* [67] measured the radial Lagrangian structure function in a laboratory acoustic particle tracking experiment in a counter-rotating disk device similar to ours and obtained a maximum value of 4 for C_0, which may be depressed due to the filtering effect of their relatively large tracer particles. Lien and D'Asaro [59] have estimated a value of 5.5 from the spectral data published by Mordant *et al.* [67]. However none of these experiments addressed the anisotropy of C_0.

In figure 2.7a, I show the full structure function tensor measured at $R_\lambda = 815$. Two features of this tensor are particularly noteworthy. We see very short plateau regions for all three diagonal components of the structure function tensor, consistent with the K41 scaling, though without a fully developed Lagrangian inertial range. It is clear, however, that this tensor is not isotropic, contradicting the K41 hypothesis of local isotropy. The zz component, measured in the axial direction of our cylindrical flow chamber, shows a peak value roughly 25% lower than that of the xx and yy components, measured in the radial direction. The xx and yy components are identical within experimental precision, reflecting the axisymmetry of the large-scale flow. We note that the peak values of the compensated structure functions occur at very short times, less than a factor of 10 larger than the Kolmogorov time τ_η , the characteristic timescale of the fastest turbulent motion. It is also interesting to note that, though it is reduced, anisotropy remains even at the smallest scales.

The anisotropy can also be investigated via the Lagrangian velocity spectrum. Though the spectrum is essentially nothing but the Fourier space representation of the second order structure function just discussed it can emphasize different information of the analyzed data [31]. Following K41 phenomenology, the Lagrangian spectrum should scale as $E_L(\omega) = B_0\epsilon\omega^{-2}\delta_{ij}$, and like the structure function it should be isotropic. The constant B_0, which is related to C_0 simply by a factor of π ($C_0 = \pi B_0$) [23], is the Lagrangian analog of the Kolmogorov constant. The spectral representation also exhibit the same pronounced anisotropy between, the axial and the radial components (the bump at high frequencies is very likely due to noise in the measurements, though by adjusting filter parameters in our post-processing we have checked that inertial range values of the spectrum are not affected by the noise).

The anisotropy found between the radial and axial components of both the structure function and the spectrum persists at all the investigated Reynolds numbers. In figure 2.8a, I show values of C_0 determined from the plateaux of the compensated structure functions as a function of R_λ . For both the axial and radial structure functions, we also observe that C_0 increases weakly with Reynolds number. It is encouraging to note that figure 2.8 shows that the C_0 estimates seem to saturate as the Reynolds

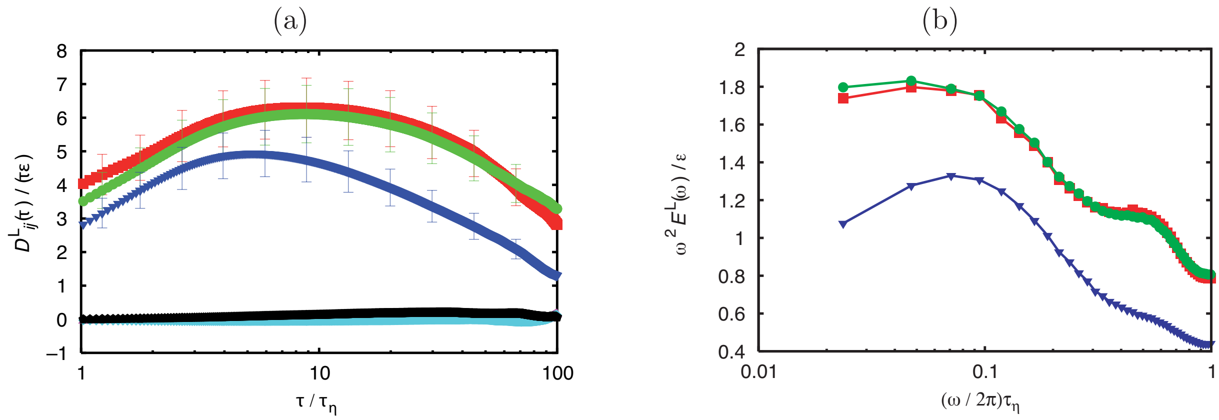

FIG. 2.7 – (a) The xx (■), yy (●) and zz (▼) components of the compensated Lagrangian structure function at $R_\lambda = 815$. The other symbols show the off-diagonal components. The time axis has been normalized by the Kolmogorov time. The relative magnitude of the radial and axial components reflects the anisotropy of our large-scale flow. (b) Compensated Lagrangian velocity spectra at $R_\lambda = 690$ in the x-direction (■), y-direction (●) and z-direction (▼). By scaling the spectra by $\epsilon\omega^{-2}$, we expect to see a plateau in the inertial range with value B_0. The frequency axis has been scaled by the Kolmogorov frequency. As before, we note that the difference in magnitude between the radial spectra and the axial spectrum reflects the large-scale structure of our flow. The bump in the spectrum at high frequencies is due to noise in the measurements, but the inertial range behaviour is unaffected.

number increases ; this result suggests that we may measure true inertial range behavior at high Reynolds number despite the very short scaling range of the structure function. To model this Reynolds number dependence of C_0, Sawford [93] has proposed that

$$C_0 = \frac{C_0^\infty}{1 + AR_\lambda^{-1.64}}, \tag{2.8}$$

where C_0^∞ is the asymptotic value of C_0 at infinite Reynolds number. From simulation data, Sawford estimated that $C_0^\infty \simeq 7$ and $A \simeq 365$. Fits of this function to our C_0 data are shown in figure 2.8a. We find that $C_0^\infty = 6.2 \pm 0.3$ for the radial structure functions and $C_0^\infty = 5.0 \pm 0.4$ for the axial structure function (similar values for A are found in both cases).

2.5.1 Discussion and conclusions

Our measurements of C_0 remain anisotropic even at the highest Reynolds number investigated. In figure 2.8b, is plotted the ratio of the radial measurements to the axial measurements. The anisotropy drops weakly with Reynolds number, but the decrease is very slow and the anisotropy remains strong even at the highest Reynolds number investigated. Taken together, these results suggest that any symmetries (or lack thereof) present at the large scales of the flow will also be reflected in the small-scale turbulent fluctuations. Clearly, therefore, great care must be exercised when applying the results of isotropic turbulence theory to real experimental, industrial and natural flows. For instance, any climate or pollutant transport models must take the significant anisotropies present in the atmosphere into account. The significant difference between the scaling constants measured in the radial and axial directions reflects the large-scale axisymmetry in our flow. Extrapolation based on the Sawford's model even predicts a persistence of small-scale anisotropy in the limit of infinite R_λ. Though such an extrapolation is highly speculative as long as the limits of validity of the model are not well controlled, it is clear that the recovery of isotropy (if any) with increasing Reynolds number is much slower than expected. We do, however, observe K41 scaling ranges for both the Lagrangian structure function and spectrum, suggesting that while our results contradict the K41 hypothesis of local isotropy, the K41 scaling hypotheses are fulfilled for second order statistics.

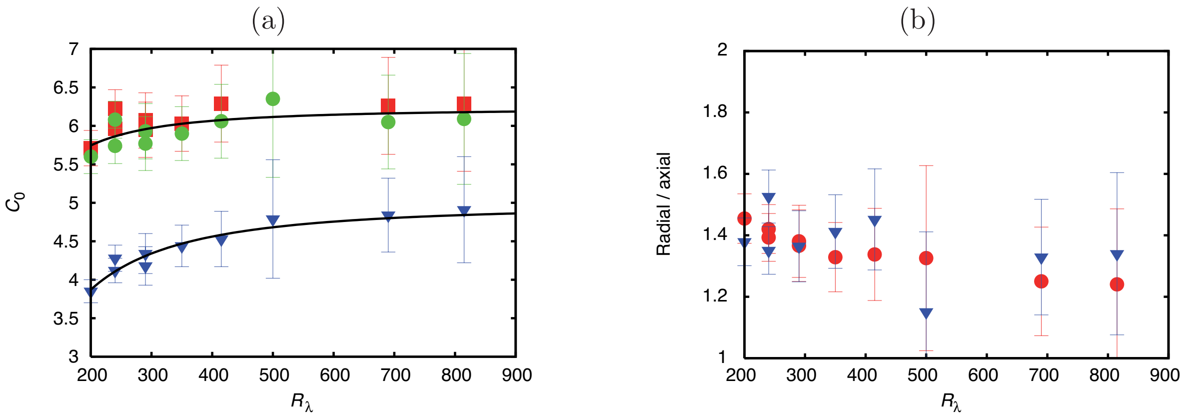

FIG. 2.8 – (a) Measurements of C_0 from the Lagrangian structure function tensor for the xx component (■), yy component (●) and zz component (▼) as a function of Reynolds number. The zz component C_0 values are smaller than those measured for the two radial components, presumably due to the large-scale axisymmetry of our flow. C_0 is observed to increase weakly with Reynolds number. The solid lines are fits of Sawford's model 2.8 for the Reynolds number dependence of C_0 [93]. We note that due to the time resolution in the $R_\lambda = 500$ data run, we encountered large uncertainties and were not able to measure a C_0 value from the xx component. We have therefore not included the $R_\lambda = 500$ data points in the fits of 2.8. (b) The ratio of the radial to the axial measurements of C_0 as a function of Reynolds number from both the structure function (●) and the spectrum (▼). While the anisotropy decreases weakly with increasing Reynolds number, the measurements remain far from isotropic even at the highest Reynolds numbers measured.

It is also intriguing to notice that in spite of the clear persistence of small scale anisotropy seen on the second moment of Lagrangian velocity increments, this anisotropy does not seem to significantly affect the second order moment of the Lagrangian position increments (*i.e.* the root mean separation investigated in the relative dispersion problem), for which the Btachelor superdiffusive law (which is established using a local isotropy hypothesis), fits almost perfectly the data. As the root mean separation between particles is directly related to the second moment of *Eulerian* velocity increments, this observation suggests that Lagrangian statistics may be more sensitive to small scale anisotropy than Eulerian's.

To summarize, this investigation shows that the local isotropy hypothesis, generally considered in models and simulations might be more controversial than usually believed. Large scale anisotropy appears to persist at small scales, even in the limit of large Reynolds numbers (approaching $R_\lambda \sim 10^3$). This reinforces the interrogation already pointed in the conclusions of the relative dispersion study, concerning the relevance (or at least of the real meaning) of the common expression "high Reynolds number limit". Is there such a limit for which Kolmogorov's original hypothesis would be satisfied ? The final chapter of this manuscript presents some ongoing studies and prospective projects aiming at pursuing the investigation of the influence of large scale properties of turbulent flows, which I hope may contribute further to this questioning.

Chapter 3

Turbulent transport of material particles

3.1 General context

Previous chapter was dedicate to the investigation of Lagrangian turbulence, that is of the dynamics of fluid tracers. In experiments these are materialized with neutrally buoyant particles significantly smaller than the dissipation kolmogorov scale of the flow η. In the present chapter I consider the dynamics of material particles which do not necessarily fulfill these conditions. Such particles, with density different than the fluid and/or size larger than η are expected to behave differently than fluid tracers and are generically called *inertial particles*. Several inertial effects have been known for long and can be interpreted qualitatively in terms of particle interaction with turbulent eddies. For instance the well known preferential concentration effect leading to the formation of clusters of inertial particles separated by depleted regions is generally interpreted as the centrifugal expulsion of denser particles from the turbulent eddies. However an accurate quantitative description of such effects is still lacking. One of the reasons is our inability to write a proper equation of motion for such particles in a turbulent environment. Actually, a rigorous analytical expression only exists in two limit situations : (i) for fluid tracers, whose equation of motion is directly related to Navier-Stokes equations and Lagrangian aspects of turbulence and (ii) for point particles, for which the BBOT (Basset-Boussinesq-Oseen-Tchen) equation - revisited in 1983 by Maxey & Riley [62] and Gatignol [39] - offers a suitable model. In the latter limit, forcing terms acting on the particle come from : (i) the local fluid acceleration ; (ii) the added mass ; (iii) the drag force ; (iv) a history term due to the interaction of the particle with its own wake ; (v) gravity, if present. As a first approximation the history term is generally neglected, so that in the absence of gravity the equation of motion can be written as :

$$\dot{\boldsymbol{v}} = \beta \frac{\mathrm{D}\boldsymbol{u}}{\mathrm{D}t} + \frac{1}{\tau_p}(\boldsymbol{u} - \boldsymbol{v}) \tag{3.1}$$

with $\beta = 3\rho_f/(\rho_f + 2\rho_p)$ and τ_p the viscous relaxation time of the particle, which quantifies its inertia. It is common to consider the dimensionless form of the relaxation time, namely the Stokes number of the particle $St = \tau_p/\tau_\eta$. In the crudest approximation, expected to be valid when $\beta St << 1$ only the drag term is conserved

$$\dot{\boldsymbol{v}} = \frac{1}{\tau_p}(\boldsymbol{u} - \boldsymbol{v}) \tag{3.2}$$

In a more general situation (finite size particles with arbitrary density), apart from some first order corrections to the BBOT equation (as Faxén corrections for instance [39, 24]), a valid equation for the turbulent motion of material particles remains to be found. This has motivated several recent experimental and numerical investigations on inertial particle acceleration statistics, which is a direct image of the turbulent forcing experienced by the particles and a key ingredient in any dynamical model for particles motion. One important question concerns the actual range of validity of the simplest usual *stokesian* model (given by eq. (3.1)), in terms of particle size and density.

The goal of the work presented in this chapter is to investigate several aspects of the dynamics of material particles in a turbulent flow. I have conducted these investigations at LEGI within the team EDT, which I joined in October 2004 as *chargé de recherches* at CNRS, and in collaborabtion with Christohpe Baudet, Alain Cartelier and Yves Gagne. Between 2006 and 2010, I had the opportunity to supervise the PhD of Nauman Qureshi and the postdoctoral project of Romain Monchaux, who have greatly contributed to the results presented here.

I have performed a systematic experimental investigation of the influence of size and density effects on the turbulent dynamics of freely advected particles. In a first step I have considered isolated particles where I have focused on the characterization of the turbulent forcing experienced by the particle. These aspects were part of the PhD of N. Qureshi. An important aspect of this work has focused on characterizing particles velocity and acceleration as a function of size and density. Comparison with predictions in the point particle limit is particularly enlightening in order to perceive the actual range of validity of this limit case, which is by far the most documented from theoretical studies and numerical simulations.

In a second step I have considered the multi-particle problem, with a particular focus on the preferential concentration phenomenon. These aspects were part of the postdoctoral project of R. Monchaux. One important aim of this study is the identification of collective effects, where the dynamics of multiple particles cannot be simply derived from isolated particles considerations as subtle coupling between the particles occur. Such collective effects have been identified by Aliseda *et al.* [2], but remains a theoretical challenge.

3.2 Turbulent dynamics of isolated particles

3.2.1 Inertial particle acceleration : a brief review

As already mentioned, much effort has been put recently in characterizing the acceleration of inertial particles. In experiments, particles are primarily characterized by their diameter D and density ρ_p. In the following I will consider the dimensionless size and density parameters : $\Phi = D/\eta$ and $\Gamma = \rho_p/\rho_f$, where η is the carrier flow dissipation scale and ρ_f is the carrier fluid density. In the point particle limit, particle inertia is generally parametrized by the so-called particle response time τ_p, which for a real particle in a smooth flow is given by the Stokes time $\tau_p = D^2(\rho_f + 2\rho_p)/(36\nu\rho_f)$ (the dimensionless Stokes number $St = \tau_p/\tau_\eta$ is commonly used). In this limit, particle response time therefore combines in a single parameter both the role of size and density. The response time characterizes particles inertia (*i.e.* its inability to rapidly adapt to the local flow), hence the usual denomination of *inertial particles*. However one should keep in mind that this denomination is *a priori* only justified for particles whose dynamics is indeed dominated by a Stokesian forcing term, as in eq. 3.1.

During the past decade the emergence of high resolution Lagrangian particle tracking techniques has allowed a detailed characterization of particle acceleration statistics. I have compiled in figure 3.1 particle classes, in the (Φ, Γ) parameter space, which have been recently investigated experimentally. It appears that most existing studies have considered either tracer particles ($\Phi << 1, \Gamma \simeq 1$) or particles much denser than the carrier fluid ($\Gamma >> 1$) but small ($\Phi << 1$), or particles over a wider range of sizes (including $\Phi > 1$) but with a moderate density ratio ($\Phi > 1, \Gamma < 4$).

In the case of tracers, highly intermittent Lagrangian dynamics (as presented in previous chapter) and highly non-Gaussian acceleration statistics (with high acceleration events occuring with a probability orders of magnitude higher than a Gaussian distribution with the same variance) have been reported [57, 65]. For inertial particles, numerical simulations in the point particle limit predict a reduction of these non-Gaussian statistical tails of acceleration probability density function (PDF) and a trend to become Gaussian as particle Stokes number is increased [10, 107]. The reduction of tails seems to be confirmed by recent experiments [5, 6] on water droplets in active grid generated turbulence, though only for particles with moderate Stokes number (red circles in figure 3.1). For real finite size

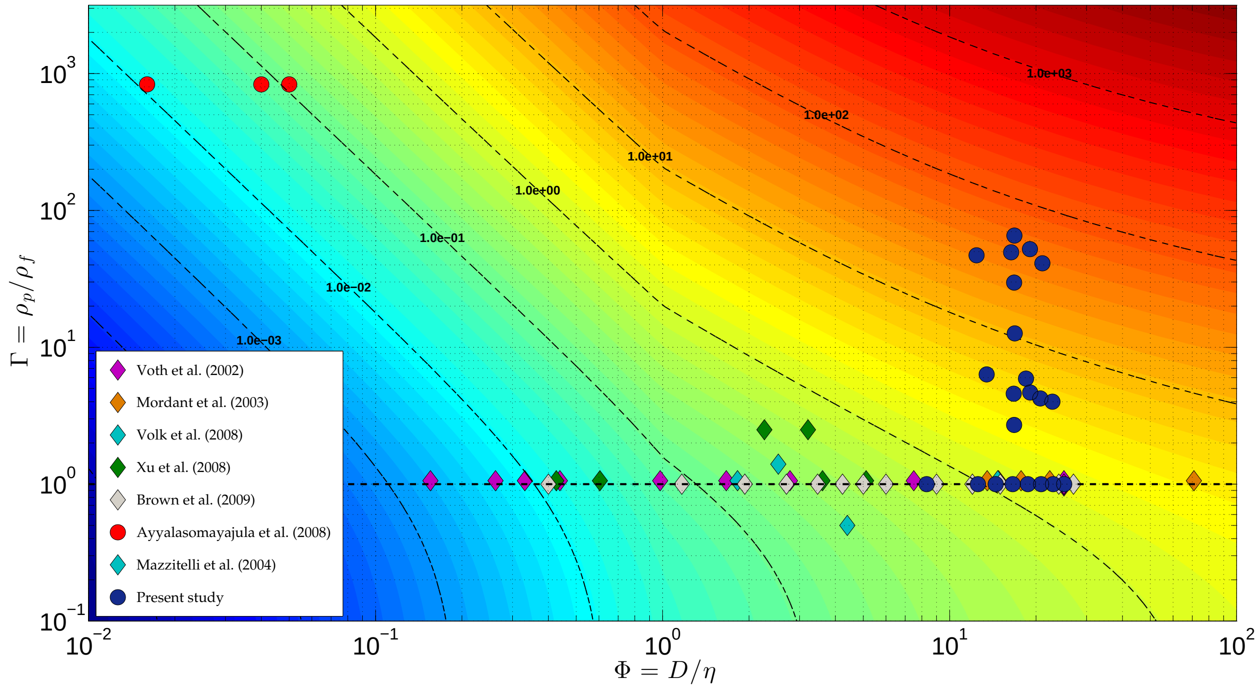

FIG. 3.1 – Particle size and density parameter space explored in previous experimental investigations of acceleration statistics. Present studies (blue circles) concern particles which are both large and dense. Background countours indicate the corresponding particle Stokes number.

particles (with $\Phi > 1$) experiments had mainly considered so far only the case of weakly inertial particles ($\Phi > 1, \Gamma < 4$). In this situation, no evidence of gaussianization of acceleration PDF with increasing Stokes number has been observed ; at most a reduction of acceleration flatness has been recently reported by R. Volk for neutrally buoyant particles with size crossing $\Phi > 1$ [106]. In all cases however, a trend of acceleration variance to decrease with increasing Stokes number has been reported.

In this work I present the first systematic Lagrangian measurements of particles which are both much larger than the dissipation scale of the carrier flow and significantly denser than the carrier flow (we cover the range $10 < \Phi < 30$ and $1 < \Gamma < 70$, corresponding to the blue circles in figure 3.1).

3.2.2 Experimental setup

Our experiment runs in a large wind tunnel with a measurement section of 75x75 cm downstream a grid (with a 7.5 cm mesh size) which reproduces almost ideal isotropic turbulence (figure 3.2). The mean velocity of the fluid is $U = 15$ ms^{-1} and the turbulence level is $u_{rms}/U \sim 3\%$. The corresponding Reynolds number, based on Taylor microscale, is of the order of $R_\lambda = 175$. The Kolmogorov dissipation scale (giving the typical size of the smallest turbulent eddies) is $\eta = (\nu^3/\epsilon)^{1/4} \sim 240$ μm (where $\nu = 1.5$ m^{2}s^{-1} is the air viscosity at working temperature and $\epsilon \sim 1.0$ m^{2}s^{-3} is the turbulent energy dissipation rate per unit mass) and the energy injection scale (giving the typical size of the largest eddies) is $L \sim 6$ cm.

In order to vary the size and density of the particles, I have used a versatile particle generator which produces *in situ* adjustable, spherical soap bubbles. The bubble generator was originally developed by C. Baudet to produce neutrally buoyant particles to seed a turbulent jet flow [41]. For the present study I have extended the range of accessible densities, and I have implemented precise measurements of the size and of the density of the generated particles. The density of the particles can now be adjusted from neutrally buoyant to about 70 times denser than air. Neutrally buoyant particles are obtained by inflating the bubbles with Helium in order to compensate the weight of the soap film. Heavier particles

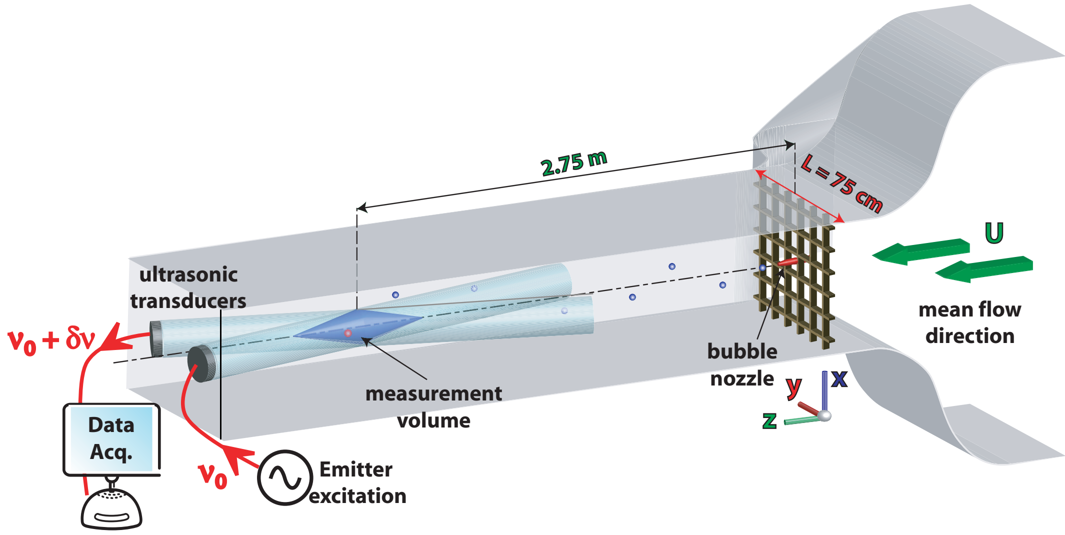

Fig. 3.2 – Turbulence is generated downstream a grid in a wind tunnel. The measurement volume is located 2.75 m downstream the grid, in a region where turbulence is fully developed, homogeneous and isotropic. Particles are injected individually at the grid with a bubble nozzle and tracked individually by Doppler velocimetry : an ultrasonic plane wave of frequency ν_0 is emitted by a transducer and a receiver records the wave scattered by a moving particle with velocity ν in the measurement volume (which is the intersection of the emitting and receiving acoustical beams, represented by the light colored tubes on the sketch) ; the component v_q of the particle velocity along the scattering vector is directly given by the Doppler shift $\delta\nu$ of the frequency of the recorded scattered wave. In the present experiment, transducers are arranged in order to measure the streamwise component v_z of particles velocity.

are inflated with air, and their density is essentially controlled by the thickness of the soap film. Bubble diameter can be adjusted independently. In all cases bubbles Weber number remains extremely small, so that they do not deform and behave as rigid spheres. The seeding density is extremely low (particles are injected individually) so that particles can be considered as isolated and do not backreact on the carrier flow.

Particles are individually tracked by 1D Lagrangian acoustic Doppler velocimetry [67, 85, 84] (see figure 3.2). With this technique the streamwise velocity component v_z of the particles is directly measured as they are tracked along their trajectory. Acceleration component a_z is obtained by differentiation of the velocity. I have performed these measurements with sell-type acoustic transducers previously used in the group by C. Baudet for spectral vorticity measurements and Lagrangian tracking of neutrally buoyant bubbles in a turbulent jet [82, 41]. I have improved the resolution and efficiency of the tracking as done in the jet experiment by implementing an iterative version of the maximum of likelihood tracking algorithm developed in N. Mordant's thesis [66].

3.2.3 Particle dynamics

In this section I present results on the Lagrangian dynamics of particles. The first subsection deals with single time velocity and acceleration statistics while the second one presents some results on two time statistics, with a main focus on Lagrangian intermittency and acceleration Lagrangian correlation.

Single time statistics

Figures 3.3a & b show typical velocity signals for large particles ($\Phi = 16.5$) either neutrally buoyant (figure 3.3a) or much heavier than the fluid (figure 3.3b). Interestingly, we observe that though individual trajectories appear to be smoother for heavier particles, the overall ensemble fluctuations cover essentially the same range for both, light and heavy, particles. More precisely, particle velocity statistics are found to have Gaussian fluctuations regardless of the size and the density, as shown in figure 3.4a,

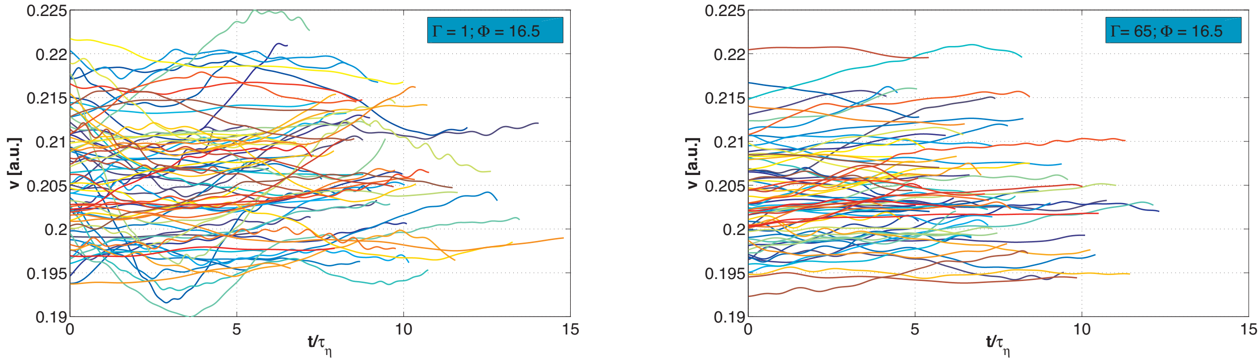

(a) (b)

FIG. 3.3 – *(a) Velocity signals for neutrally buoyant particles ($\Gamma = 1$) with size 16.5η. (b) Velocity signals for heavy particles ($\Gamma = 65$) with size 16.5η.*

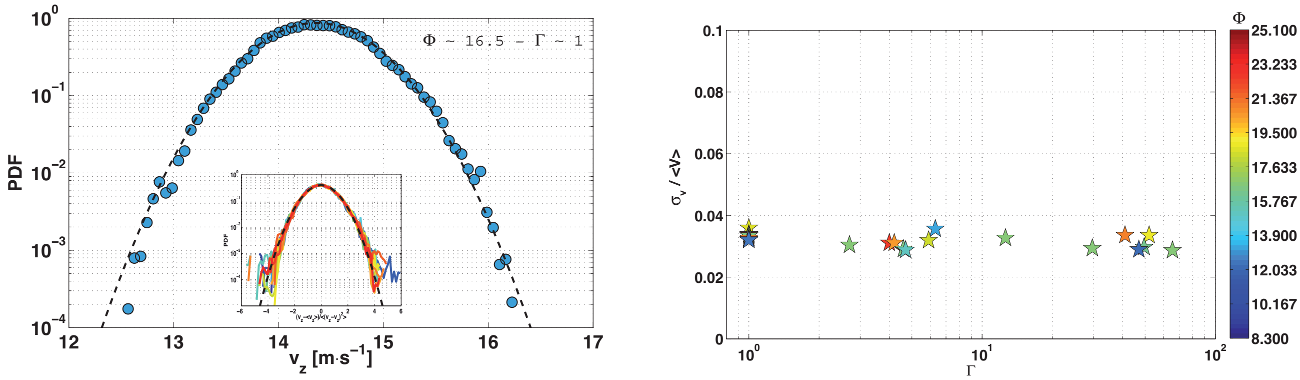

(a) (b)

FIG. 3.4 – *(a) Typical particle velocity probability distribution function. Inset shows the centered reduced velocity PDF for all particles class investigated. (b) Velocity flucutation rate as a function of particle density (color code indicates particle size).*

with a fluctuation level also independent of the size and the density. If we define the particle turbulent fluctuation rate as the ratio of the velocity standard deviation σ_v to the average velocity $< V >$ (which is identical to the mean streamwise velocity U of the carrier flow), this fluctuation level is indeed found to be independent of particle properties and does not present any trend either with particle size or with particle density (figure 3.4b). The corresponding fluctuation level, of the order of 3%, is identical to the turbulence level of the carrier flow itself measured from classical hot-wire Eulerian anemometry. While Eulerian and Lagrangian velocity fluctuations are indeed expected to coincide for tracer particles, this result is in contrast with predictions from inertial point particle stokesian models considering the drag force as a dominant one acting on the particle, where a monotonic decrease of velocity fluctuations is predicted as particle inertia increases. In these models, the predicted decrease of velocity variance is trivially expected as an inertial low pass filtering effect due to particles response time to turbulent solicitations. In the Tchen-Hinze approach [32] for instance, equation (3.1) is considered for the motion of the particles ; this equation is indeed a low pass filter with cut-off time scale τ_p acting on the carrier velocity $\vec{u}$ along particles track. Our observations clearly show that such a filtering does not occur, at least not trivially. As already mentioned, figures 3.3a & b show however that there is some kind of low-pass filtering associated to increasing inertia, as individual trajectories for heavier particles are indeed smoother than for lighter. However no filtering is observable for the overall velocity fluctuations over the global ensemble of particles. Filtering appears therefore to operate at a small scale level but not at large scales, and it does not affect velocity variance which mainly reflects large scale fluctuations.

This suggests that if there is any significant change in particles dynamics, it should better be looked for in the small scales rather than in the large scales fluctuations. A typical small scale quantity is the particle acceleration.

Figure 3.5a shows acceleration probability density functions for all the particle classes I have investigated. Note that in this plot PDFs have been normalized to variance unity. It is striking to observe that all such normalized PDFs collapse onto almost a single curve, indicating a very robust statistical signature of acceleration fluctuations which remain independent of particle size and density. This observation is again in contrast with predictions based on point particle models where the filtering Stokes number effect has been shown to induce a Gaussianization of acceleration PDF with increasing particle inertia. A clear influence of particle size and density can however be observed when PDFs are not normalized to unity variance. PDFs tend then to narrow and to peak as particle density increases. The evolution of acceleration PDFs is therefore entirely coded by acceleration variance only, while the global PDF shape remains unchanged when normalized to unity variance (this shape is well described by a lognormal distribution for the acceleration amplitude). Size and density effects on particles acceleration statistics can therefore be entirely characterized by the single investigation of acceleration variance $< a^2 >$. Figure 3.5b represents the evolution of $< a^2 >$ as a function of particle size and density. Several important features need to be stressed. For neutrally buoyant particles, a monotonic decrease of $< a^2 > \sim \Phi^{-2/3}$ is observed for particles larger than $\Phi \lesssim 12$ (smaller particles reach the fluid tracer limit). This trend has already been reported by Voth *et al.* [109]. I have shown that such a law can be derived by assuming pressure forces at particle size dominate the turbulent forcing onto the particle. Under an ergodic assumption, particles acceleration statistics can indeed then be related to Eulerian pressure increments statistics. In particular, by integrating in this context the pressure forces exerted by the carrier flow at the particles surface, the acceleration variance of a particle with diameter D can be related to the second moment of the pressure increments at the scale of the particle : $\left\langle a_z^2 \right\rangle_{\text{particle}}(D) \propto \frac{S_2^P(D)}{D^2}$,where $S_2^P(r) = \left\langle (p(\vec{x}+\vec{r}) - p(\vec{x}))^2 \right\rangle$, is the Eulerian second order pressure structure function (which only depends on $r = |\vec{r}|$ in homogeneous isotropic conditions). In the frame of Kolmogorov 41 phenomenology, the classical inertial scaling for $S_2^P(r)$ is $(\epsilon r)^{4/3}$ [71, 64] (or equivalently $\epsilon^{4/3} k^{-7/3}$ for the pressure spectrum). Although this scaling is still controversial [103, 45], there are experimental [40, 68] and numerical [103] evidences suggesting that it is most likely correct in ranges of Reynolds numbers and scales consistent with our flow and particle sizes. As a consequence, the acceleration variance of particles with diameter D in inertial range scales should follow the scaling :

$$\left\langle a_z^2 \right\rangle_{\text{particle}}(D) = a_0' \epsilon^{4/3} D^{-2/3}. \tag{3.3}$$

Though such a relation can be directly derived by simple dimensional considerations in the framework of Kolmogorov's inertial range hypotheses [64], I would like to stress here the dynamical correspondence with the pressure increments statistics. Recently, further experiments by G. Voth *et al.* [22] and pseudo-penalization numerical simulations with finite size resolved particles seem to confirm the idea of a leading pressure increment forcing at particle scale for finite size neutrally buoyant particles.

Concerning density effects, for a fixed particle size Φ, $< a^2 >$ is found to decrease monotically when particle density is increased and to reach a finite limit a_0^∞ for large density values. An interesting finding is the non trivial size dependence of a_0^∞ which is found to increase abruptly for increasing particle size around $\Phi \sim 18$. This counter-intuitive observation (it shows an increase of fluctuations with increasing particle size and therefore with increasing particle Stokes number) needs to be understood and will be discussed later.

Two time statistics

Previous single time statistics analysis has shown that large scales (as represented by velocity fluctuations) and small scales (as represented by acceleration fluctuations) are affected differently by particle inertia. As discussed in the previous chapter, in spite of its limitations the most classical way to investigate scale by scale turbulent dynamics is to consider velocity increments. Figure 3.6a presents PDFs of Lagrangian velocity increments ($\delta_\tau v(t) = v(t+\tau) - v(t)$) for one class of particle ($\Phi = 16.6, \Gamma = 1$).

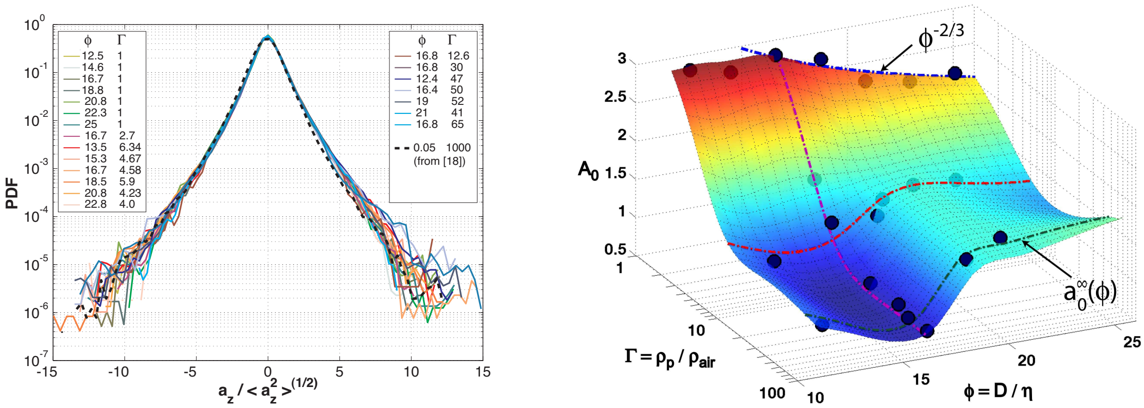

(a) (b)

FIG. 3.5 – *(a) Particle acceleration probability density function.* (b) Acceleration variance as a function of particle size and density ($< a^2 >$ is presented in the dimensionless form $A_0 =< a^2 > \epsilon^{-3/2}\nu^{1/2}$ - Heisenberg-Yaglom scaling).

We observe a continuous deformation from highly non-Gaussian fluctuations for small scale increments (which reflect acceleration) to Gaussian fluctuations at large scale increments (which reflect velocity itself). This evolution of increments statistics with is representative of the intermittent nature of particle Lagrangian dynamics. An interesting finding of the present work is that intermittency is observed for all the particles which have been investigated. However, the fine signature of this intermittent dynamics is found to depend on particle inertia. To illustrate this point, figure 3.6b presents the evolution of increment flatness $\mathcal{F}$ (which measures the extent of PDF tails) as a function of time scale τ for two different classes of particles with fixed size and increasing density. Within error bars, flatness is comparable for both at small sub-Kolmogorov scales (this only reflects the robustness of acceleration PDF shape, already discussed above) and at large scales (flatness tend to a value of 3, which corresponds to large scale Gaussian fluctuations, as previously shown for the velocity of the particles). However the evolution between small and large scales is strongly dependent on the particle class ; in particular for time scales near the dissipation time scale τ_η of the carrier flow. At such scales, a clear drop $\Delta\mathcal{F}$ of the flatness (corresponding to a sudden reduction of increments PDF tails) can be observed, with an increasing amplitude as particle density is increased. Subsequently to this drop flatness smoothly tends to its large scale Gaussian limit as larger time scales are considered. This indicates that the main deviations from fluid particle dynamics occur for time scales near τ_η, though inertial effects are usually expected to occur at a time scale related to the particle response time τ_p. Therefore, a natural question at this point is : what is the actual response time of the particle ? As already mentioned, usual estimations of τ_p are based on particle Stokes time. In the limit of vanishing particles Reynolds number it is given by $\tau_p = D^2(\rho_f + 2\rho_p)/(36\nu\rho_f)$. For finite particle Reynolds number, empirical corrections to this relation can be found in the litterature [28] (these corrections have been used to estimate the Stokes time in figure 3.8a for instance). In addition to this a priori estimation of τ_p, an experimental measurement of actual particle response time to the turbulent solicitations τ_p^{exp} can be obtained from the analysis of the particle acceleration Lagrangian correlation function R_a. Such a typical correlation function is shown in figure 3.7a. I define the experimental particle forcing time as $\tau_p^{exp} = \int_0^{t_0} R_a(t)dt$, where t_0 is the first zero crossing of R_a. Figure 3.7b shows the evolution of a priori estimated Stokes time τ_p (stars) and experimentally measured response time τ_p^{exp} (circles) as a function of particle size and density. It is striking to observe that, while the estimated τ_p is expected to vary over more than one order of magnitude among the different particles we have investigated, the actual measured response time does not exhibit any significant change with particle size and density and remains of the order of τ_η. Not only is the actual response time different to the estimated one, but also it appears to be determined mainly by the carrier flow itself and not to change significantly with particle properties.

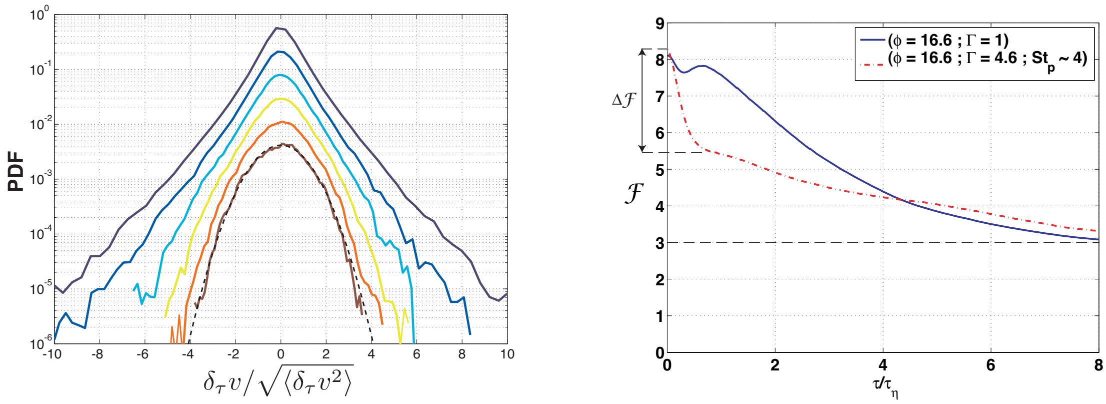

(a) (b)

FIG. 3.6 – *(a) Typical evolution of velocity Lagrangian increments. (b) Increment flatness coefficient as a function of time lag.*

3.2.4 Dicussion and conclusions

The results presented here on the investigation of finite sized inertial particles indicate that : (i) velocity statistics are not affected by particle inertia ; (ii) acceleration statistics have a very robust signature, where only acceleration variance is affected by inertia ; (iii) inertial particles always have intermittent dynamics ; (iv) intermittency signature depends on particle inertia ; (v) particle actual response time to turbulent forcing remains of the order of the carrier flow dissipation time rather than any particle dependent time (the Stokes time for instance). Most of these observations cannot be interpreted by a simple filtering effect (or Stokes number effect) as suggested by usual stokesian models in the limit of point particles. A first correction to this limit can be made by including in the point particle equation of motion the so called Faxèn corrections, which account for the local curvature of the unperturbed flow at particle position. In a recent numerical investigation in collaboration with R. Volk and E. Calzavarini at Laboratoire de Physique de l'École Normale Supérieure de Lyon [24] we have shown that including these corrections does improve qualitative trends of the stokesian model when compared to experiments for neutrally buoyant particles (the case of heavy particles has not been extensively investigated yet), in particular regarding the shape of acceleration statistics, the decrease of acceleration variance and the robustness of velocity fluctuation level. More recently, using pseudo-penalization method where finite size particles are fully resolved, Homann *et al.* [49] have shown that these corrections are relevant for particles with size up to $\Phi \sim 5$. For larger particles, their simulations show that pressure increments considerations robustly describe several observations, in particular the constance of velocity statistics and the robustness of acceleration statistics. Put together, my interpretation of these experimental and numerical results clearly show that departure from fluid tracer behavior for finite size neutrally buoyant particles has essentially nothing to do with inertia (*i.e.* it is not related to a simple Stokes number effect) : for particles with size close to dissipation scale it is simply related first to Faxén corrections (accounting at first orider for the non-uniformity of the flow around the particle) and then for larger particles it is dominated by the integrated pressure field around the particle. The impressive superposition of normalized acceleration PDFs of heavy particles compared to neutrally buoyant, in contrast with usual Stokesian models, suggests that the same dominant effects of pressure still prevail for particles much denser than the fluid. Such a dynamical forcing, mostly independent of particles properties is also consistent with the observed forcing time, which remains of the order of τ_η regardless of size and density. It should also be noted that for large particles other forces, as the lift, may become important. In a recent experiment carried out at the Laboratoire de Physique de l'École Normale Supérieure de Lyon in collaboration with R. Volk, J.-F. Pinton, A. Pumir and R. Zimmermann, we have for instance shown that the translational dynamics of large neutrally buoyant particles (with size smaller but comparable to the integral scale of the flow) is coupled to its rotational dynamics via lift force (Magnus effect). The importance of this term in the overall equation of motion of the particle remains to be quantified).

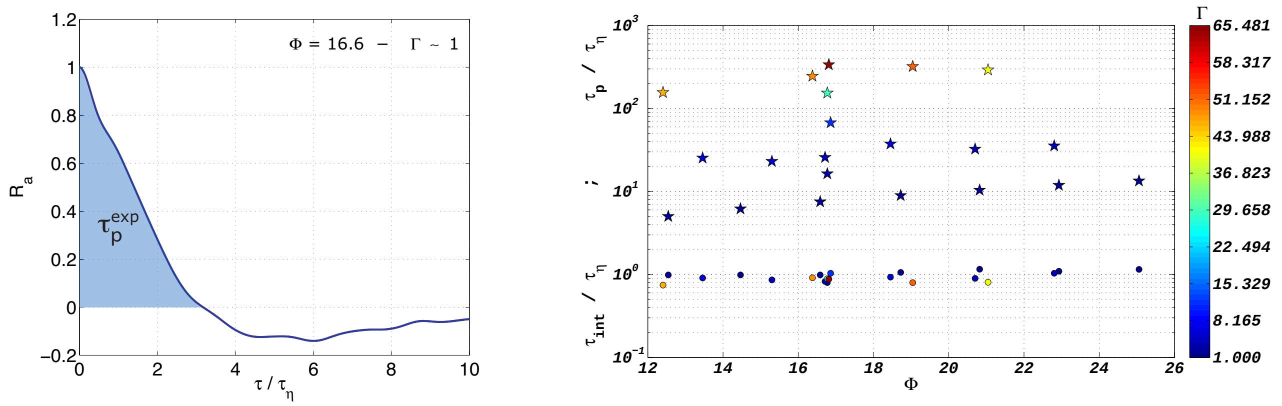

(a) (b)

FIG. 3.7 – *(a) Typical acceleration correlation function R_a and definition of the experimental particle response time τ_p^{exp}. (b) A priori estimated Stokes time τ_p (stars) and experimentally measured particle time τ_p^{exp} (circles) as a function of particle size (color codes particles density).*

The simple filtering effect predicted by usual models, seems therefore inadequate for finite size inertial particles. *I believe that* the observations reported here can be better understood in terms of a sampling effect, related to the preferential sampling by the particle of certain turbulent structures in the carrier flow, rather than a filtering response time effect. Such preferential sampling is expected due to trend of inertial particles to cluster in the quietest regions of the flow. In such a scenario, we expect inertia (Stokes number effects) to play an important role for creating the preferential sampling, but the turbulent dynamics of the particles then mainly reflects the preferentially sampled turbulent conditions. As possible sampling mechanisms, we can mention the centrifugal preferential concentration effect [61] (where inertial particles are ejected from turbulent eddies and concentrate in low vorticity regions) and the stick-sweep mechanisms [29] (where particles tend to stick to zero-acceleration points of the carrier flow). According to numerical simulations, it is likely that the first mechanism dominates for weakly inertial particles ($St < 1$) and the second for highly inertial particles [29]. Such a scenario would exhibit several features shared with our observations :

(i) Numerical simulations of stick-sweep mechanisms [44] show that inertial particles tend to cluster near low acceleration points of the carrier flow. Though these simulations were carried with a simple Stokesian dynamics for the particles, they show that inertial mechanisms do generate a preferential sampling with lower acceleration fluctuations, consistent with the decrease of acceleration variance we measured for increasing particle density. A detailed investigation of acceleration PDFs in the context of the stick-sweep mechanism is however still lacking for finite size particles. This is work in progress.

(ii) Velocity statistics of such zero-acceleration points have been shown to be identical to the overall velocity statistics of the carrier flow. This is consistent with our observation of particle *rms* velocity which is found to remain independent of particles size and density ;

(iii) Such a sampling scenario is expected to be efficient only if particles can *hide* efficiently in the quiet regions of the flow. Though, when particles become too large (larger than the typical size of these quiet regions), an increase of fluctuations is expected as particles experience again the influence of more active surrounding structures. On top of this purely steric effect it has also been observed that particle preferential sampling efficiency decreases for very inertial particles (preferential sampling is known to be maximun for particles with Stokes number of order unity, this will be further discussed in the next section). These effects would explain the increase of $< a_0^\infty >$ observed for particles with increasing size at constant density. However, what fixes the critical scale for which this increase appears ($\Phi > 18$) remains unknown. It may be related for instance to a typical size of zero-acceleration clusters (though the existence of such a scale remains controversial).

Of course several other points still need to be investigated further. Important questions remain. What fixes the shape of acceleration PDFs (our results suggest that this may require a closer investigation of pressure statistics in the carrier flow) ? What fixes the limit $< a_0^\infty >$ for acceleration variance at high density ratios ? Why is the particle forcing time so weakly affected by particle properties ? And finally, what adequate equation of motion is needed to model the dynamics of finite sized particles ?

3.3 Collective dynamics of particles in turbulent flow

3.3.1 Introduction

In this section we consider no more the case of an isolated particle, but on the contrary the situtation where many particles are simultaneously investigated. This investigation has been done in collaboration with A. Cartellier and R. Monchaux (during his postdoctoral project at LEGI). A striking feature observed in such situation, is the trend to preferential concentration, which has been reported for long [96, 34] and which is still thoroughly studied [92, 91, 95, 73]. This phenomenon has a fundamental and practical interest *per se* and is also possibly relevant for a better understanding of the sampling scenario discussed in the context of isolated particles dynamics in the previous section. Another related feature is the enhancement of the settling velocity of particles which has been surprisingly measured to depend on particle seeding density by Aliseda *et al.* [2]. Since an explanation of this phenomenon through collective effects related to particles clustering has been proposed by Aliseda *et al.*, different authors have tried to quantify and characterize particles clustering from numerical simulations. However, as emphasized in previous section, since an appropriate equation of motion for an accurate modeling of particle dynamics is still lacking experimental investigations are still important to reach a better understanding of the underlying mechanisms of preferential concentration and collective effects.

In the present section, I address the question of particle preferential concentration and clustering, including possible collective effects. Do clusters exist as a whole in turbulent flows ? What is their structure and how does this structure evolve with time ? Which effect do they have on the single particle dynamics ? Here are some of the questions that still need to be answered. To date, the preferential concentration/clustering problem has been studied with global or Eulerian tools (such as box counting methods, pair correlation function estimation, correlation dimension or topological indicators). A dynamical study of the Lagrangian dynamics –of particles and of the local concentration field– would bring new insight in these processes. In particular, it would be worthwhile to get access to the concentration along a particle trajectory, a quantity which has been recognized as very important in models [87, 52].

In that scope, during the postdoctoral work of R. Monchaux at LEGI, we have proposed a new approach to analyze particle concentration fields based on Voronoï tesselations which give a measure of the local concentration field at inter-particles length scale. By itself, this data processing technique is particularly enlightening to explore and quantify the preferential concentration phenomenon while, combined to Lagrangian tracking, it also gives access to simultaneous measurements of velocity, acceleration and local concentration along particles trajectories which are crucial for a better insight of clusters and particles dynamics. As a first step, the focus was put on the preferential concentration problem on a statistical ground. In section 3.3.2 below I briefly describe the experimental setup and the Voronoï approach used to post-process the data. In section 3.3.3 I show the results from the Voronoï analysis used to quantify the preferential concentration and to identify and characterize clusters.

3.3.2 Experimental setup

Two phases flow generation and characterization

Experiments are conducted in the same wind tunnel as previous section. As inertial particles we use water droplets generated by four injectors placed in the convergent part of the wind tunnel, one meter upstream the grid to ensure a homogeneous seeding of the flow. These injectors consist of two tubes carrying water and air that merge into a specifically designed nozzle (a Schlick-D sen 942 two fluids

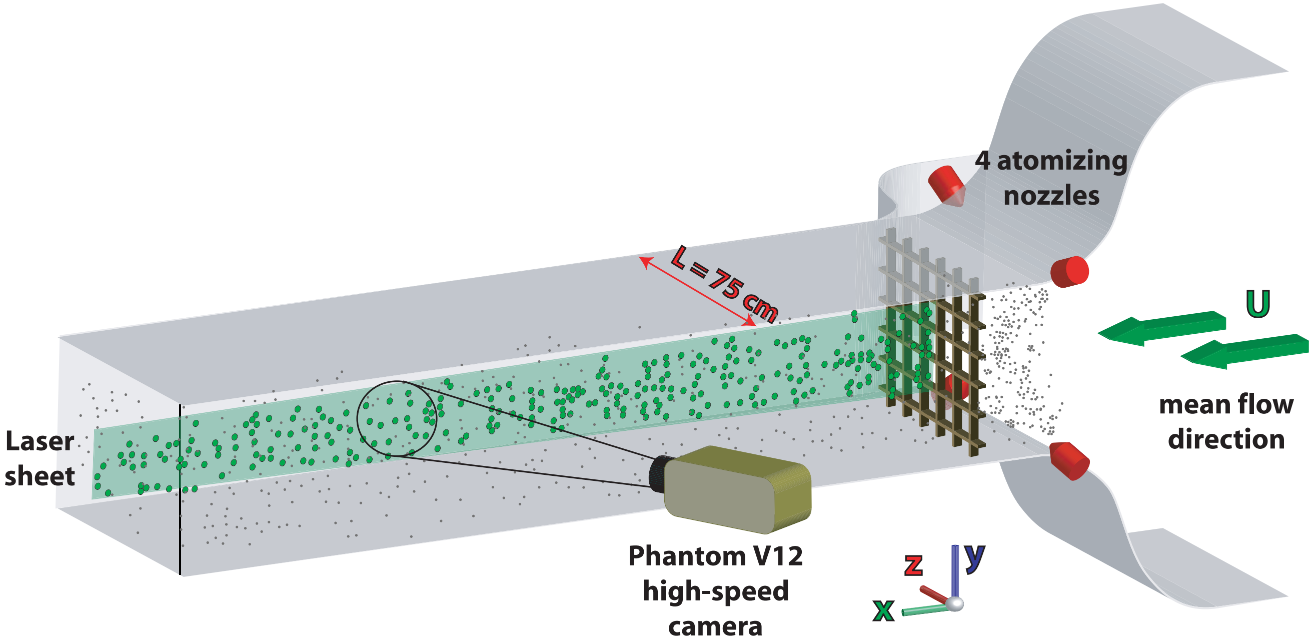

FIG. 3.8 – Experimental setup

x (cm)	V_0 (m.s^{-1})	ϵ (m^2.s^{-3}	L (mm)	λ (mm)	η (mm)	τ_η (ms)	v_η (cm.s^{-1})	R_λ
290	2.92	0.0084	61.4	12	0.79	42	1.90	72
290	4.51	0.0309	61.4	9.7	0.57	22	2.59	90
290	6.33	0.0854	61.4	8.2	0.45	13.3	3.38	114

TAB. 3.1 – Evolution of the turbulence characteristics for the single phase flow for three different velocities at our measurement volume location. x : distance downstream the grid, V_0 : mean longitudinal velocity, ϵ : dissipation rate, L, λ, η : integral, Taylor and Kolmogorov length scales, τ_η, v_η : Kolmogorov time and velocity scales, last column displays the Taylor scale based Reynolds number.

nozzle) where pressurized air atomizes the liquid and forms the exiting conic jet. Particles properties relevant to our study can be adjusted within accessible range : volume loading is directly linked to the water flow rate in the nozzles while the diameter distribution is a subtle function of both water flow rate and air pressure in the nozzles, as detailed below. We always consider regimes of relatively low particles volume loading (volume fraction in our experiments covers the range $2.10^{-6} < \phi_v < 3.10^{-5}$) so that no turbulence modulation by two-way coupling is expected to occur.

Regarding the droplets spray, one of the main goals of this study is to explore the influence of particle diameters d (or equivalently of their Stokes number) on the preferential concentration phenomenon. The two phases nozzles used to produce the spray present the advantage to easily allow a systematic variation of the mean diameter of droplets by controlling air and water flow rates in the injectors. The drawback of this versatility is the difficulty to produce a monodisperse spray. The injection process leads indeed to a polydisperse seeding of the flow for which particles diameter distribution has to be estimated. This has been done using the SprayTech instrument developed by Malvern Inc. and based on the diffusion of a laser beam by the spray. Due to the size of the SprayTech apparatus, these granulometry characterizations cannot be done simultaneously with other measurements ; therefore they have been performed once for the entire set of experimental parameters and in the same measurement volume as the main measurements. Figure 3.9a shows typical particles size distributions. Main control parameters

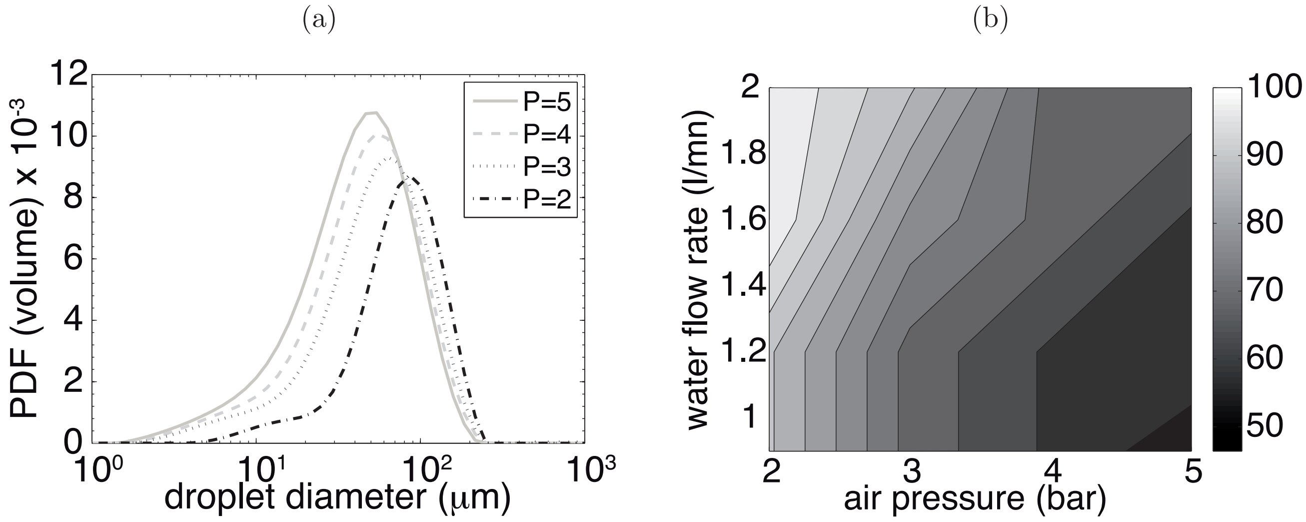

Fig. 3.9 – (a) Particles diameter Probability Density Function evolution with air pressure (varying from 2 to 5 bars) at fixed water flow rate (1.2 l/mn for each injector) and fixed wind velocity ($V_0 = 4.5$ m.s^{-1}) ; note that PDFs are given from particles volume (and not particles number). (b) Evolution of the maximum of these PDF with water flow rate and air pressure at the same fixed velocity ($V_0 = 4.5$ m.s^{-1}).

governing the diameter distributions are : the air pressure and the water flow rate in the injectors as well as the wind velocity in the tunnel. Once particles diameter distributions are obtained for a given set of injection parameters, we can define a corresponding most probable Stokes number defined as $St = (d_{\max}/\eta)^2(1 + 2\Gamma)/36$, where $d_{\max}$ corresponds to the maximum of diameters distribution (see figure 3.9a). Figure 3.9b represents the evolution of $d_{\max}$ as a function of air pressure and water flow rate in the nozzles for a given carrier flow Reynolds number. I would like to stress that because of the high polydispersity the standard deviation σ_{St} of Stokes number (based on measured diameters distribution), which could be interpreted as an error-bar for the Stokes number estimation, is large (σ_{St}/St easily exceeds 50%) and will not be displayed on the figures presented in the sequel.

To summarize, each experiment is characterized by the set of parameters (R_λ, St, C_0) with R_λ the carrier flow Reynolds number (based on Taylor microscale), St the average Stokes number obtained as described above, C_0 the global seeding density (which we cannot accurately measure, but which we assume to be directly related to the number of particles per image). Another usual relevant parameter is the Rouse number (defined as the ratio of the terminal velocity of the particles to the turbulent fluctuations intensity) which in our experiments varies in a relatively narrow range from 0.4 to 2. A total of 90 experiments covering a set of about 40 different parameter triplets (R_λ, St, C_0) have been explored in order to investigate systematic effects on preferential concentration phenomenon. Here I will mainly focus on the influence of St and C_0.

Acquisitions

Acquisitions are performed using a Phantom V12 high speed camera operated at 10 kHz and acquiring 12bits images at a resolution of 1280 pixels × 488 pixels corresponding to a 125 mm (along x)× 45 mm (along y) visualization window on the axis of the wind tunnel (covering slightly less than an integral scale in the vertical y direction and almost two integral scales in the streamwise x direction), located 2.95 m downstream the grid. The camera is mounted with a 105 mm macro Nikon lens opening at $f/D = 2.8$. An 8 W pulsed copper Laser synchronized with the camera is used to generate a 2 mm (*i.e.* 3-4η) thick light sheet illuminating the field of view in the stream-wise direction. The camera is orientated with a 50° forward scattering observation angle with respect to the laser sheet to increase the light budget. The resulting deformations are compensated by a Scheimpflug mount. Each experiment consists in a 0.9 s acquisition of 9000 images (corresponding to the available on board memory storage of the camera) at fixed wind velocity, water rate and air pressure in the injectors. Particles are identified on the recorded images as local maxima with intensity higher than a prescribed threshold. As a consistency test, we have checked that changing the threshold around the selected value does not impact significantly the number of particles found. Sub-pixel accuracy detection is obtained by locating the particles at the center of mass of the pixels surrounding the local maxima.

Post-processing : a new Voronoï analysis method

As already mentionned, the goal here is to study particles concentration fields in order to quantify preferential concentration effects and to identify particles clusters if any. Usual approaches to do this consider the pair correlation function to quantify preferential concentration effects while a box counting method is preferred to access local concentration fields. In the present study we propose to use a single tool to tackle simultaneously these two problems : the Voronoï diagrams. Such a Voronoï diagram is the unique decomposition of 2D space into independent cells associated to each particle. One Voronoï cell is defined as the ensemble of points that are closer to a particle than to any other. Use of Voronoï diagrams is very classical to study granular systems and has also been used to identify galaxies clusters. Voronoï diagrams computation is very efficient with the typical number of particles per image (up to several thousands) we have to process. Figures 3.10a&b show a raw acquired image as well as the located particles and the associated Voronoï diagram.

Why using Voronoï tessellations ? From the definition of the Voronoï diagrams, it appears that the area A of a Voronoï cell is the inverse of the local 2D-concentration of particles ; therefore the investigation of Voronoï areas field is strictly equivalent to that of local concentration field. Let me recall that usually local concentration fields are obtained through box counting methods [2] which show several disadvantages : they are computationally inefficient and they require to select an arbitrary length scale (the box size), whereas in Voronoï diagrams computation, no length scale is *a priori* chosen and the resulting local concentration field is obtained at an intrinsic resolution. Similarly, the pair correlation function only gives global (non local) information and is also associated to the choice of a length scale that spans the whole values of interest increasing dreadfully the computation time. Finally, another interest of Voronoï diagrams is that as each individual cell is associated to a given particle at each time step, thus tracking in a Lagrangian frame the particles directly gives access to the Lagrangian dynamics of the concentration field itself along particles trajectories. Though I will not discuss here such Lagrangian aspects, they represent an important opening which will be addressed in forthcoming studies.

Some relevant properties of Voronoï diagrams. Whatever the measurement and data analysis technique used, when one refers to preferential concentration, it is implicitly assumed that one deals with statistical preferential concentration compared to the case where particles would be spatially distributed as a random Poisson process (RPP). In order to quantify preferential concentration, the Probability Density Function (PDF) of the measured Voronoï areas for each experiment is compared to that expected for a RPP. Main known properties of Voronoï diagrams associated to RPP can be found in a short review by Ferenc and collaborators [33] and references herein. The first moment of Voronoï areas PDF has nothing to do with the spatial organization of the particles since the average Voronoï area, $\overline{A}$, is always identical to the mean particles concentration. Therefore, in the sequel I will generally focus on the distribution of the normalized Voronoï area $\mathcal{V} = A/\overline{A}$ which is of unit mean. The only known exact result for RPP Voronoï areas statistics concerns the second order moment in the 2D case which is equal to $< \mathcal{V}^2 >_{\mathrm{RPP}} = 1.280$, corresponding to a standard deviation $\sigma_{\mathcal{V}}^{\mathrm{RPP}} = \sqrt{< \mathcal{V}^2 >_{\mathrm{RPP}} - 1} \simeq 0.53$. Regarding the shape of the PDF of Voronoï areas statistics for a RPP, no analytical solution is known (most of the authors fit them with Gamma distributions). Ferenc and collaborators propose a compact analytical expression involving the space dimension as a single parameter : this analytical expression is used here as a RPP reference.

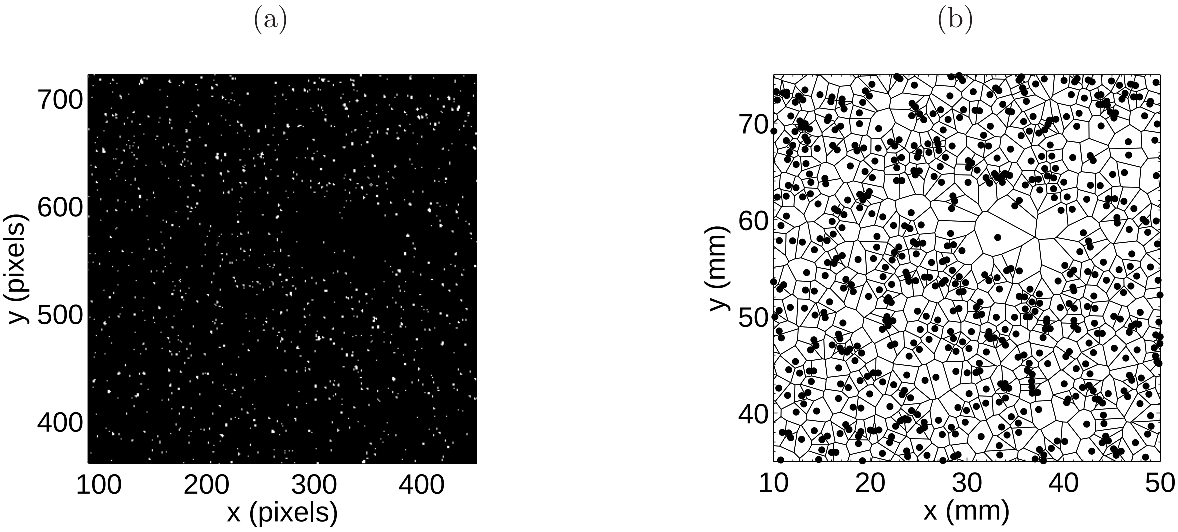

FIG. 3.10 – (a) A typical raw image. (b) Particles located in this image and the associated Voronoï diagram. For clarity, we show only one third of the full acquired image.

3.3.3 Preferential concentration evidence and quantification

Experimental Voronoï areas distributions. Figure 3.11a displays the PDFs of the dimensional Voronoï cells area, A, for 40 different experiments. When the dimensional area A is considered, one observes that the maximum of these PDFs spans over two decades. This evolution is representative of the average number of particles per image (or equivalently of the global seeding concentration C_0) which for the ensemble of experiments represented goes from 50 to 5000. Note that as the average number of particles per image decreases (*i.e.* as the mean Voronoï area increases), the scatter of the right tail on these PDFs increases as a consequence of the lesser statistical convergence. As shown in figure 3.11b, all these PDFs collapse reasonably if we consider the centered-reduced PDF of the logarithm of normalized Voronoï areas. This indicates that while Voronoï area PDFs of RPP are usually described by Gamma distributions [33] they are well described by a log-normal distribution for the investigated inertial. As seen on the figure, superimposition with a log-normal distribution is almost perfect in the interval $\pm 2\sigma_{\log(\mathcal{V})}$, where $\sigma_{\log(\mathcal{V})}$ stands for the standard deviation of $\log(\mathcal{V})$ (note that extreme PDF tails for statistics of the logarithm of $\mathcal{V}$ are beyond experimentally accessible statistical convergence). To date we do not have any theoretical interpretation of this log-normality, but this result shows that in the limit of experimental convergence, normalized Voronoï areas PDFs can be described with one single scalar quantity which we choose here to be the standard deviation of the normalized Voronoï areas $\sigma_{\mathcal{V}}$.

Quantifying preferential concentration. It is generally assumed that preferential concentration is primarily governed by particles Stokes number. Most former numerical and experimental studies have evidenced that preferential concentration effects are more significant as the Stokes number approaches unity. In figures 3.11c we present the evolution of normalized Voronoï areas standard deviation $\sigma_{\mathcal{V}}$ as a function of Stokes number in our experiments. As mentioned earlier, the standard deviation of Voronoï areas for a RPP is analytically known to be $\sigma_{\mathcal{V}}^{\mathrm{RPP}} \simeq 0.53$ which defines a reference value to compare with. A standard deviation $\sigma_{\mathcal{V}}$ significantly exceeding 0.53, reveals the existence of high and low concentration events compared to the RPP case. Oppositely, a standard deviation $\sigma_{\mathcal{V}}$ below this reference value would evidence the tendency of particles to distribute in a more organized arrangement ($\sigma_{\mathcal{V}} = 0$ in the limit of a perfect crystal). As seen on figures 3.11c, for the range of explored Stokes numbers (spanning from 0.2 to almost 6) the standard deviation of the normalized Voronoï areas always exceeds 0.57 and reaches values as high as 0.85, what shows that preferential concentration is always present over this range of Stokes numbers, consistently with former experimental and numerical investigations. Furthermore, both figures peak around $St_{\mathrm{pk}} \simeq 2-3$ which is consistent with the generally assumed feature that preferential concentration is maximal for Stokes number around unity,

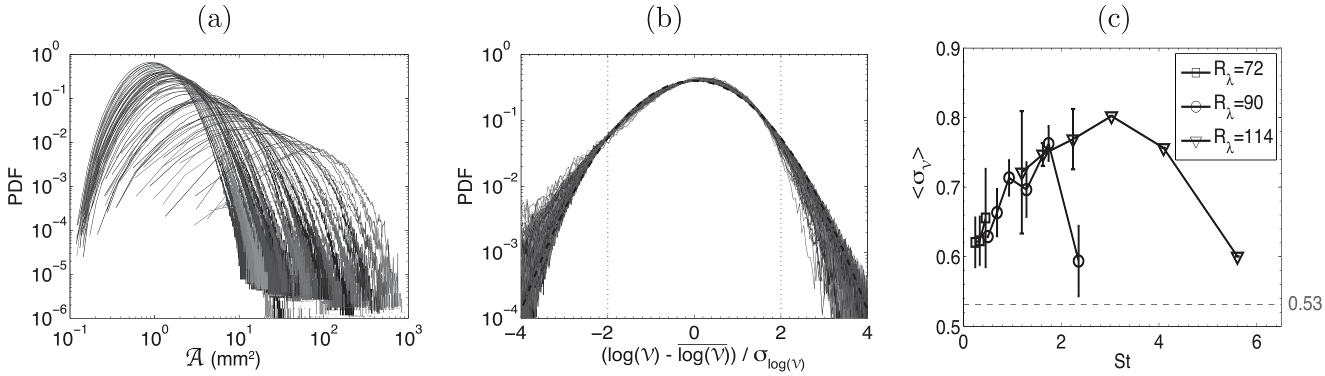

FIG. 3.11 – (a) PDF of dimensional Voronoï area $\mathcal{A}$ for 40 experiments spanning all R_λ, St and volume loading explored. (b) Centered and normalized PDF of the logarithm of Voronoï area for the 40 experiments from upper figure ; black dashed line represents a gaussian distribution. (c) Standard deviation of Voronoï areas as a function of average Stokes number. Lines connect different experiments for which Reynolds number (Error-bars represent the dispersion between experiments with different C_0).

corresponding to a better adjustment of particles response time to turbulence forcing time. In order to compare our Voronoï analysis with usual tools, we have also performed box counting and correlation dimension analysis (not shown) which are consistently found to give a maximum effect of preferential concentration also for $St_{\text{pk}} \simeq 2 - 3$. Figure 3.11c also suggests a possible Reynolds number effect as the curve for $R_\lambda = 90$ seems more peaked than curve at $R_\lambda = 114$ and appears to reach its maximum for a slightly lower value of St_{pk}. However, one can hardly be conclusive on such a Reynolds number effect as it is mainly supported by only one point on the $R_\lambda = 90$ curve (point $St = 2.2\,; \sigma_\mathcal{V} = 0.6$ in figure 3.11c) which furhtermore presents relatively large statistical error-bars ; the possible specific influence of Reynolds number on preferential concentration is being addressed more deeply in ongoing investigations, taking advantage of the active grid I have recently implemented in the wind-tunnel at LEGI.

Finally, it is also important to note that since our experiments cover a wide range of particles seeding concentrations, it is necessary to avoid any possible statistical bias on $\sigma_\mathcal{V}$ depending on the number of particles per image which are processed. Only then $\sigma_\mathcal{V}$ can be considered to be an actual quantitative indicator of preferential concentration. For instance experiments with large particles (large Stokes numbers in figures 3.11c) generally have less particles per image (typically less than 1000 ppi) than experiments with smaller particles (which typically have $3000 - 4000$ ppi). To test such a possible bias we have estimated $\sigma_\mathcal{V}$ from a set of originally highly loaded images from which we randomly removed particles. The estimation of $\sigma_\mathcal{V}$ appears to be very robust and not biased by this subsampling procedure as it is only reduced by less than 1.5% when up to 80% of the particles are randomly removed from the images.

As a partial conclusion, I emphasize that Voronoï analysis allows to robustly quantify preferential concentration with a single scalar quantity (the standard deviation of normalized Voronoï areas) which is easily accessible and efficiently computed. This analysis confirms the trend of inertial particles to preferentially concentrate with a maximal effect for particles with Stokes number of order unity. However, we note that Voronoï areas PDF on their own do not contain any information concerning the spatial structure of particles concentration field which is a key point for the study of clustering and of its dynamics. In the next section I show how Voronoï areas distributions can nevertheless be used to analyze concentration fields structure and dynamics.

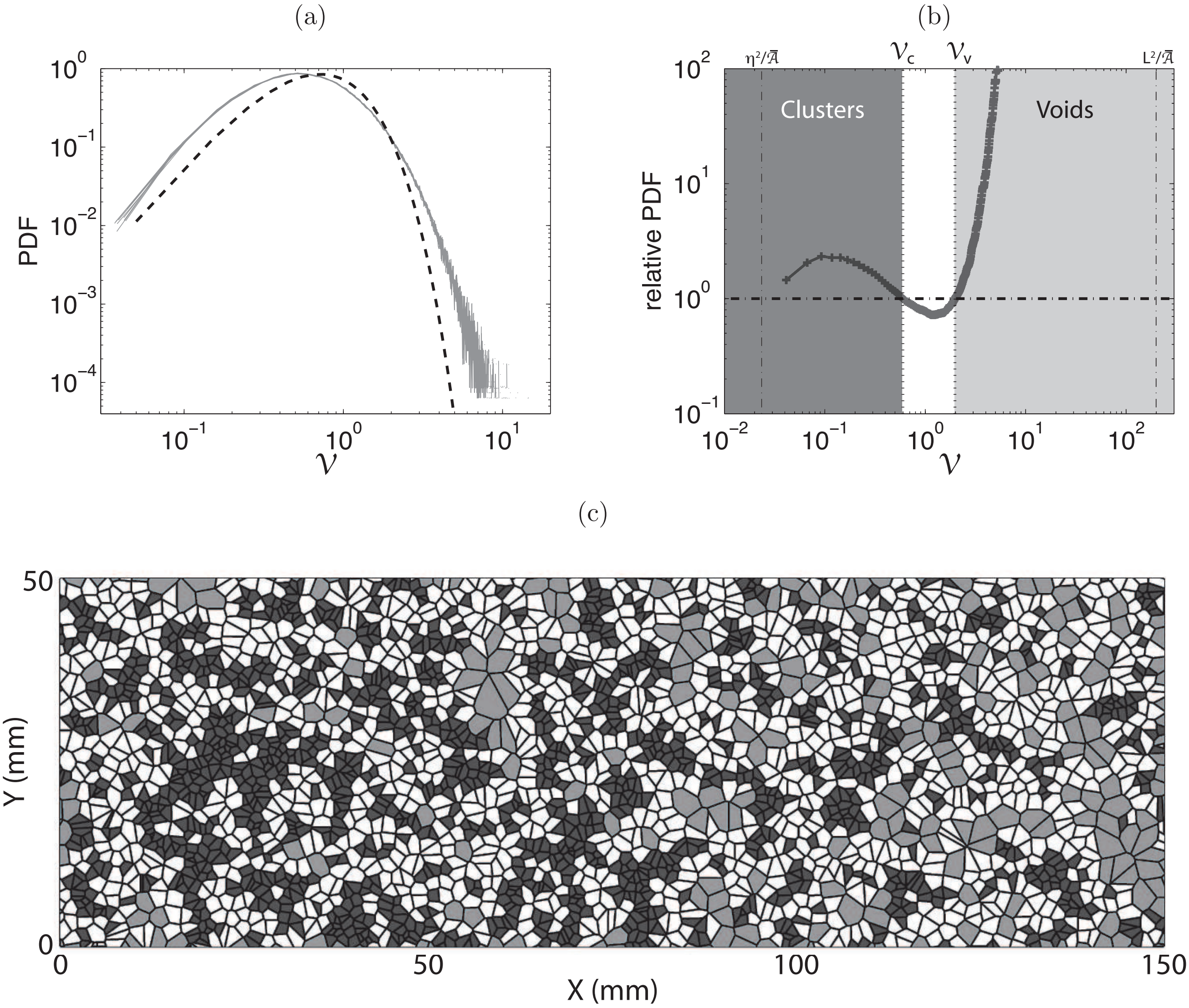

FIG. 3.12 – A way to identify clusters : (a) Superposition of the Voronoï areas PDF for a typical experiment ($R_\lambda = 85$, $St = 0.33$, $C_0 = 500$ particles per image) ; 10 continuous lines associated to ten sets of 500 UIVD are represented (dispersion is negligible) and a RPP (dotted line) ; (b) ratio of the two PDF presented on the left figure. Vertical dash-dotted lines indicates η^2 (left) and L^2 (right). (c) colored visualization of clusters (dark grey) and voids (light gray).

Toward clusters identification and characterization from Voronoï analysis

Voronoï areas PDF may be used to identify clusters of particles as follows. Consider figure 3.12a which presents the Voronoï PDF for a typical experiment and for a RPP. These PDFs intersect twice (which is more visible on figure 3.12b showing the ratio of both PDFs) : for low and high values of normalized Voronoï area, corresponding respectively to high and low values of the local concentration, experimental PDF is above the RPP one, while we observe the opposite for intermediate area values. This is consistent with the intuitive image of preferential concentration : inertial particles concentration field is more intermittent than the RPP, with more probable *preferred* regions where concentration is higher than the Poisson case and subsequently also more probable *depleted* regions where concentration is lower than in the Poisson case. These intersection points $\mathcal{V}_c$ and $\mathcal{V}_v$ can be taken as an intrinsic definition of particle *clusters* and *voids* : for a given experiment, Voronoï cells whose area is smaller than the first intersection $\mathcal{V}_c$ are considered to belong to a cluster while those whose area is larger than the second intersection $\mathcal{V}_v$ are associated to voids. I insist on the fact that these thresholds are intrinsically chosen experiment wise and so vary from one experiment to another ; in particular their value depends on the number of particles per image and their evolution with the seeding concentration C_0 is find to be affine. Figure 3.12c displays a full Voronoï diagram corresponding to one image taken from one experiment. On this diagram, cells corresponding to clusters (*resp.* to voids) have been colored in dark gray (*resp.* light gray) while the remaining cells have been patched with white. It appears that dark gray cells (*resp.* light gray cells) tend to be connected in groups of various sizes and shapes that are identifed as clusters (*resp.* voids) whenever they belong to the same connected component.

Clusters geometry. Let analyze now the geometrical structure of the identified clusters and voids. Their area and perimeter are computed from the area and perimeter of the constitutive Voronoï cells. Figure 3.13a presents the distributions of the clusters area $\mathcal{A}_c$ and figure 3.13b shows the scatter plot of their perimeter $\mathcal{P}_c$ versus $\mathcal{A}_c^{1/2}$. This last figure shows that for small and compact clusters, $\mathcal{P}_c$ and $\mathcal{A}_c^{1/2}$ are almost linearly related while large structures exhibit a fractal behavior as also reported in previous experimental and numerical studies (see Aliseda *et al.* [2] and references herein). As shown in figure 3.13a, clusters areas $\mathcal{A}_c$ are found to be algebraically distributed with an exponent -2 which is found to be independent of both R_λ and St within measurements accuracy (see inset). This interesting observation implies that clusters do not have a typical size (not even an average). This result is in contrast with the previous study by Aliseda *et al.* [2] who fitted clusters area distributions (measured from a box counting method) with a decaying exponential from which they could estimate a typical cluster size. However this estimation is questionable as the clusters area distributions they report are not clearly exponential and generally defined on so few points that an algebraic behavior cannot be ruled out. The same geometrical analysis has been performed for the empty regions (not shown) which are found to exhibit very similar trends than for clusters : large depleted regions have a fractal structure and their areas are algebraically distributed with an exponent close to -1.8. This last result is in agreement with recent direct numerical simulations [113] where void regions between inertial particles have been analyzed.

Clusters inner concentration. Let consider now the concentration within the clusters formerly identified. We define C, the mean concentration inside a cluster, as the inverse of the mean Voronoï area within this cluster and C_0 as the average particles concentration in the whole images during one experiment (C_0 is the average number of particles per image divided by the area of the whole visualization domain). Figure 3.14a presents the PDF of C/C_0 for 9 typical experiments spanning our control parameters space. Though these PDF are poorly converged due to an evident lack of statistics (each identified cluster counts as one statistical sample) they are still well described, at first order, by a gaussian distribution. Their means $< C/C_0 >$ define the averaged normalized concentrations within clusters for each experiment ; it measures the average relative overloading of particles inside clusters. In our experiments, mean concentration in clusters is generally found to exceed twice the global seeding concentration and it can reach up to eight times the latter depending on experimental conditions (see figures 3.14b&c).

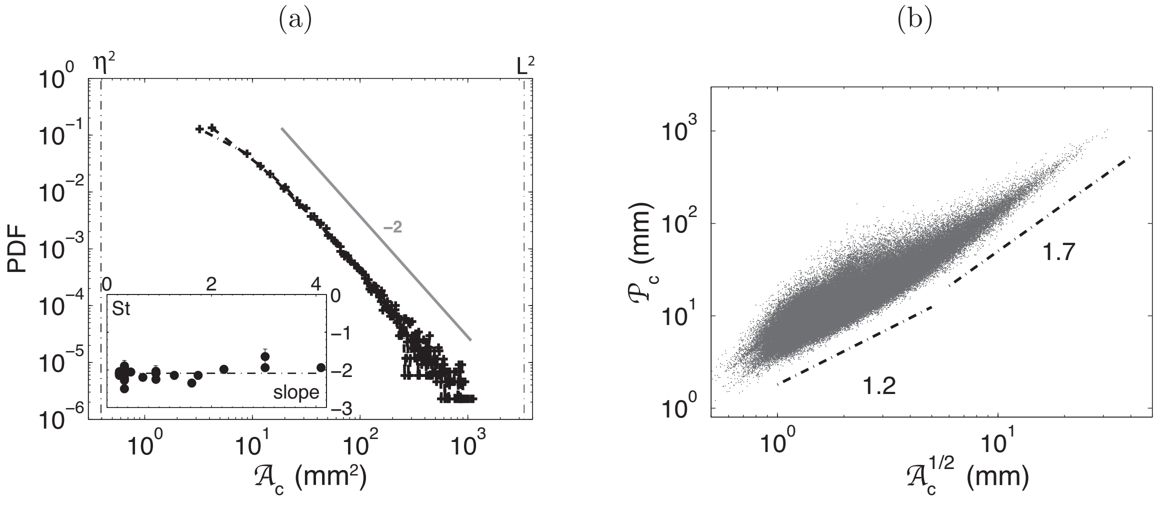

FIG. 3.13 – (a) PDF of clusters area, inset shows the evolution of the fitted power law exponent with Stokes number for the 40 experiments of fig. 3.11a. Vertical dash-dotted lines indicates η^2 (left) and L^2 (right). (b) Geometrical characterization of clusters for the same 40 experiments.

Figure 3.14b shows the evolution of these mean normalized concentration with Stokes number, a globally growing trend with St can be seen, though scattering of data points is relatively large. On the contrary, as evidenced in figure 3.14c, the mean normalized concentration in clusters turns to be clearly dependent on the global seeding concentration C_0 following a decreasing power law $< C/C_0 >\propto C_0^{-0.39}$. While one might have expected the concentration inside the clusters to grow linearly with the global concentration ($< C/C_0 >$ remaining constant) as a trivial geometric effect, this surprising decreasing power law dependency shows that the average concentration inside clusters grows more slowly than the global seeding concentration. As a consequence, the relative overloading of particles inside the clusters is reduced when the global seeding increases : for the lowest values of C_0 clusters are up to 8 times overloaded while they are only twice as dense as the average for the largest values of C_0. To rule out any possible bias due for instance to a statistical under-sampling of low concentration experiments, the same whole analysis on artificially subsampled data has been performed : starting from the highest concentration experiment (containing several thousands particles per image), up to 90% of the particles are randomly removed and Voronoï tesselations and clusters identification are recomputed. The subsampled data show that the algebraic distribution of clusters area is always maintained with the same −2 exponent, that the distribution of concentration within clusters is still gaussian, and that mean normalized concentration in the clusters with the subsampled number of particles per image is weakly affected by the subsampling (see dots data on figure 3.14c). This robustness of the analysis to arbitrary subsampling shows that the effect observed in figure 3.14c does result from a physical process related to particles loading and not from a statistical bias. Such a non trivial effect, which has never been reported to our knowledge, is therefore intrinsic to the clustering of dense particles by turbulence. It probably reveals the existence of collective effects inside the clusters, and certainly deserves further investigations as well as cross-analysis with other experiments and numerical simulations. In particular, it should be underlined that this behavior is most probably not due a steric effect. If so one should expect both a linear increase of $< C >$ with C_0 in the dilute limit and a saturation of $< C >$ (irrespective of C_0) at very large concentrations. None of these trends appear in figure 3.14c (note that the concentration covers more than one decade in this figure).

Finally, a possible dependency of $< C/C_0 >$ on Stokes number (which was not clearly visible at first sight in figure 3.14b) has been further checked by considering data on figure 3.14b divided by the empirical power law $< C/C_0 >\propto C_0^{-0.39}$ (obtained from figure 3.14c) as a first attempt to separate Stokes number effects from the global seeding concentration effects just described. The result is presented in figure 3.14d which shows a possible dependency on Stokes number with a maximum mean concentration in clusters occurring around $St \simeq 2$, reminiscent of the maximum of preferential

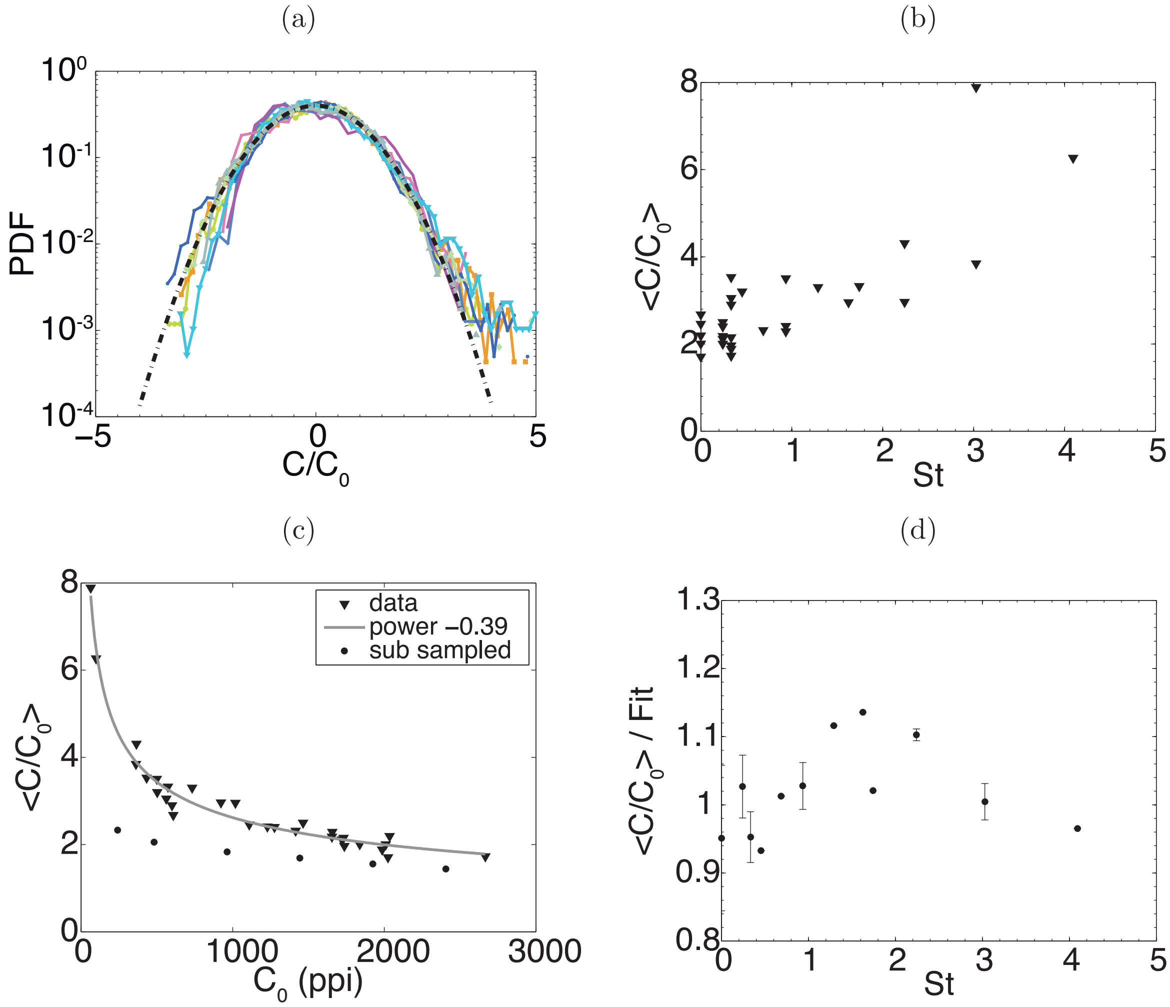

Fig. 3.14 – (a) PDF of normalized-reduced concentration C/C_0 within clusters. (b) Evolution of the means of PDFs in figure (a) with particles Stokes number. (c) Evolution of the means of PDFs in figure (a) with the global seeding concentration C_0 given in particles per image ($\bigtriangledown$: all our experiments, $\bigcirc$: one single experiment randomly subsampled). (d) Evolution of the means of PDFs in figure (a) with the Stokes number after compensation by the seeding concentration dependance evidenced in figure (c).

concentration observed in figures 3.11c. Though further investigations will be needed to be conclusive on this point, as discussed in the concluding section, such a dependency can be consistently interpreted in the framework of a sweep-stick mechanism [43, 29].

3.3.4 Conclusions and outlooks

We have introduced, together with R. Monchaux and A. Cartellier, the analysis of preferential concentration in turbulent particles laden flows using Voronoï diagrams as a new tool to get a quantitative insight of the phenomenon. This very computationally efficient tool, not only gives access to the concentration field at an intrinsic local resolution (inverse of Voronoï areas directly gives local particles concentration) but it also offers a remarkably simple and non-ambiguous way to define particles clusters (as well as complementary voids) and to analyze their structural properties. Several known behaviors (previously reported in experimental and numerical works based on classical tools, mainly pair correlations, correlation dimension and box counting), as the maximum of heterogeneity of the concentration field for particles with Stokes numbers around unity, have been successfully recovered and further analyzed at the light of this new tool. By systematically varying the triplet of parameters (St, R_λ, C_0), we have shown that particles Voronoi's areas distributions are always reasonably log-normal, so that preferential concentration can be quantitatively measured by a single scalar (the standard deviation of these distributions). We have characterized clusters (and voids) geometries and their inner concentration. Geometrical properties (mainly the algebraic distribution of mean cluster areas and the fractal structure of clusters) may be interpreted as an evidence of the self-similar nature of preferential concentration in particle laden flows ; in particular clusters do not appear to have any characteristic typical scale. The analysis of particles concentration inside the clusters have revealed two new and so far unpredicted results : *(i)* average particles concentration inside clusters depends on the global particle loading in a non trivial way and *(ii)* after compensation of this particle loading dependency, average concentration inside clusters exhibits a non monotonic dependency on Stokes number, with a maximum around unity values.

To summarize Stokes number effects, we find that overall preferential concentration is enhanced for particles with Stokes number around unity, cluster sizes and geometries do not depend on Stokes number while mean concentration within clusters is also enhanced (at second order, when seeding concentration effects are decoupled) around unity Stokes numbers. All together these results can be consistently interpreted in the framework of recently introduced sweep-stick mechanism by Vassillicos and co workers [43, 29]. They propose a new physical process for particles preferential concentration phenomena where clusters form around zero acceleration points of the carrier flow to which particles tend to stick and to be advected with. These special points of the carrier flow have been thoroughly investigated in DNS [43, 29] and found to have at least two main remarkable properties : (i) their spatial distribution is not uniform, and they tend to clusterize and (ii) inertial particles tend to stick to these points with an optimal stickiness when the Stokes number is around unity. Physically, the sticking mechanism is dominated by the convergence of particles toward zero acceleration points along the maximum compression direction of acceleration gradients tensor of the carrier flow. This convergence is optimal when particles response time τ_p is of the order of the inverse of the corresponding contraction rate [29](if the response time is too small contraction is too slow, while for too large response times contraction is fast but overshot by particles inertia). In the context of the stick-sweep mechanism, clusters shape and size are therefore expected to be mostly prescribed by the carrier turbulence itself (in terms of clustering properties of zero acceleration points themselves). For instance the fractal structure of zero acceleration points distribution has been identified in DNS [29]. This is consistent with the self similarity we have observed in our experiment. In the same time, as a result of the Stokes number dependency of the stickiness of zero acceleration points, the concentration of particles within clusters is also expected in the context of this model to depend on Stokes number (with an optimum around $St \sim 1$) and consequently so does the overall preferential concentration. This is also consistent with Stokes number trends observed experimentally. However some observations still remain to be understood. Yet, considering the sweep-stick mechanism alone, it is hard to qualitatively identify the origin of a departure from a linear increase of $< C >$ with C_0. Such a quantification remains to be done from available simulations [43, 29]. One possibility could be the indirect role of gravity (gravity was not accounted for in the above mentioned simulations). Indeed, particle-turbulence interactions are known to enhance the settling velocity of dense inclusions [62, 2, 114]. One may expect that such a settling velocity would tend to decorrelate somewhat the particles locations from those of zero acceleration points, making clustering less efficient than expected. An argument in favor of such a scenario is that the enhanced settling velocity of inclusions in clustered regions is a collective effect that arises from the local concentration alone and thus is not Stokes dependent [2]. In this framework, the influence of turbulence intensity on settling velocity enhancement is not completely clarified. If, as identified from simulations [62], this enhancement is proportional to the turbulence intensity, one may expect an evolution of the relationship between $< C >$ and $< C_0 >$ with Reynolds number. Such a possibility will to be addressed in future investigations.

Similarly, a thorough comparative Voronoï analysis of zero acceleration points and particles clusters as well as a parametric Reynolds number study would shed more light on our results. The former is only accessible to numerical works so far, and regarding the latter, a drastic and challenging reduction of the polydispersity of the seeding fog is crucial for any experimental attempt. Numerical studies are

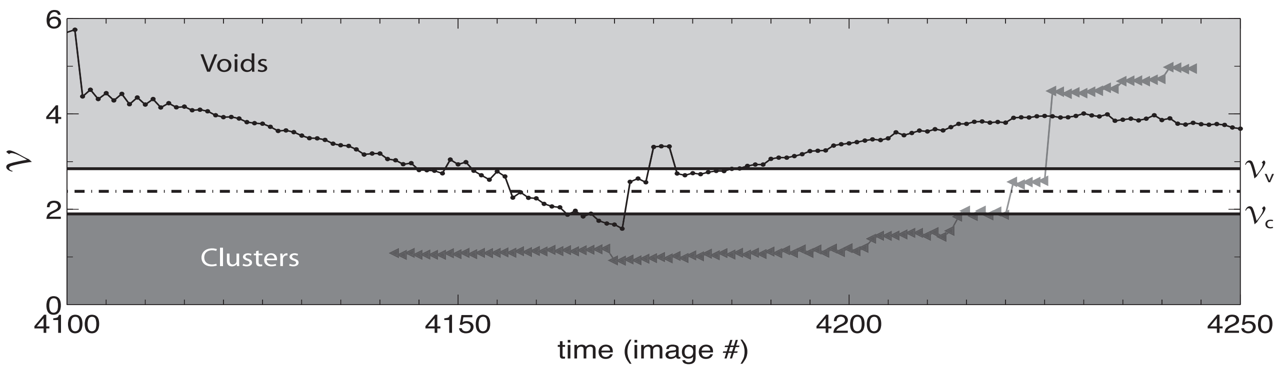

FIG. 3.15 – Voronoï area trajectories for two particles. The dashed-dotted horizontal line shows the cluster threshold defined above, the continuous lines are respectively 80% and 120% of this threshold. The track with triangles is clearly associated to a particle that is ejected from a cluster around $t = 4225$.

naturally monodisperse and could also be of great help to this regard. Incorporating gravity effects in these simulations would also be useful regarding the question of the amount of demixing. To finish, I would like to stress the great potential of Voronoï tesselations which offer a whole range of new openings for further investigations of particle laden flows. In particular combined to classical Lagrangian particle tracking, it allows to follow the local concentration in a Lagrangian frame (see figure 3.15 which illustrates preliminary attempts of such Lagrangian local concentration tracking), giving simultaneous access to statistics of particles dynamics (velocity and acceleration) and local concentration field around particles. Other important aspects concern clusters dynamics, and more specifically clusters life-time as well as statistics of particles residence time inside clusters (Lagrangian evolution of local concentration in figure 3.15 shows for instance two particles travelling between clustered and void regions). Such conditional and dynamical information are expected to be key ingredients to improve our understanding and modeling capabilities for turbulent particle laden flows.

Chapter 4

Transport of magnetic field by a turbulent flow of liquid metal : MHD and dynamo effect

4.1 General Context

The magnetic field of the Earth and of most astrophysical bodies results from a magnetohydrodynamic (MHD) instability, *the dynamo effect*, where mechanical energy of the flow of a conducting fluid is spontaneously converted into magnetic energy. For the Earth, the mechanical energy is given by the convection of the liquid iron forming the outer core. The dynamo instability is intimately related to the capacity of the flow to transport the magnetic field, as a result of MHD induction processes. All flows are not capable of sustaining a dynamo instability, but specific flow topologies are requested. Basically the geometry of the flow must be complex enough so that the magnetic field is stretched and folded in such a way that it superimposes to itself, therefore generating a positive feedback which may become unstable and initiate the exponential growth of any infinitesimal magnetic seed. Unfortunately existing theorems only predict geometries which are *not* capable of sustaining dynamos ; they are called *anti-dynamo* theorems. No *dynamo* theorem giving sufficient geometric conditions for a flow to

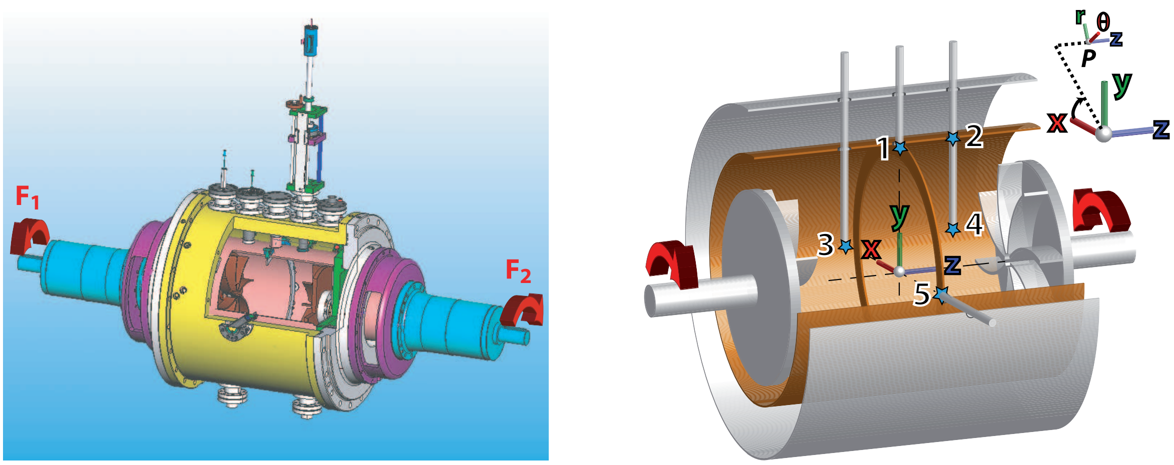

FIG. 4.1 – Sketch of the VKS experiment which drives a von Kármán swirling flow of liquid sodium in a cylindrical vessel. The total mechanical power is 300 kW and the total volume of sodium in the outer vessel is 150 L. The right figure shows details of the the experimental configuration for the first dynamo run (september 2006), including soft iron impellers, an inner copper shell and an inner annulus in the mid-plane. Typical location of magnetic probes are also shown.

be favorable for a dynamo is known. However, helicity and differential rotation have been shown to be important topological ingredients, favorable to efficiently stretch and fold the magnetic field for a dynamo mechanism. They are therefore the most common topological ingredients in dynamo models. The condition on the flow geometry needs then to be completed by an energetic condition, requiring that the transport of the magnetic field overpass the magnetic diffusion due to Joule dissipation in the conducting fluid. This is generally written in terms of the magnetic Reynolds number $R_m = UL/\eta$ (with U the typical velocity of the flow, L the typical length scale and $\eta = (\mu\sigma)^{-1}$ the magnetic diffusivity with μ the magnetic permeability and σ the electric conductivity of the conducting fluid) having to exceed a certain threshold R_m^*, which is flow topology dependent.

The difficulty of this double condition (favorable flow topology and $R_m > R_m*$) explains the long time lag between the original theoretical idea of Larmor, who was the first to suggest in 1919 that such a MHD instability might be responsible for the magnetic field of the sun, and the first experimental verification of the phenomenon which has only been observed in the year 2000, almost simultaneously in two different liquid sodium experiments (one in Karlsruhe [98], the other in Riga [37]). Sodium is the liquid metal with the highest conductivity (and hence the lowest magnetic diffusivity), what makes it the ideal fluid for high R_m experiments (in spite of practical difficulties due to its high chemical reacitivity). Eventhough, largest sodium experiments nowadays hardly exceed magnetic Reynolds number above 50 which is already a very large number for laboratory conditions, but unfortunately not necessarily sufficient for overpassing the dynamo threshold. The success of these two experiments has therefore required a rigourous optimization of the flow topology in order to make the dynamo threshold as low as possible. As a consequence, the geometry of the flow was very constrained (using pipes, diverters and internal boundaries) to force the flow to follow as close as possible ideal topologies shown theoretically to be able to sustain a dynamo (Roberts' flow [89] for the Karlsruhe experiment and Ponomarenko's flow [80] for the experiment in Riga). Since these historical experiments, new challenges in dynamo research concern the release of these constraints in order to investigate the role of fluctuations and turbulence on magnetic field generation process, its saturation and its dynamics. These questions are important in the context of natural dynamos which are generated in turbulent conditions. It should also be noted that any liquid metal dynamo experiment with an unconstrained flow is also necessarily turbulent. In the absence of internal boundaries guiding the flow the characteristic length scale for the velocity and the magnetic fields are indeed the same ; as a consequence the kinetic Reynolds number of the flow, $Re = UL/\nu$, is then related to the magnetic one, $R_m = UL/\eta$ via the magnetic Prandtl $P_m = \nu/\eta$ which for all liquid metals is a very small quantity of the order $10^{-5} - 10^{-6}$. Having a large magnetic Reynolds number (what is required to exceed the dynamo threshold R_m^*) then implies that the kinetic Reynolds number must be huge. In a more general context this is related to the turbulent transport of passive and active fields and to instabilities in presence of noise.

My MHD activities are done in collaboration with Jean-François Pinton's group at Laboratoire de Physique de l'École Normale Supérieure de Lyon. The work reported here is primarily experimental and encompasses to liquid metal facilities : (i) the VKS experiment, which uses liquid sodium and has recently become the third experimental dynamo and the first operating in fully turbulent conditions and (ii) a smaller experiment using liquid gallium, which is dedicated to the investigation of induction processes and MHD coupling between a magnetic field and a conducting flow. The VKS experiment, presented in section 4.2, results from a large collaboration involving ENS-Lyon, ENS-Paris and CEA-Saclay and the experiment itself is located at CEA Cadarache. The Gallium experiment, presented in sections 4.3 runs at the Laboratoire de Physique de l'École Normale Supérieure de Lyonand the results presented here were obtained together with Nicolas Plihon, Philippe Odier, Jean-François Pinton and Gautier Verhille (then PhD student).

4.2 VKS2 - turbulent dynamo experiment

The VKS (von Kármán Sodium) experiment results from a large collaboration including ENS-Lyon, ENS-Paris and CEA-Saclay. It aims at producing and investigating the generation of a magnetic field by

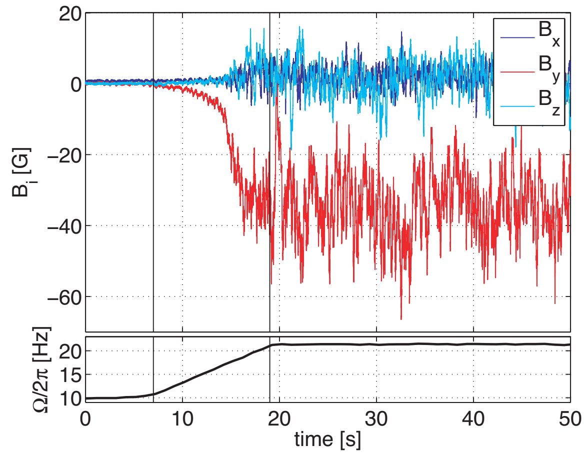

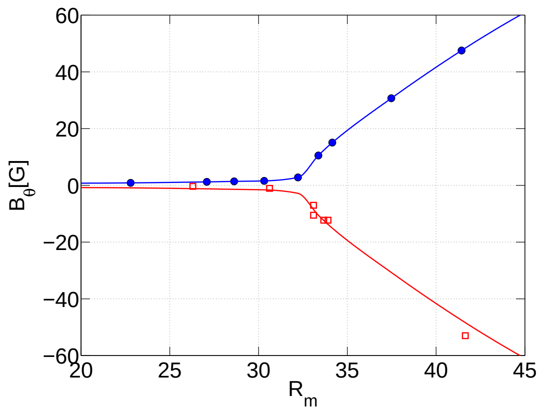

FIG. 4.2 – (a) Three components of the magnetic field generated by dynamo action measured at point P1 in the when the flow is driven in exact counter-rotation. The bottom plot shows the rotation rate, which is increased from 10 Hz to 22 Hz. (b) Bifurcation curves of the Azimuthal field measured at P1, growing with either polarity. The solid lines correspond to a best fit with a scaling behavior $B = (Rm - 32)^{0.77}$ above threshold.

dynamo effect in a turbulent von Kármán flow of liquid Sodium (figure 4.1). I joined the collaboration during my PhD in 2000 and participated to the two generations of the experiment (only results of the second one, VKS2, after the first dynamo run in 2006 will be discussed here). The choice of von Kármán configuration for this investigation relies on its large scale topological properties, dominated by helicity and differential roation (when the impellers are counter-rotating), which are known to be very efficient ingredients for induction processes, and for its high intrinsinc level of turbulent fluctuations. The experiment is hosted by CEA Cadarache and benefits from the expertise and infrastructures available there for handling large volumes of liquid sodium.

4.2.1 First experimental observation of a turbulent dynamo

In 2006, the second generation of the VKS experiment gave the first experimental evidence of the dynamo instability from a fully turbulent flow of liquid metal. This success was recognized worldwide and is the result of almost ten years of research during which the experiment was successively incremented and optimized in order to improve the efficiency of the induction mechanisms (this included optimizing the forcing geometry and electromagnetic boundary conditions, increasing the mechanical power, adding a temperature regulation, etc.). A crucial factor, which has so far been identified as determinant for the instability onset in VKS, relies on the material used for the impellers : at the moment the dynamo is only observed when the impellers are made of soft iron. No dynamo is observed when the flow is driven with impellers with identical geometry but made for instance out of copper or stainless steel. This point, which will be discussed later remains one of the mysteries of VKS.

When the flow is driven with soft iron impellers in perfect counter-rotation, the spontaneous growth of the magnetic field is observed when the rotation frequency of the impellers exceeds a certain threshold (figure 4.2a), which corresponds to a critical magnetic Reynolds number $R_m^* = UL/\lambda \sim 30$, following a typical evolution of a super-critical bifurcation 4.2(b). The observed magnetic field is statistically stationnary, with an average value of the order of 40 G (hence two orders of magnitude larger than the magnetic field at the surface of the Earth) measured at point 3 in figure 4.1. The field presents an important fluctuation level (of the order of 30%). The topology of the field, as inferred from the several measurements available inside the experiment (see figure 4.1), appears to be essentially that of an axisymmetric dipole. To be consistent with the Cowling theorem, which forbids axisymmetric dynamos, this observation suggests that non-axisymmetric fluctuations of the von Kármán flow play a crucial role in the dynamo process. Consistently with the symmetry $\vec{B} \to -\vec{B}$ of the equations of the

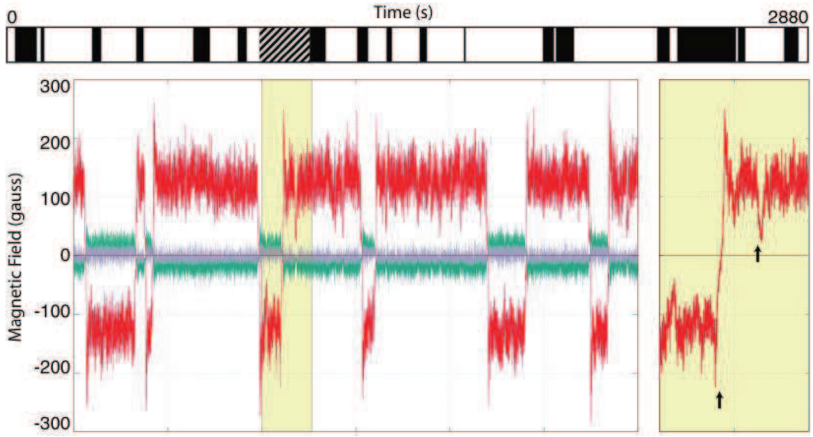

FIG. 4.3 – Magnetic field measured inside the flow vessel, by a 3-dimensional Hall probe when the flow is driven with counter-rotating soft iron disks at frequencies F1 = 16Hz and F2 =22Hz. The main component (red) is the azimuthal one. Note that all components decay to zero at a reversal. Top : Chronos of the magnetic field orientation, white for a positive direction, black for the negative direction, for 2 successive recordings 900 and 1800 seconds long (separated by the shaded area, the first sequence corresponds to the main graph).

dynamo problem, both polarities of the dipole can be observed when the experiment is stopped and re-run (see figure 4.2(b)) but the chosen polarity is statiticaly stationary once the field has grown.

4.2.2 Dynamical regimes

We have seen in the previous paragraph that a statistically stationary magnetic field is generated by dynamo effect when the impellers are in exact counter-rotation. The scenario is changed if the forcing is asymmetric (one of the disks rotating faster than the other). In that case a wide variety of dynamical regimes appears, among which one particularly interesting where the magnetic field experiences random erratic reversals (see figure 4.3). During a reversal the amplitude of the dipolar field vanishes before it grows with opposite polarity. Events (known as excursion) are also observed where the amplitude of dipole decreases but then increases with the same polarity. The duration on which the reversal occurs (a few seconds, what is comparable to the magnetic dissipation time) is much shorter than the average duration of a given polarity. Interestingly, all these properties recall the erratic reversals of the Earth magnetic field. A more detailed exploration of the parameter space of the experiment with asymmetric forcing, shows a rich variety of dynamo classes depending on the relative rotation rate of the two impellers (see figure 4.4), including periodic oscillations and intermittent bursts. It is also striking to note that the phase space trajectory of the magnetic field over these several dynamical regimes is particularly robust (see figure 4.4(b)), and to be connected only to four fixed points (noted P, -P, Q and -Q). This is characteristic of a low dimensional dynamical system, where despite the high level of turbulence, only a few modes are responsible of the dynamics. In this context, a model based on the interaction between a dipolar and a quadrupolar mode with similar threshold instability has been proposed by Pétrélis and Fauve [78].

4.2.3 Discussion and conclusions

Many unknowns remain on the VKS dynamo. Among them the actual mechanism responsible for the instability and the role played by the material of the impellers are crucial. It is highly unlikely that the instability is purely generated by the iron disks only. Several observations point indeed toward a fluid dynamo mechanism : (i) as the disks are driven with a constant rotation rate regulation, if the dynamo was generated only by the disks, the staturation of the magnetic field would be limited only by the available torque (or power) of the motors, so that a sharp increase of the amplitude of

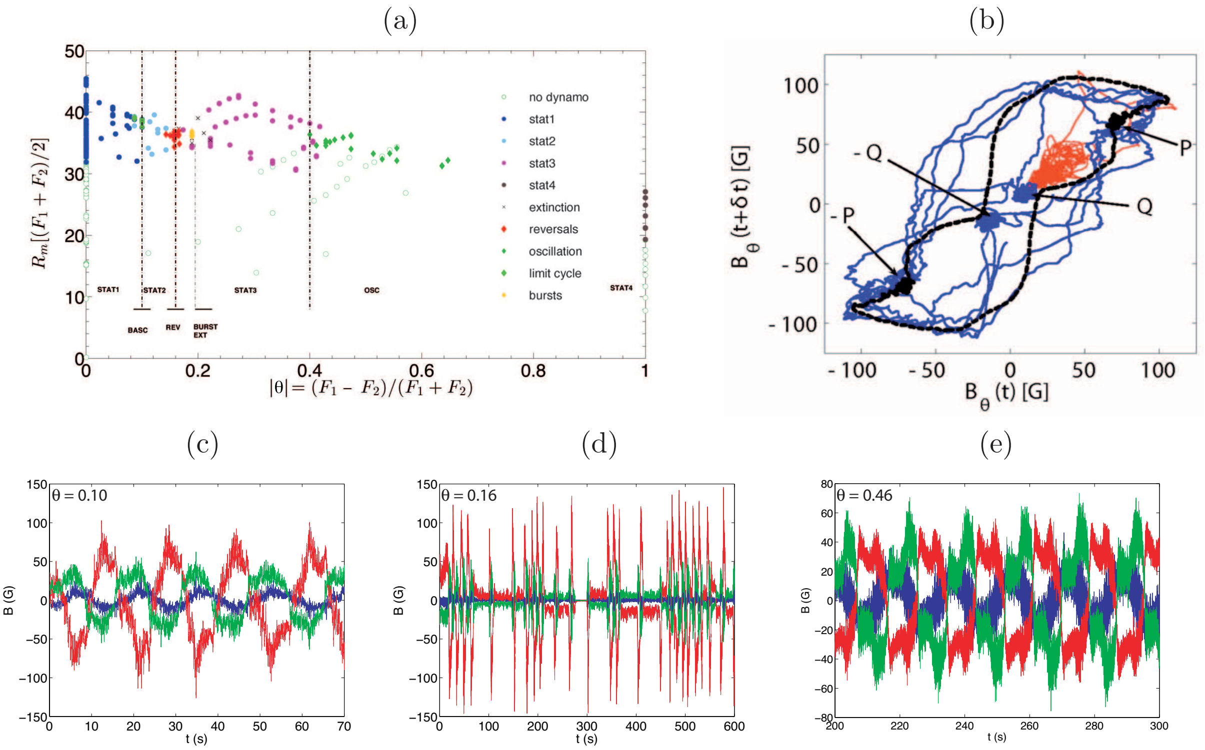

FIG. 4.4 – Top : Parameter space and dynamo regimes for VKS2 experiment, vertical axis is the magnetic Reynolds number based on the average rotation rate of the two impellers $((F_1+F_2)/2$ and the horizontal axis is the normalized rotation rate difference $\theta = (F_1 - F_2)/(F_1 + F_2)$. Bottom : Examples of times series of three different dynamical regimes (time periodic regime at $\theta = 0.1$, bipolar intermittent bursts at $\theta = 0.16$ and oscillations at $\theta = 0.46$).

the magnetic field would happen at the instability onset at the same time as the limit torque (or power) of the motors should be reached ; this is highly contrasting with the progressive and continous bifurcation curve (figure 4.2b) and the small impact on the power consumption of the motors at the onset ; (ii) we have observed in the experiment that removing the inner annulus in the mid-plane of VKS changes drastically the threshold of the dynamo when the impellers counter-rotate "backwards" (the blades of the impellers being curved, we call "forward" counter-rotation the unscooping direction and "backward" counter-rotation the scooping direction), what clearly shows that the threshold is related to the hydrodynamics ; (iii) the bifurcation curve of the instability is relatively scattered when the amplitude of the magnetic field is directly plotted as a function of the rotation rate of the impellers, but it collapses onto a single curve when plotted against the magnetic Reynolds number based on the temperature dependent conductivity of sodium. A possible $\alpha\omega$ mechanism for the observed dynamo has been proposed by Pétrélis *et al.* [79] involving a poloidal to toroidal conversion by the usual ω-effect associated to the counter-rotation of the flow [20] while the toroidal to poloidal conversion would be related to the α-effect associated to the large scale swirls generated in the wake of the eight blades of the impellers. In such a scenario, induction mechanisms generated by the flow in the vicnity of the disks are of primary importance, however the specific and crucial role of the material of the disks (I recall that dynamo action has only been observed in VKS when the flow is driven by soft iron disks) remains unexplained.

To better understand this role, we have recently investigated how induction mechanisms are affected depending on the material of the disks. This study has been done at the Laboratoire de Physique de l'École Normale Supérieure de Lyon, in the context of Gautier Verhille PhD and in collaboration with N. Plihon, J.-F. Pinton and P. Odier, in a von Kármán flow of liquid Gallium (VKG) with similar geometry than VKS, but significantly lower magnetic Reynolds number (the dynamo threshold in particular is unreachable). The study consists in measuring the induced magnetic field B_i when an external field B_A

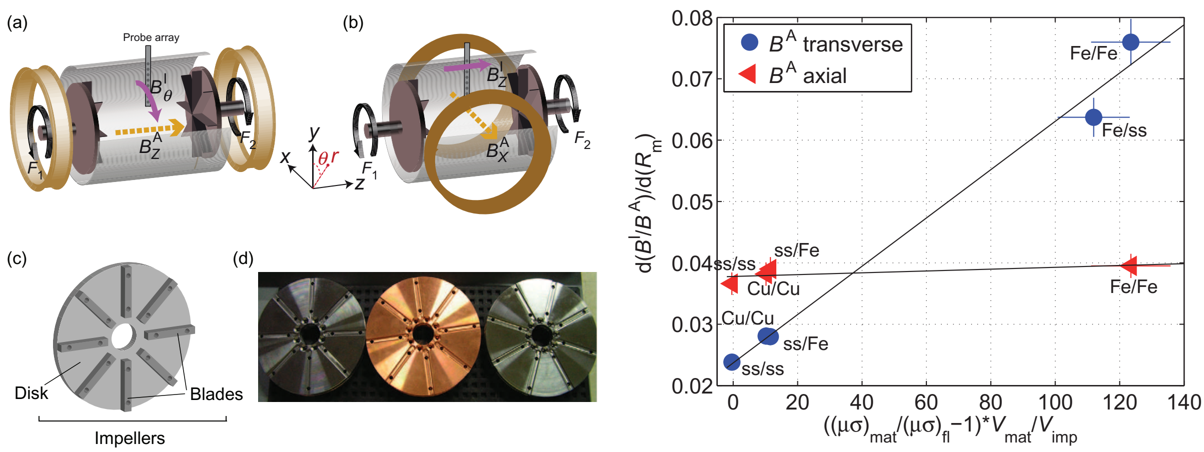

FIG. 4.5 – Left : VKG experiment with axial or transverse applied magnetic field and driven with different impellers. Note that the disk and the blades of the impellers can be of different materials (stainless steel, copper or soft iron), allowing for multiple combinations. Right : Indicator of the efficiency of induction mechanisms in VKG experiments (given by the slope of the evolution of the induced magnetic field as a function of R_m) when it is driven with disks made out of different combinations of stainless steel, copper and soft iron. The different configurations are characterized by $(\mu\sigma)_{mat}/(\mu\sigma)_{fluid}-1)V_{mat}/V_{imp}$, where $(\mu\sigma)_{mat}$ is the inverse of the magnetic diffusivity of the specific material, $(\mu\sigma)_{fluid}$ is the inverse of the magnetic diffusivity of Gallium, V_{mat}/V_{imp} is the volumic fraction of the specific material in the impeller.

is applied to the flow which is driven with disks made out of different materials (see figure 4.5a). These measurements have proven that for an identical flow geometry the efficiency of the induction processes is significantly enhanced when the magnetic permeability of the propellers is increased. More precisely, we have shown that (at least within the moderate range of magnetic Reynolds number accessible in VKG) the additional contributions to the induction processes vary linearly with the change in $\mu\sigma$ between fluid and impeller (see figure 4.5). As a consequence, this shows that a large value of $\mu\sigma$ (hence a low magnetic diffusivity) of the impellers significantly enhances the efficiency of the induction processes in the fluid, therefore contributing to reducing the threshold of the dynamo instability. These induction measurements also show that such impellers also tend to promote the induction of axial magnetic fields, what is consistent with the observation that the dynamo field generated in VKS is dominated by an axial dipole. Finally, the localization of dynamo sources near the impellers may also help understand why the evolution of the VKS dynamo field shares many features with low-dimensional chaos, as it would result from nonlinear interactions of two weakly coupled dynamos (one in the vicinity of each impeller). Note that this is also consistent with two interacting near critical dipole and quadrupole modes as proposed in the model by Pétrélis *et al.*.

Though the detailed role of the soft iron and the exact mechanism generating the dynamo in VKS are not yet completely elucidated, the observations just described point to a scenario dominated by induction mechanisms in the bulk (though in the vicinity of the disks) which are enhanced by the contrast in magnetic permeability between the fluid and the disks. This is also supported by recent numerical simulations where the discontinuity of magnetic permeability at the impellers is taken into account [42, 47].

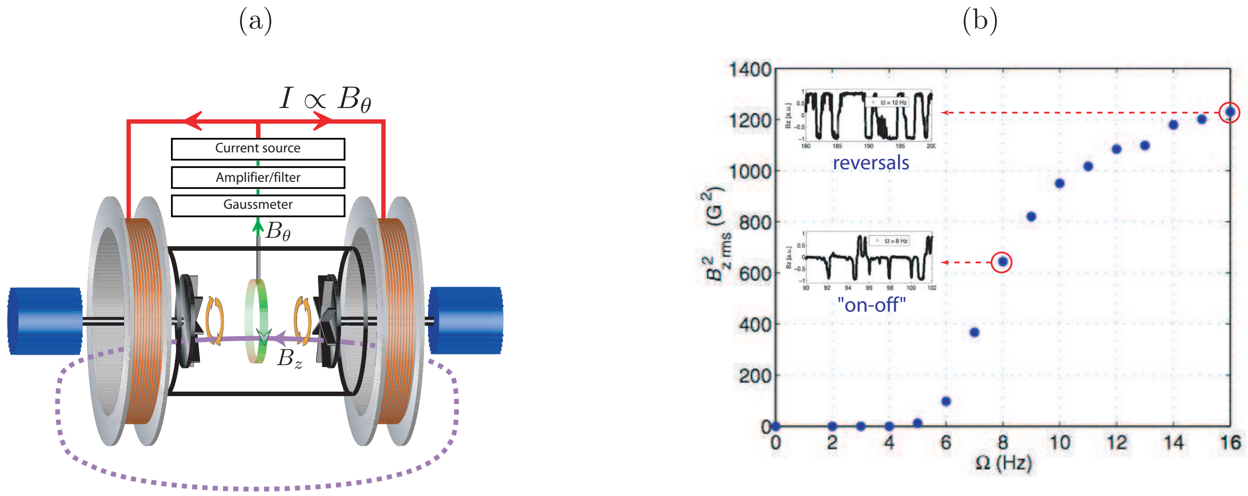

FIG. 4.6 – (a) BVK experimental set-up : a von Kármán flow of liquid gallium is generated in a cylindrical vessel between two counter-rotating disks driven by two AC-motors. The differential rotation advects and stretches an axial field Bz produced by two Helmholtz coils so as to generate a toroidal component B_θ. The amplitude of B_θ is then used to drive the power source which generates the current in the coils, which closes the dynamo feedback loop. (b) The main figure shows the evolution of the variance of the time fluctuations of the axial magnetic field B_z as the disks counter-rotation rate is increased (bifurcation diagram). The insets show two time series of the magnetic field near threshold (8Hz) where an intermittent "on-off" dynamic is observed and far above threshold (16Hz) where a fully developed reversing regime is observed.

4.3 An experimental model of a Bullard-von Kármán (BVK) dynamo

4.3.1 The BVK experiment

As illustrated by the VKS experiment history, building an actual fluid dynamo experiment is a complex and expensive task. Only three successful experimental dynamos have ever been built (Karlsruhe, Riga and VKS). One of the specific goals when the VKS project started was to produce a fully turbulent dynamo experiment. This required almost ten years of research and optimization. Considering the difficulty of the task, before the success of VKS in 2006, I proposed the idea of building a synthetic experimental turbulent dynamo, inspired by the classical hompolar dynamo (also known as Bullard dynamo, after the theoretical work on this specific configuration made by Sir E. Bullard in 1955 [23]), where part of the dynamo feedback mechanism is artificially forced using external wiring and coiling but where the flow turbulence is still included in the whole process and has a leading role. That is, we relax the requirement that the current path be fully homogeneous, and we effectively prescribe the mechanism by which a toroidal magnetic field generates a poloidal one. However, the poloidal to toroidal conversion remains the result of a fully magnetohydrodynamic ω-effect process (including the flow fluctuations). The experiments are carried out in the set-up sketched in figure 4.6. The flow is produced by the rotation of two disks inside a stainless steel cylindrical vessel filled with liquid gallium. A magnetic field can be applied using two axial coils. For a constant and uniform axial field applied, one obtains in the quasi-static limit at low magnetic Reynolds numbers, a toroidal magnetic field induced by the differential rotation of the flow. This is the ω induction mechanism [19] which converts a poloidal field into a toroidal one. It is a linear effect, and the time average of the toroidal field at the measurement location verifies $B_\theta = kR_m B_{0,z}$, where k is a "geometric" constant which in our experiment has been measured of the order of 0.1. However, due to the turbulent nature of the flow, the instantaneous values $B_\theta(t)$ have strong fluctuations : the standard deviation is of the order of the mean. The poloidal to toroidal conversion is then obtained when a signal linearly proportional to B_θ is used to drive the current source that feeds the coils, which, in turn, generate $B_{0,z}$. As a result, $B_{0,z} = GB_\theta$ with G an adjustable gain. In the end the overall feedback mimics an $\alpha\omega$ mechanism, where the α effect is artificially forced using the external wiring, but the ω effect fully includes the complexity of the flow. In this closed loop the average axial field obeys $B_z = GkR_mB_z$. A necessary condition for a self-sustained state is then $R_m > R_m^* = 1/kG$. Clearly, the adjustable gain of the linear amplifier allows us to set the value of the critical magnetic Reynolds number to an experimentally accessible range.

4.3.2 The BVK dynamo

I consider now the case where no external field is initially applied. Figure 4.6b shows the bifurcation diagram of the instability. As the rotation rate of the driving disks is progressively increased, the magnetic field remains null until a sufficient rotation rate is reached. At this point, one observes the occurrence of intermittent bursts : the magnetic field grows spontaneously at irregular intervals, with either polarity. This corresponds to times when the fluctuations in the differential rotation reach a level high enough to satisfy the instability condition $R_m > 1/kG$. During these dynamo bursts, the magnetic field reaches a finite value $\pm B_{sat}$, held for durations,$T_{burst} \sim 5\ s$ on average (or $T_{burst}\lambda/R^2 \sim 10$ if one compares to the diffusion time of the magnetic field across the flow volume). Interestingly, the bifurcation occurs via an "on-off" regime, a scenario which has been previously hypothesized for dynamo experiments and models [69, 99], but which was not observed in Karlsruhe, Riga and VKS. The fact that either polarity is realized is due to the symmetry of the induction equation. As the disks rotation rate is increased further, the dynamo bursts growlonger until a regime is reached when the magnetic field is always present, with either polarity. The polarity of the field is not constant in time : the magnetic field spontaneously reverses its direction, at irregular time intervals. One also notes the occurrence of excursions, *i.e.* times when the magnetic field decreases as if about to reverse, but then returns to its initial value and polarity. We note also that the time of a reversal is short compared to the magnetic diffusion time of the system and that the reversals proceed via a robust trajectory (as is the case for the Earth and VKS).

4.3.3 Discussion and conclusions

Though the dynamo cycle is here artificially forced, this setup appears to be an easy model for versatile experiments which shares interesting behaviours with actual homogeneous dynamos. Several issues related to dynamo and nonlinear bifurcations can be addressed using this experimental arrangement and will be explored in forthcoming studies :

• The external gain in the feed-back loop amplifies induction effects. The effective magnetic Reynolds number in the system is then $R_m^{eff} = GR_m$. One consequence is that one can tune independently the magnetic Reynolds number and the kinetic Reynolds number of the flow. It will be interesting to analyse to which extend our arrangement provides a way to study MHD at varying magnetic Prandtl numbers (here defined as the ratio R_m/Re).

• The use of a mean and a fluctuating component in the feed-back amplification stage provides a tool to study experimentally the role of fluctuations and noise in the bifurcation dynamics. Firstly, one can set the threshold by adjusting the gain of the feed-back loop so that one may choose to operate far above the dynamo onset. Secondly, several kinds of noise (coloured, correlated, etc) can be inserted into the feed-back loop, and the effects can be quantified. Some studies have shown that the dynamo threshold would be increased due to the presence of noise while others suggested that small scale turbulence may not modify it or eventually help. The nature of the bifurcation may also change with the characteristics of the noise, particularly for the "on–off" regime.

• One may also ask whether it is possible to synchronize the reversals by adding a periodic forcing (mechanical or applied field) in connection with stochastic resonance issues.

• Finally, a promising possible development is the use of a current source such that the field at saturation is large enough for Lorentz forces to alter the flow (at the moment the instability saturation is entirely due to the saturation of the electrical source driving the current in the coils). One of the open questions is how the field dynamics, including reversals, is changed in this case. This is currently under investigation by Nicolas Plihon in the context of Sophie Miralles PhD.

Chapter 5

Conclusion

The studies presented in this memory report experimental results on turbulent transport of particles (both tracers and non tracers) and magnetic fields to which I have personnaly contributed during the past years.

During my collaboration with Pr. Bodenschatz at Cornell University, I have developped, together with Haitao Xu and Nick Ouellette, the first multiple ultra-high-speed-camera system, capable of tracking simultaneously hundreds of 3D-trajectories in a turbulent flow at Reynolds number up to almost $R_\lambda \sim 1000$, with sufficient spatial and temporal resolution. Thanks to this unique system, I have explored three important aspects of Lagrangian turbulence (from the dynamics of fluid tracers) : (i) the pair dispersion problem, (ii) the validity of the local isotropy hypothesis and (iii) the Lagrangian intermittency phenomenon. Results from points (i) and (ii) have shown that two usually accepted features for turbulent flows actually need to be revisited. Concerning pair dispersion, we have indeed shown that within the accessible range of Reynolds number and initial separations explored, the usually accepted superdiffusive Richardson t^3 dispersion regime is not observed. On the contrary a ballistic (t^2) and initial separation dependent regime predicted by Batchelor in 1952 is very robustly observed. Similarly our measurements of 3D Lagrangian spectra of particles velocity have shown that recovery of isotropy at small scales might be much slower than expected, and at least far from being reached, even at the smallest scales in an axisymmetric turbulent flow at R_λ approaching 10^3. Point (iii) has given what still remains the standard for Lagrangian anomalous exponents measurements. In a more general context, these experiments are also important as they explicitly address the question of what a *high Reynolds number limit* might be and at which rate usual idealizations of turbulence are eventually approached.

More recently, my activities in the team EDT at LEGI have addressed the problem of the transport of material particles, with a specific focus on finite size, density and collective effects. The theoretical approach of this problem is extremely complex, as even writing an appropriate equation of motion modeling the coupling of the carrier turbulent flow and particle dynamics remains a challenge. I have considered the case of individual finite size particles from acoustical Lagrangian tracking experiments (this was done in collaboration with Christophe Baudet, Alain Cartellier and Yves Gagne, and was also the topic of Nauman Qureshi's PhD which I supervised) and the multiple particle case, with a particular focus on the preferential concentration phenomenon (this was done in collaboration with Alain Cartellier and was part of the postdoctoral project of Romain Monchaux). My contribution to the investigation of the turbulent dynamics of individual particle have shown that usual stokesian models may be actually limited only to extremely small particles. This is not really surprising as these models have been developed based on a point particle assumption. However I have shown that even simple predictions (as for instance for particles *rms* velocity) cannot be extrapolated to inertial particles with size even only slightly larger than the dissipation scale. These findings show indeed that many dynamical features of turbulent particles generally referred as “inertial” in the litterature are actually not attributable to particle inertia. For instance, velocity fluctuations, normalized acceleration PDF and forcing correlation time are found not to depend significantly on particle inertial properties. On the contrary the pressure fluctuations integrated at the particle scale are found to be an essential ingredient. Instead of the classical Stokes number filtering scenario where particles fluctuations are expected to be damped simply because of their inertial response time, this study suggests that a preferential sampling scenario is more realistic to account for statistical deviations from tracer behaviour. In this scenario, particles preferentially sample certain regions of the flow ; the sampling itself is expected to result from particles preferential concentration induced by inertia, while the subsequent dynamics of the particles then mostly reflect the dynamics of the flow in these preferentially sampled regions. The dynamical features I have measured for the particles seem particularly consistent with the *stick-sweep* sampling mechanism proposed by J. C. Vassilicos. In a second step I have investigated the preferential concentration phenomenon when many particles are dispersed in a turbulent flow. To this scope, together with A. Cartellier and R. Monchaux, we have proposed a new approach based on Voronoi tesselations analysis which we have shown to be a particularly complete tool compared to previous classical analysis. Important results in this context are : (i) the maximum efficiency of clustering for particles with Stokes number close to unity ; (ii) the absence of typical scale of clusters ; (iii) and the evidence of collective effects within the clusters. Further work is in progress to explore more specifically the influence of Reynolds number on preferential concentration as well as the impact on the individual and collective dynamics of particles.

Though much remains to be done, it is my hope that these studies will contribute to the fundamental understanding and practical modeling of turbulent transport phenomena. For instance relative dispersion is often a key ingredient for turbulent mixing modeling, as the fluctuations of a mixing passive scalar can be related to the pair dispersion law. Choosing the appropriate law (let say Batchelor versus Richardson) can lead to radically different predictions, with important consequences when it comes for instance to improve mixers efficiency or to estimate security levels of toxic substances dispersion. Concerning inertial particles, though we do not have yet an appropriate equation of motion, our results may support the validity of new modeling approaches where particles are fully resolved, which are becoming computationally accessible [49, 102]. Coupling such novel numerical simulations with highly resolved experiments will help testing possible scenarios (as the leading role of pressure and sampling proposed in this work) and give soon a less speculative understanding of the subtle turbulence-particle coupling. This conviction has encouraged me to reinforce my collaborations with numerical groups.

Finally, I have contributed to experimental investigations on the transport of magnetic fields by turbulent conducting flows, with the particular focus of better understanding the spontaneous generation of a magnetic energy by dynamo action. This work involved experiments in liquid sodium, as a member of the VKS collaboration, and also experiments in liquid Gallium, in collaboration with Jean-François Pinton, Nicolas Plihon and Philippe Odier at ENS-Lyon. I have joined the VKS collaboration during my PhD, in 2000, but it is only in 2006, after years of optimization of the experiment that VKS became the first experimental dynamo produced by a fully turbulent flow of liquid metal. Interestingly dynamo action has only been observed up to now in VKS, when the flow is driven with soft iron impellers. Though the exact role of iron remains one of the main interrogations of VKS, the investigation of induction processes in the Gallium experiment done in Lyon, shows that usual induction mechanisms in the bulk of the flow are significantly enhanced when the magnetic diffusivity of the impellers is much lower than that of the driven conducting fluid. A remarkable feature of VKS is that only two macroscopic control parameters (the rotation rate of each impeller) are sufficient to reproduce a wide variety of dynamical regimes of the generated magnetic field (statistically stationnary, random reversals, intermittent bursts, periodic oscillations, etc.) which are all known to exist in natural astrophysical bodies. All these regimes evolve within a robust phase space, and behave as a low-dimensional dynamical system. As shown by Pétrélis & Fauve, this dynamical landscape results from the interaction of two nearly critical modes with different symmetry properties (in the present case a magnetic dipole and a magnetic quadrupole). Measurements in Gallium suggest that this may result from the non-linear coupling between two dipoles generated in the vicinity of each impeller. The role of turbulence in this scenario remains unclear. Surprisingly, in spite of the high level of fluctuations, VKS behaves mainly as a determinisitc low dimensional system where the role of turbulence may be limited to that of noise trigering the departure from a few stable points. To better understand the role of turbulence in such MHD processes, I have proposed and implemented a simple experiment mimicking a dynamo cycle in the Gallium experiment (the Bullard-von Kármán dynamo), which is more versatile and modulable than Sodium experiments. The first studies on this synthetic dynamo show interesting dynamical features (including reversals and "on-off" intermittency. Furhter studies are being carried out, which I hope will help the investigation of fluctuations impact on MHD processes and instabilities. It should also be noted that the role of fluctuations in such von Kármán flows is not limited to small scales. A remarkable feature of von Kármán flow is also the existence of long term fluctuations, over time-scales covering thousands of eddy turnover times. This long term dynamics is known for purely hydrodynamic flows (whitout magnetic field), and seems to be enhanced in the presence of a dynamo. I am currently investigating the origin of this slow dynamics by combining experimental data and numerical simulations in collaboration with Pablo Mininni (University of Buenos Aires).

I would like to conclude by discussing the general fact that fundamental turbulence research has longly dealt with idealized situations, generally assuming homogeneous, isotropic, stationary turbulence, often in the so called *high Reynolds number limit*, which constitutes the favorite playground for theoretical investigations. Though they are not sufficient to solve Navier-Stokes equations, these assumptions are justified by the fact that they allow simplifications which help the development of analytical and/or numerical models. However such idealization generally remains at odds of most real situations making in particular difficult any unambiguous comparison between experiments and models. During the past decades a clear effort has emerged in the turbulence community to enlarge existing studies in order to address these kind of difficulties. Theoretical approaches start including non ideal effects at the same time as new technologies allow experiments to cover a wider range of situations and to explore the real impact of theoretical simplifications. I like to believe that the work presented in this memory is part of this effort. Many novel and challenging experiments are being carried out worldwide. These include cryogenic turbulence, new windtunnel technologies, adjustable isotropy level flows, high Reynolds number rotating turbulence, etc.. Combined with the latest high resolution measurements techniques (high speed particle imaging, acoustical measurements, Laser velocimetry, instrumented particles, etc.) they open new possibilities of experimental investigations never reached before. On the other side, non ideal conditions start to be included in modeling and simulations. This is the case for instance for anisotropy effects, or for simulations of resolved finite size inertial particles. It is extremely encouraging and exciting to realize that, for the first time, experimental, numerical and theoretical turbulence research start playing in a significantly overlapping field of common parameters.

Chapter 6

Research perspectives

6.1 General context

My research perspectives for the coming years aim at exploring new aspects of transport of particles and fields in complex flows. This is at the same time in the continuity of the questions raised by present activities but also in the scope of proposing new approaches, developing new experiments and stimulating new collaborations. My projects articulate around five main axis :

- study of the **influence of large scale properties of turbulent flows** on the small scale dynamics and on the transport of particles ;
- study of **the role of turbulent drag** on the motion of finite objects ;
- study of **collective effects of inertial particles** in turbulent flow, including the impact on collision, coalescence and mass transfer phenomena ;
- study of the **influence of nano and micro-scale interfacial properties on the macroscopic mixing of particles** ;
- study of the **MHD processes in turbulent plasmas**.

The following pages briefly describe these different axis, giving the origin of the associated questions and the intended investigation tracks.

6.2 Influence of large scale properties of turbulence

This work aims at investigating the influence of large scale properties (mainly homogeneity, anisotropy, confinement and Reynolds number) of a turbulent flow on the small scales dynamics, the transport phenomena, but also the long-term stability of the flow.

This investigation requires the ability to produce turbulent flows with different –and ideally, tunable– large scale properties. To this end I will take advantage of several apparatuses available at LEGI and at Laboratoire de Physique de l'École Normale Supérieure de Lyon, and more particularly of the active grid which I have recently implemented in the wind-tunnel at LEGI, of a water tunnel available at LEGI and of the LEM (Lagrangian Exploration Module) which I have contributed to develop at the Laboratoire de Physique de l'École Normale Supérieure de Lyon (and also in collaboration with the Max Planck Institute of Göttingen).

Our active grid is made of 8 horizontal and eight vertical rotating bars, each mounted with square flaps (figure 6.1a). Each bar is independently driven by a dedicated step motor. Active grids [60, 81] are known for their versatility and their capacity to increase the size of the large structures of the flow. As a consequence they offer simultaneously the possibility to significantly increase the available Reynolds number in our wind-tunnel and to modify the large scale homogeneity and isotropy of the flow, which can be tuned depending on the forcing protocol of the rotating bars.

The water tunnel, originally designed and built by J.-P. Thibault for MHD investigations in salted water, is being redesigned in collaboration with N. Mordant, for wall turbulence studies. In particular, the cross section of the tunnel, which is at the moment square (10cm x 10cm) will be changed to an elongated rectangular section (2.5cm x 30cm).

The L.E.M. is somehow to the usual von Kármán flow, what the active grid is to the classical passive grid. It consists of a closed icosahedron full of water, with 12 independent impellers driving the flow (figure 6.1b). The large scale isotropy of the flow can be tuned depending on the driving protocol of the 12 motors.

Besides their individual interest, these flows are also complementary as for instance L.E.M. is a confined and bounded flow where the turbulence is constantly forces, while wind and water tunnels are an open flows where the turbulence decays downstream. All together, these facilities will therefore allow to explore Reynolds number effects, large scale anisotropy and homogeneity effects and confinement/forcing effects.

I plan to investigate the influence of these large scale properties on different aspects :

• *Influence on the small scales of turbulence.* This is in the continuity of the study on the validity of the local isotropy hypothesis already described in section 2.5. The focus will be put on exploring the return to isotropy when the large scale properties are progressively finely tuned to almost perfect isotropy to highly non-isotropic. The influence of confinement in the return to isotropy at small scales will also be explored. The results are potentially important for the refinement of sub-scale models in LES simulations.

• *Influence on the long term dynamic of the flow.* The von Kármán flow is known to exhibit long term dynamics, especially concerning the random motion of the shear layer in the mid plane which fluctuates on time scales exceeding thousands of turn over times [30]. The origin of this slow dynamics remains mysterious, but may be related to the large scale symmetry properties of the flow. I will use the versatility of the LEM to investigate the role of symmetries on this slow scale dynamics. This can be done for instance by considering only two face-to-face motors in the LEM in a counter-rotating von Kármán configuration, the other ten being used to perturb the large scale symmetry of the base flow.

• *Influence of the large scale properties on the transport of particles.* I will in particular focus on the possible influence of large scale anisotropy and confinement of the flow on the shape of finite size particles acceleration PDFs. This is motivated by the observation that for a given flow acceleration PDFs of finite size particles has been shown to be robust (see section 3.2), but that it is found different, at equivalent Reynolds number, for particles in the wind-tunnel and in von Kármán flows. The possible influence of confinement on acceleration statistics has been recently proven numerically by Kadoch *et al.* [53].

I would also like to mention here other ongoing collaborations which will contibrute to these investigations :

– I collaborate with B. Rousset at CEA/SBT and other members of the SHREK project to investigate turbulence in a von Kármán flow of liquid Helium (fluid and super-fluid).
– I coordinate a project aiming at investigating classic grid turbulence in the very large scale wind-tunnel S1MA at ONERA in Modane. This experiment should run in 2013 and will give unprecedented high resolution data of simultaneous Eulerian and Lagrangian statistics which we expect will become the standard for experimental characterization of homogeneous isotropic turbulence.

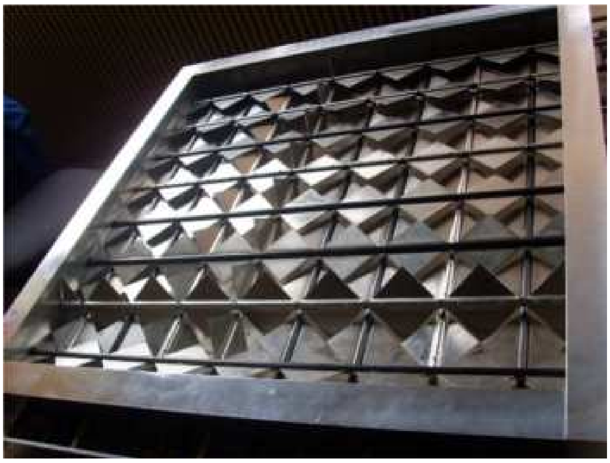

(a)

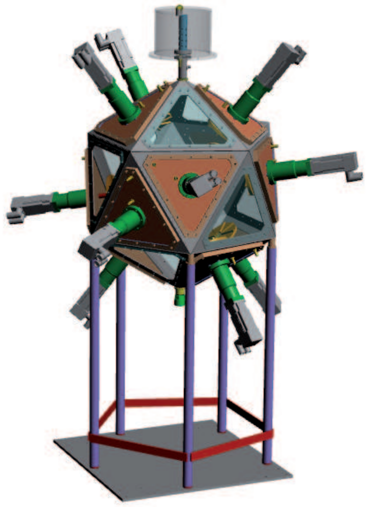

(b)

FIG. 6.1 – (a) New active grid at L.E.G.I.. (b) The Lagrangian Exploration Module at Laboratoire de Physique de l'École Normale Supérieure de Lyon.

– I also coordinate the work-package "particles and fields" of the EuHIT I^3 European proposal submitted at the end 2011. The proposed investigations aim at investigating several aspects of Lagrangian turbulence and transport phenomena in different large scale European facilities (including the SF6 wind-tunnel in Göttingen, the Coriolis platform and cryogenic flows at CEA and CERN).

6.3 Collective effects of particles in turbulence

This work aims at characterizing and improving the modeling of collective effects of particles transported in a turbulent flow. Such collective effects can arise for instance inside clusters of inertial particles, as subtle couplings between the particles (either via hydrodynamics interactions or direct collisions) appear.

• *Influence of spray polydispersity.* The characterization of clustering and preferential concentration carried so far with the water spray in the wind-tunnel has revealed the difficulty to produce monodisperse sprays and the difficulty to interpret the results the polydispersity is high. In order to improve the study of the size dependence (or equivalently the Stokes number dependence) of preferential concentraion, it is required either to produce a more monodisperse spray or to measure particles size simultaneously with their dynamics and concentration field characterization. The latter solution is being explored by coupling the Voronoï analysis to a Mie scattering technique [46].

•*The relevance of Stokes number as indicator of preferential concentration.* Preferential concentration is generally quantified in terms of particles Stokes number. The investigation reported in chapter 3 shows indeed that preferential concentration is optimal for Stokes number around unity. However, the results presented for the turbulent transport of individual finite size particles in the same chapter clearly indicate that their dynamics is weakly affected by Stokes number effects. A natural continuation of these two observations is then to investigate the preferential concentration phenomenon for finite size particles. This is part of the postdoctoral work of Lionel Fiabane (which I supervise in collaboration with R. Volk), who is presently investigating in the LEM the clustering properties of neutrally buoyant particles significantly larger than the dissipation scale (which are known not to behave as fluid tracers). The first results on such particles, over a range of Stokes number from 1 to 20, indicate that their distribution

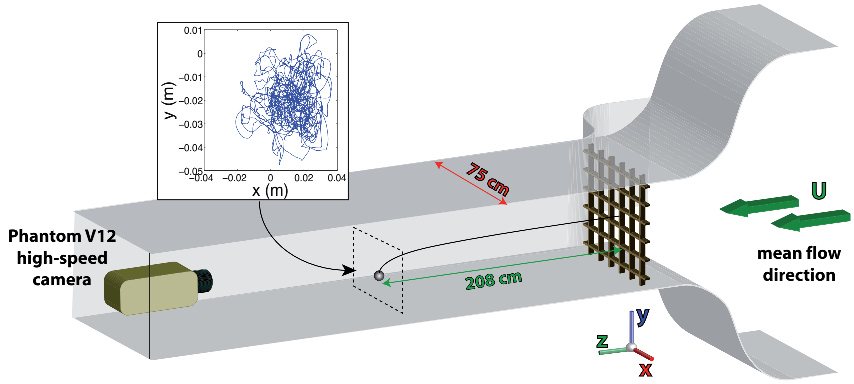

Fig. 6.2 – Investigation of the dynamics of a towed particle in the wind-tunnel at LEGI. Particle motion in the transverse direction is recorded using a high-speed camera.

is exactly that of a random process with no sign of clustering. This study is now being completed by considering finite size glass particles (hence denser than water) in the same range of Stokes number.

• *Study of the structure and dynamics of the clusters.* I will use the developed Voronoï analysis to investigate the 3D structure of particle clusters and their temporal dynamics. The 3D structure will be studied by illuminating the tunnel with a transverse laser sheet, the third dimension being probed thanks to the advection of the spray (using a usual frozen field Taylor hypothesis). The temporal dynamics will be investigated by pursuing the effort in coupling Voronoï analysis to Lagrangian tracking. This study will consider on one side particles individually, looking for correlation between their Lagrangian dynamics and the local concentration given by the area of their Voronoï cell along their trajectory, and on the other side the collective dynamics of the cluster as a whole. This information is believed to be important for the modelisation of collective effects [2].

• *Study of particles mass transfer.* I will investigate several aspects of mass transfer in presence of turbulence, including the influence of turbulence rate on accretion processes and the measurement of particles collision kernel. Accretion processes will be investigated by considering the mass increase of a fixed sphere in the wind-tunnel seeded with a water spray (subsequently the drying rate of the same wet sphere, and the influence of turbulence level will also be investigated). The turbulence level will mainly be varied by considering successively the wind-tunnel without grid (fluctuation level is then of order a few per thousands) with the passive grid (a few percents) and with the active grid (about 20 percent). Collisions between water droplets in the spray will also be investigated by measuring the relative velocity between particles pairs to estimate the collision kernel. An important aspect will be to correlate this estimation to the preferential concentration analysis and to evaluate the impact on particles coalescence rate.

6.4 The role of turbulent drag on the motion of finite size objects

Most of theoretical and numerical works for freely advected particles in a turbulent flow only consider the drag force acting on the particle, resulting from the slippage velocity between the particle and the fluid induced by the inertia of the particle. However, the results on the Lagrangian of finite size particles in chapter 3 show that these stokesian models fail to predict even simple features of the dynamics of the particles. In particular the filtering scenario by which particles dynamics is related to that of the carrier flow by a low-pass filtering effect at the particle viscous response time does not appear as relevant. This observations motivate new experiments trying to emphasize the role of hydrodynamics forces related to the relative velocity between the particle and the fluid.

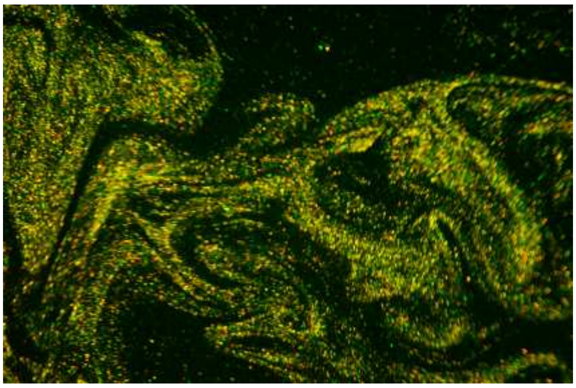

(a)

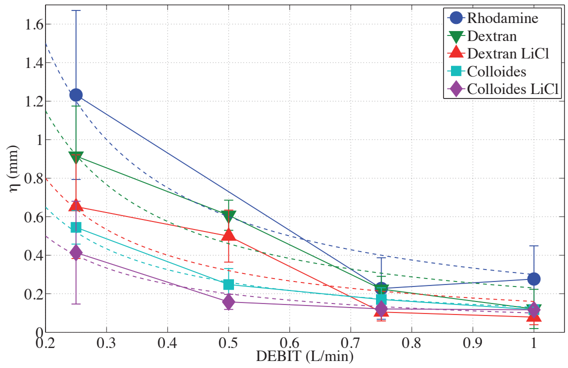

(b)

FIG. 6.3 – (a) Concnetration field of rhodamine colloids from LIF measurements in a turbulent jet. (b) Mixing indicator (corresponding to coarse-grained length scale as defined in [104]) for differente substances with and without gradient of LiCl.

This will be achieved by considering objects in the wind-tunnel with a constrained motion. At the moment I plan to investigate two main situations :

• *The dynamics of of a towed particles in a turbulent environment.* I want to investigate the dynamics of a semi-constrained particle with an imposed dominant motion relative to the surrounding fluid. This is achieved by considering a particle attached to a thin longitudinal wire in a wind tunnel experiment (see figure 6.2) ; as the particle is attached its streamwise motion is blocked what imposes a strong slippage velocity and therefore a strong drag force. On the other hand, the particle is free to move in the transverse directions x and y. In the reference frame moving at the mean wind velocity, this situation is equivalent to that of a particle towed at constant velocity. The first preliminary results on this geometry, obtained during Martin Obligado's PhD which I supervise, show that a filtering scenario is realistic. An important role to be explored now is the role of fluctuation rate of the dynamics of the towed particle. This question will be address by successively exploring the case without any grid, with the classic grid and with the active grid.

• *The behavior of a pendulum in a turbulent mean flow.* I want to investigate the equilibrium and the oscillations of a pendulum in the wind-tunnel with different fluctuation levels and different shapes of pendulum. A first study using a flat circular plate (4 cm in diameter) at the tip of a pendulum have revealed an hysteric behavior of the equilibrium position (when the mean wind velocity is increased and then decreased) with a domain of forbidden angular positions. The hysteresis seems to be reduced when the turbulence level increases. It is likely that this behavior results from the coupling between drag and lift forces acting on the disc. Further experiments and simulations are been carried. I also plan to investigate the case of a sphere, for which only drag is present. This geometry will be particularly enlightening for the exploration of the influence of turbulent fluctuation rate on the drag coefficient of a sphere. Most experimental studies on this question have essentially been limited to low fluctuation rates (of the order of a few percents) while our active grid will allow to push above 20%.

6.5 Influence of nano and micro-scale interfacial properties on the macroscopic mixing of particles

This work aims at investigating the role played by subtle interfacial effects on the macroscopic mixing of particles. This is primarily motivated by the recent observation that the diffusion of colloids in microfluidic devices can be enhanced or reduced when coupled to salt gradients, via an effect called diffusiophoresis [1]. This study, carried by the group "Liquids at Interfaces" at LPMCN (University of

Lyon) has shown that the effective diffusivity D of particles or macromolecules can be varied up to two orders of magnitude in the presence of salt gradients. In collaboration with LPMCN, we propose a "bottom-up" approach in order to explore the possible role of diffusiophoresis on macroscopic mixing. Turbulent mixing is indeed known to be affected by the Schmidt number ($Sc = \nu/D$, where ν is the kinematic viscosity of the fluid and D the molecular diffusivity) of the mixed substance [104] ; it is therefore possible that the influence on the effective diffusivity due to the nanoscale diffusiophoretic effect, may impact the large scale mixing.

To this end a first series of experiments has been carried out to investigate the influence of salt gradients on the mixing of colloids injected in a turbulent jet (this was done in collaboration with R. Volk at the Laboratoire de Physique de l'École Normale Supérieure de Lyon during the Master's training of N. Machicoane which I supervised). Measurements are done using Laser Induced Fluorescence (LIF) (see figure 6.3).

First results are very encouraging. We have shown that the mixing of rhodamine colloids is indeed decelerated when they are injected together with salt water, consistently with an increase of the effective Schmidt number of the colloids induced by a diffusiophoretic mechanism. We have now to quantify more precisely this phenomenon and to check that mixing is accelerated when the salt gradient is reversed.

6.6 MHD processes in turbulent plasmas

This work will be done at Laboratoire de Physique de l'École Normale Supérieure de Lyon, as part of the DYPTIC project coordinated by N. Plihon. It is a natural continuation of previous investigations of MHD coupling between magnetic fields and turbulence I carried in liquid metals. As already discussed, because of the low value of the magnetic Prandtl number of liquid metals ($P_m = \nu/\eta$ with ν the kinematic viscosity and η the magnetic diffusivity), high magnetic Reynolds number R_m can only be achieved in highly turbulent conditions (because $R_m = P_m Re$, where Re is the kinetic Reynolds number). As a consequence, the scales of magnetic fluctuations in liquid metals are much larger than that of the velocity field (the ratio between the magnetic and the viscous dissipation scales as P_m). This is particularly problematic for instance for numerical simulations of the dynamo instability in liquid metals which would require unreachable resolution (state of the art direct numerical simulations of the dynamo instability are limited to magnetic Prandtl numbers of the ordre $P_m \sim 0.1$). An interesting property of plasmas is the capacity to vary their Prandtl number of the medium over several order of magnitudes. The benefit is mulitple : (i) this will help bridging the gap between existing liquid metals experiments (at $P_m \sim 10^{-5}$) and direct numerical simulations (at $P_m \sim 0.1$) ; (ii) it will allow investigating separately the influence of P_m and R_m on MHD processes and (iii) it will offer a new experimental tool to investigate turbulence in plasmas. Beyond the fundamental interest, these questions are also of practical importance as such MHD coupling in turbulent conditions dominate in fusion plasmas.

Bibliographie

[1] B. Abecassis, C. Cottin-Bizonne, C. Ybert, A. Ajdari, and L. Bocquet. Boosting migration of large particles by solute contrasts. *Nature Materials*, 7(10) :785–789, OCT 2008.

[2] A. Aliseda, A. Cartellier, F. Hainaux, and J.C. Lasheras. Effect of preferential concentration on the settling velocity of heavy particles in homogeneous isotropic turbulence. *Journal of Fluid Mechanics*, 468 :77–105, 2002.

[3] F Anselmet, Y Gagne, Ej Hopfinger, and R. A. Antonia. High-order velocity structure functions in turbulent shear flows. *Journal of Fluid Mechanics*, 140(MAR) :63–89, 1984.

[4] A. Arneodo, C. Baudet, F. Belin, R. Benzi, B. Castaing, B. Chabaud, R. Chavarria, S. Ciliberto, R. Camussi, F. Chillà, B. Dubrulle, Y. Gagne, B. Hebral, J. Herweijer, M. Marchand, J. Maurer, J. F. Muzy, A. Naert, A. Noullez, J. Peinke, F. Roux, P. Tabeling, W. van de Water, and H. Willaime. Structure functions in turbulence, in various flow configurations, at reynolds number between 30 and 5000, using extended self-similarity. *Europhysics Letters*, 34(6) :411, 1996.

[5] S. Ayyalasomayajula, A. Gylfason, L.R. Collins, E. Bodenschatz, and Z. Warhaft. Lagrangian measurements of inertial particle accelerations in grid generated wind tunnel turbulence. *Physical Review Letters*, 97 :144507, 2006.

[6] Sathyanarayana Ayyalasomayajula, Armann Gylfason, and Zellman Warhaft. Lagrangian measurements of fluid and inertial particles in decaying grid generated turbulence. In Yukio Kaneda, editor, *IUTAM Symposium on Computational Physics and New Perspectives in Turbulence*, volume 4, pages 171–175, Nagoya, Japan, September, 11-14 2006. Nagoya University, Springer.

[7] G. K. Batchelor. The theory of axisymmetric turbulence. *Proceedings of The Royal Society of London Series A-Mathematical and Physical Sciences*, 186(1007) :480–502, 1946.

[8] G. K. Batchelor. The application of the similarity theory of turbulence to atmospheric diffusion. *Quarterly Journal of the Royal Meteorological Sociey*, 76(328) :133–146, 1950.

[9] G. K. Batchelor. Diffusion in a field of homogeneous turbulence II. The relative motion of particles. *Proceedings of the Cambridge Philosophical Society*, 48(2) :345–362, 1952.

[10] Jeremy Bec, Luca Biferale, Guido Boffetta, Antonio Celani, Massimo Cencini, Alessandra Lanotte, S. Musacchio, and Federico Toschi. Acceleration statistics of heavy particles in turbulence. *Journal of Fluid Mechanics*, 550 :349–358, 2006.

[11] R. Benzi, L. Biferale, R. Fisher, D. Q. Lamb, and F. Toschi. Inertial range Eulerian and Lagrangian statistics from numerical simulations of isotropic turbulence. *JOURNAL OF FLUID MECHANICS*, 653 :221–244, JUN 25 2010.

[12] Roberto Benzi, Sergio Ciliberto, R. Tripiccione, Christophe Baudet, F. Massaioli, and S. Succi. Extended self-similarity in turbulent flows. *Physical Review E*, 48 :R29, 1993.

[13] L. Biferale, G. Boffetta, A. Celani, B. J. Devenish, A. Lanotte, and F. Toschi. Lagrangian statistics of particles pairs in homogeneous isotropic turbulence. *Physics of Fluids*, 17 :115101, November 2005.

[14] L Biferale, G Boffetta, A Celani, BJ Devenish, A Lanotte, and F Toschi. Multifractal statistics of Lagrangian velocity and acceleration in turbulence. *Physical Review Letters*, 93(6), AUG 6 2004.

[15] L Biferale, G Boffetta, A Celani, A Lanotte, and F Toschi. Particle trapping in three-dimensional fully developed turbulence. *Physics Of Fluids*, 17(2), FEB 2005.

[16] L Biferale and I Procaccia. Anisotropy in turbulent flows and in turbulent transport. *PHYSICS REPORTS-REVIEW SECTION OF PHYSICS LETTERS*, 414(2-3) :43–164, JUL 2005.

[17] G Boffetta and A Celani. Pair dispersion in turbulence. *Physica A*, 280(1-2) :1–9, MAY 15 2000. International Conference on Statistical Mechanics and Strongly Correlated Systems, ROME, ITALY, SEP 27-29, 1999.

[18] M. S. Borgas. The multifractal lagrangian nature of turbulence. *Philosophical Transactions of the Royal Society of London Series A-Mathematical Physical And Engineering Sciences*, 342(1665) :379–411, FEB 15 1993.

[19] M. Bourgoin, R. Volk, P. Frick, S. Khripchenko, Ph. Odier, and J.-F. Pinton. Induction mechanisms in von karman swirling flows of liquid gallium. *Magnetohydrodynamics*, 40(1) :13–31, 2004.

[20] Mickaël Bourgoin, Louis Marié, François Pétrélis, Cécile Gasquet, Alain Guigon, Jean-Baptiste Luciani, Marc Moulin, Frédéric Namer, Javier Burguete, Arnaud Chiffaudel, François Daviaud, Stephan Fauve, Philippe Odier, and Jean-François Pinton. Magnetohydrodynamics measurement in the von kármán sodium experiment. *Physics of Fluids*, 14(9) :3046–3058, 2002.

[21] Mickaël Bourgoin, Nicholas T. Ouellette, Haitao Xu, Jacob Berg, and Eberhard Bodenschatz. The role of pair dispersion in turbulent flow. *Science*, 311 :835, February 2006.

[22] Rachel D. Brown, Z. Warhaft, and Greg A. Voth. Acceleration Statistics of Neutrally Buoyant Spherical Particles in Intense Turbulence. *PHYSICAL REVIEW LETTERS*, 103(19), NOV 6 2009.

[23] Edward C. Bullard. The stability of a homopolar dynamo. *Proceedings of the Cambrdige Philosophical Society*, 51(744), 1955.

[24] Enrico Calzavarini, Romain Volk, Mickaël Bourgoin, Emmanuel Lévêque, Jean-François Pinton, and Federico Toschi. Acceleration statistics of finite-sized particles in turbulent flow : the role of faxen forces. *Journal of Fluid Mechanics*, in press, 2009.

[25] S Chandrasekhar. The theory of axisymmetric turbulence. *Philosophical Transactions of The Royal Society of London Series A-Mathematical and Physical Sciences*, 242(855) :557–577, 1950.

[26] SY Chen, B Dhruva, S Kurien, KR Sreenivasan, and MA Taylor. Anomalous scaling of low-order structure functions of turbulent velocity. *Journal Of Fluid Mechanics*, 533 :183–192, JUN 25 2005.

[27] Laurent Chevillard, Stéphane G. Roux, Émmanuel Lévêque, Nicolas Mordant, Jean-François Pinton, and Alain Arnéodo. Lagrangian velocity statistics in turbulent flows : Effects of dissipation. *Physical Review Letters*, 91(21) :214502, 2003.

[28] R. Clift, J. R. Grace, and M. E. Weber. *Bubbles, drops and particles*. Academic Press, New York, 1978.

[29] S. W. Coleman and J. C. Vassilicos. A unified sweep-stick mechanism to explain particle clustering in two- and three-dimensional homogeneous, isotropic turbulence. *Physics of Fluids*, 21(11) :113301, November 2009.

[30] E. Crespo Del Arco, J. J. Sanchez-Alvarez, E. Serre, A. De La Torre, and J. Burguete. Numerical and experimental study of the time-dependent states and the slow dynamics in a von karman swirling flow. *Geophysical and Astrophysical Fluid Dynamics*, 103(2-3) :163–177, 2009.

[31] P. A. Davidson and B. R. Pearson. Identifying turbulent energy distributions in real, rather than fourier, space. *Phys. Rev. Lett.*, 95(21) :214501, Nov 2005.

[32] E. Deutsch and O. Simonin. Large eddy simulation applied to the motion of particles in stationary homogeneous fluid turbulence. *in Turbulence Modification in Multiphase Flow, ASME-FED*, 110 :35–42, 1991.

[33] Jarai-Szabo Ferenc and Zoltan Neda. On the size distribution of poisson voronoi cells. *Physica A-Statistical Mechanics and Its Applications*, 385(2) :518–526, November 2007.

[34] Jr Fessler, Jd Kulick, and Jk Eaton. Preferential concentration of heavy-particles in a turbulent channel flow. *Physics of Fluids*, 6(11) :3742–3749, November 1994.

[35] U. Frisch. *Turbulence : The Legacy of A. N. Kolmogorov*. Cambridge University Press, Cambridge, England, 1995.

[36] Y. Gagne, M. Marchand, and B. Castaing. Conditional velocity pdf in 3d-turbulence. *Journal de Physique II*, 4 :1–8, 1994.

[37] Agris Gailitis, Olgerts Lielausis, Sergej Dement'ev, Ernests Platacis, Arnis Cifersons, Gunter Gerbeth, Thomas Gundrum, Frank Stefani, Michael Christen, Heiko Hänel, and Gotthard Will. Detection of a flow induced magnetic field eigenmode in the riga dynamo facility. *Physical Review Letters*, 84 :4365–4368, 2000.

[38] S Garg and Z Warhaft. On the small scale structure of simple shear flow. *PHYSICS OF FLUIDS*, 10(3) :662–673, MAR 1998.

[39] Renée Gatignol. The faxen formulas for a rigid particle in an unsteady non-uniform stoke flow. *Journal de Mécanique théorique et appliquée*, 2(2) :143–160, 1983.

[40] W. K. George, P. D. Beuther, and R. E. A. Arndt. Pressure spectra in turbulent free shear flows. *Journal of Fluid Mechanics*, 148 :155, 1984.

[41] Philippe Gervais. *Mesure acoustique de vitesse Lagrangienne dans un jet d'air turbulent*. PhD thesis, Université Joseph Fourier, Grenoble, France, Mai 2005.

[42] André Giesecke, Frank Stefani, and Gunter Gerbeth. Role of soft-iron impellers on the mode selection in the von kármán˘sodium dynamo experiment. *Phys. Rev. Lett.*, 104 :044503, Jan 2010.

[43] S. Goto and J. C. Vassilicos. Self-similar clustering of inertial particles and zeroacceleration points in fully developed two-dimensional turbulence. *Physics of Fluids*, 18 :115103, 2006.

[44] Susumu Goto and J. C. Vassilicos. Sweep-stick mechanism of heavy particle clustering in fluid turbulence. *Physical Review Letters*, 100(5) :054503, 2008.

[45] Toshiyuki Gotoh and Daigen Fukayanna. Pressure spectrum in homogeneous turbulence. *Physical Review Letters*, 86(17) :3775–3778, 2001.

[46] A Grassmann and F Peters. Size measurement of very small spherical particles by mie scattering imaging (msi). *Particle & Particle Systems Characterization*, 21(5) :379–389, December 2004.

[47] J.-L. Guermond, J. Léorat, F. Luddens, C. Nore, and A. Ribeiro. Effects of discontinuous magnetic permeability on magnetodynamic problems. *Journal of Computational Physics*, 230 :6299–6319, 2011.

[48] S. R. HANNA. Lagrangian and Eulerian time-scale relations in the daytime boundary-layer. *Journal Of Applied Meteorology*, 20(3) :242–249, 1981.

[49] Holger Homann and Jeremie Bec. Finite-size effects in the dynamics of neutrally buoyant particles in turbulent flow. *Journal of Fluid Mechanics*, 651 :81–91, MAY 25 2010.

[50] Holger Homann, Daniel Schulz, and Rainer Grauer. Conditional eulerian and lagrangian velocity increment statistics of fully developed turbulent flow. *Physics of Fluids*, 23(5) :055102, 2011.

[51] Norden E. Huang, Zheng Shen, Steven R. Long, Manli C. Wu, Hsing H. Shih, Quanan Zheng, Nai-Chyuan Yen, Chi Chao Tung, and Henry H. Liu. The empirical mode decomposition and the hilbert spectrum for nonlinear and non-stationary time series analysis. *Proceedings of the Royal Society of London. Series A : Mathematical, Physical and Engineering Sciences*, 454(1971) :903–995, 1998.

[52] R. H. A. Ijzermans, M. W. Reeks, E. Meneguz, M. Picciotto, and A. Soldati. Measuring segregation of inertial particles in turbulence by a full lagrangian approach. *Physical Review E*, 80 :015302, 2009.

[53] B. Kadoch, Wouter Bos, and K. Schneider. Extreme lagrangian acceleration in confined turbulent flow. *Physical Review Letters*, 100 :184503, 2008.

[54] A Kolmogoroff. The local structure of turbulence in incompressible viscous fluid for very large Reynolds numbers. *Dokl. Akacl. Nauk SSSR*, 30 :301–305, 1941.

[55] AN Kolmogoroff. Dissipation of energy in the locally isotropic turbulence. *Dokl. Akad. Nauk SSSR*, 32 :16–18, JUL 1941.

[56] A. N. Kolmogorov. Refining the notions of the local structure of turbulence in an incompressible viscous fluid at high reynolds numbers. In *Mecanique de la turbulence*, pages 447–458. CNRS, Paris, 1962.

[57] Arthur LaPorta, Greg A. Voth, Alice M. Crawford, Jim Alexander, and Eberhard Bodenschatz. Fluid particle accelerations in fuly developped turbulence. *Nature*, 409 :1017, February 2001.

[58] R-C. Lien, E. A. D'Asaro, and G. T. Dairiki. Lagrangian frequency spectra of vertical velocity and vorticity in high-reynolds-number oceanic turbulence. *Journal of Fluid Mechanics*, 362 :177, 1998.

[59] RC Lien and EA D'Asaro. The Kolmogorov constant for the Lagrangian velocity spectrum and structure function. *Physics Of Fluids*, 14(12) :4456–4459, DEC 2002.

[60] Hideharu Makita. Realization of a large-scale turbulence field in a small wind tunnel. *Fluid Dynamics Research*, 8 :53–64, 1991.

[61] M. Maxey. The gravitational settling of aerosol-particles in homogeneous turbulence and random flow-fields. *Journal of Fluid Mechanics*, 174 :441–465, January 1987.

[62] Martin R. Maxey and James J. Riley. Equation of motion for a small rigid sphere in a nonuniform flow. *Physics of Fluids*, 26(4) :883–889, 1983.

[63] IM Mazzitelli and D Lohse. Lagrangian statistics for fluid particles and bubbles in turbulence. *New Journal Of Physics*, 6, DEC 22 2004.

[64] A. S. Monin and A. M. Yaglom. *Statistical fluid mechanics*, volume II. MIT press, 1975.

[65] N. Mordant, J. Delour, E. Léveque, O. Michel, A. Arnéodo, and J.-F. Pinton. Lagrangian velocity fluctuations in fully developed turbulence : scaling, intermittency and dynamics. *Journal of Statistical Physics*, 113 :701–717, 2003.

[66] Nicolas Mordant. *Mesures Lagrangiennes en turbulence : mise en oeuvre et analyse*. PhD thesis, École Normale Supérieure de Lyon, Lyon, France, Novembre 2001.

[67] Nicolas Mordant, Pascal Metz, Olivier Michel, and Jean-François Pinton. Measurement of lagrangian velocity in fully developed turbulence. *Physical Review Letters*, 87(21) :214501, 2001.

[68] Mark Nelkin. Universality and scaling in fully developed turbulence. *Advances in Physics*, 43(2) :143–181, 1994.

[69] M. D. Nornberg, E. J. Spence, R. D. Kendrick, C. M. Jacobson, and C. B. Forest. Intermittent magnetic field excitation by a turbulent flow of liquid sodium. *Physical Review Letters*, 97 :044503, 2006.

[70] A. M. Oboukhov. On the distribution of energy in the spectrum of a turbulent flow. *Izv. Akad. Nauk SSSR*, 5 :453–466, 1941.

[71] A. M. Obukhov. Pressure fluctuations in a turbulent flow. *Doklady Akademii Nauk SSSR*, 3 :49–68, 1949.

[72] A. M. Obukhov. Some specific features of atmospheric turbulence. *Journal of Fluid Mechanics*, 13 :77–81, 1962.

[73] Piero Olla. Preferential concentration versus clustering in inertial particle transport by random velocity fields. *Phys. Rev. E*, 81(1) :016305, Jan 2010.

[74] Soren Ott and Jakob Mann. An experimental investigation of the relative diffusion of particle pairs in three-dimensional turbulent flow. *Journal of Fluid Mechanics*, 422 :207–223, 2000.

[75] Nicholas T. Ouellette, Haitao Xu, and Eberhard Bodenschatz. A quantitaive study of three-dimensional lagrangian particle tracking algorithms. *Experiments in Fluids*, 39(4) :722–729, 2005.

[76] M Ould-Rouiss. The axisymmetric equivalent of Kolmogorov's equation. *European Physical Journal B*, 23(1) :107–120, SEP 2001.

[77] G. Parisi and U. Frisch. A multifractal model of intermittency. In M.Ghil, R. Benzi, and G. Parisi, editors, *Turbulence and predictability in geophysical fluid dynamics and climate dynamics*, pages 84–87, Amsterdam, 1985. Eds. North Holland.

[78] François Pétrélis and Stephan Fauve. Chaotic dynamics of the magnetic field generated by dynamo action in a turbulent flow. *Journal of Physics : Condensed Matter*, 20 :494203, 2008.

[79] François Pétrélis, Nicolas Mordant, and Stephan Fauve. On the magnetic fields generated by experimental dynamos. *Geophysical and Astrophysical Fluid Dynamics*, 101 :289, 2007.

[80] Yu. B. Ponomarenko. On the theory of hydromagnetic dynamo. *J. Appl. Mech. Tech. Phys.*, 14 :775–778, 1973.

[81] R. Poorte and A. Biesheuvel. Experiments on the motion of gas bubbles in turbulence generated by an active grid. *Journal of Fluid Mechanics*, 461 :127–154, JUN 25 2002.

[82] Cedric Poulain, Nicolas Mazellier, Philippe Gervais, Yves Gagne, and Christophe Baudet. Spectral vorticity and lagrangian velocity measurements in turbulent jets. *Flow, Turbulence and Combustion*, 72 :245–271, 2004.

[83] Alain Pumir and Boris I. Shraiman. Persistent small scale anisotropy in homogeneous shear flows. *Phys. Rev. Lett.*, 75(17) :3114–3117, Oct 1995.

[84] Nauman M. Qureshi, Unai Arrieta, Christophe Baudet, Yves Gagne, and Mickaël Bourgoin. Acceleration statistics of inertial particles in turbulent flow. *European Physical Journal B*, 66 :531–536, 2008.

[85] Nauman M. Qureshi, Mickaël Bourgoin, Christophe Baudet, Alain Cartellier, and Yves Gagne. Turbulent transport of material particles : an experimental study of finite size effects. *Physical Review Letters*, 99 :184502, 2007.

[86] Mark Peter Rast and Jean-Fran çois Pinton. Pair dispersion in turbulence : The subdominant role of scaling. *Phys. Rev. Lett.*, 107 :214501, Nov 2011.

[87] MW Reeks. On probability density function equations for particle dispersion in a uniform shear flow. *Journal of Fluid Mechanics*, 522 :263–302, January 2005.

[88] Lewis F. Richardson. Atmospheric diffusion shown on a distance-neighbour graph. *Proceedings of the Royal Society of London, Series A*, 110(756) :709–737, April 1926.

[89] G. O. Roberts. Dynamo action of fluid motions with two-dimensional periodicity. *Phil. Trans. R. Soc. London, Ser. A*, 271 :411–454, 1972.

[90] H. C. RODEAN. The universal constant for the lagrangian structure-function. *Physics of Fluids A*, 3(6) :1479–1480, JUN 1991.

[91] Juan P. L. C. Salazar, Jeremy de Jong, Lujie Cao, Scott H. Woodward, Hui Meng, and Lance R Collins. Experimental and numerical investigation of inertial particle clustering in isotropic turbulence. *Journal of Fluid Mechanics*, 600 :245–256, 2008.

[92] Ewe Wei Saw, Raymond A. Shaw, Sathyanarayana Ayyalasomayajula, Patrick Y. Chuang, and Armann Gylfason. Inertial clustering of particles in high-reynolds-number turbulence. *Physical Review Letters*, 100(21), MAY 30 2008.

[93] B. L. Sawford. Reynolds number effects in lagrangian stochastic models of tur bulent dispersion. *Physics of Fluids A*, 3(6) :1577–1586, 1991.

[94] Brian Sawford. Turbulent relative dispersion. *Annual Review of Fluid Mechanics*, 33 :289–317, 2001.

[95] Stephen J. Scott, Aditya U. Karnik, and John S. Shrimpton. On the quantification of preferential accumulation. *INTERNATIONAL JOURNAL OF HEAT AND FLUID FLOW*, 30(4) :789–795, AUG 2009.

[96] K. D. Squires and J. K. Eaton. Preferential concentration of particles by turbulence. *Physics of Fluids A*, 3(5) :1169–1178, 1991.

[97] K. R. Sreenivasan. On the universality of the kolmogorov constant. *Physics of Fluids*, 7(11) :2778–2784, NOV 1995.

[98] R. Stieglitz and U. Müller. Experimental demonstration of a homgeneous two-scale dynamo. *Physics of Fluids*, 13 :561, 2001.

[99] D. Sweet, E. Ott, J. M. Finn, T. M. Jr Antonsen, and D. P. Lathrop. Blowout bifurcations and the onset of magnetic activity in turbulent dynamos. *Physical Review E*, 63 :066211, 2001.

[100] G. I. Taylor. Diffusion by continuous movements. *Proceedings of London Mathematical Society*, 20(1) :196–212, 1922.

[101] H. Tennekes and J. L. Lumley. *A first course in turbulence*. MIT press, 1992.

[102] M Uhlmann. An immersed boundary method with direct forcing for the simulation of particulate flows. *Journal of Computational Physics*, 209(2) :448–476, November 2005.

[103] Prakash Vedula and P. K. Yeung. Similarity scaling of acceleration and pressure statistics in numerical simulations of isotropic turbulence. *Physics of Fluids*, 11(5) :1208–1220, 1999.

[104] E. Villermaux and J. Duplat. Coarse grained scale of turbulent mixtures. *Physical Review Letters*, 97(14), October 2006.

[105] Marko Virant and Themistocles Dracos. 3D PTV and its application on lagrangian motion. *Measurement science and technology*, 8 :1539–1552, 1997.

[106] R. Volk, E. Calzavarini, E. Leveque, and J-F Pinton. Dynamics of inertial particles in a turbulent von karman flow. *Journal of Fluid Mechanics*, 668 :223–235, February 2011.

[107] R. Volk, E. Calzavarini, G. Verhille, D. Lohse, N. Mordant, J. F. Pinton, and F. Toschi. Acceleration of heavy and light particles in turbulence : Comparison between experiments and direct numerical simulations. *Physica D*, 237(14-17) :2084–2089, 2008.

[108] GA Voth, K Satyanarayan, and E Bodenschatz. Lagrangian acceleration measurements at large reynolds numbers. *Physics of Fluids*, 10(9) :2268–2280, September 1998.

[109] Greg A. Voth, Arthur LaPorta, Alice M. Crawford, Jim Alexander, and Eberhard Bodenschatz. Measurement of particle accelerations in fully developed turbulence. *Journal of Fluid Mechanics*, 469 :121–160, 2002.

[110] Z. Warhaft and J. L. Lumley. Experimental-study of decay of temperature-fluctuations in grid-generated turbulence. *Journal Of Fluid Mechanics*, 88(OCT) :659–684, 1978.

[111] KA Weinman and AY Klimenko. Estimation of the Kolmogorov constant C-0 by direct numerical simulation of a continuous scalar. *Physics of Fluids*, 12(12) :3205–3220, DEC 2000.

[112] P. K. Yeung. Lagrangian investigations of turbulence. *Annual Review of Fluid Mechanics*, 34 :115–142, 2002.

[113] H. Yoshimoto and S. Goto. Self-similar clustering of inertial particles in homogeneous turbulence. *Journal of Fluid Mechanics*, 577 :275, 2007.

[114] L. I. Zaichik and V. M. Alipchenkov. Statistical models for predicting pair dispersion and particle clustering in isotropic turbulence and their applications. *New Journal of Physics*, 11 :103018, 2009.